

Nanotribological surface characterization by frequency modulated torsional resonance mode AFM

Dissertation
der Fakultät für Geowissenschaften
der Ludwig-Maximilians-Universität München



Ayhan Yurtsever

27. March 2008

Disputation: 04. July 2008

Referees: PD Dr. Robert W. Stark
Prof. Dr. Wolfgang W. Schmahl

Abstract

The aim of this work is to develop an experimental method to measure in-plane surface properties on the nanometer scale by torsional resonance mode atomic force microscopy and to understand the underlying system dynamics. The invention of the atomic force microscope (AFM) and the advances in development of new AFM based techniques have significantly enhanced the capability to probe surface properties with nanometer resolution. However, most of these techniques are based on a flexural oscillation of the force sensing cantilever which are sensitive to forces perpendicular to the surface. Therefore, there is a need for highly sensitive measurement methods for the characterization of in-plane properties. To this end, scanning shear force measurements with an AFM provide access to surface properties such as friction, shear stiffness, and other tribological surface properties with nanometer resolution.

Dynamic atomic force microscopy utilizes the frequency response of the cantilever-probe assembly to reveal nanomechanical properties of the surface. The frequency response function of a cantilever in torsional motion was investigated by using a numerical model based on the finite element method (FEM). We demonstrated that the vibration of the cantilever in a torsional oscillation mode is highly sensitive to lateral elastic (conservative) and visco-elastic (non-conservative) in-plane material properties, thus, mapping of these properties is possible in the so-called torsional resonance mode AFM (TR-mode).

The theoretical results were then validated by implementing a frequency modulation (FM) detection technique to torsion mode AFM. This method allows for measuring both conservative and non-conservative interactions. By monitoring changes of the resonant frequency and the oscillation amplitude, we were able to map elastic properties and dissipation caused by the tip-sample interaction. During approach and retract cycles, we observed a slight negative detuning of the torsional resonance frequency, depending on the tilt angle between the oscillation plane and the surface before contact to the HOPG surface. This angle leads to a mixing of in-plane (horizontal) and out-of-plane (vertical) sample properties. These findings have a significant implication for the imaging process and the adjustment of the microscope and may not be ignored when interpreting frequency shift or energy dissipation measurements.

To elucidate the sensitivity of the frequency modulated torsional resonance mode AFM (FM-TR-AFM) for the energy dissipation measurement, different types of samples such as a compliant material (block copolymer), a mineral (chlorite) and a macromolecule (DNA) were investigated. The measurement of energy dissipation on these specimens indicated that the

TR-AFM images reveal a clear difference for the domains which have different mechanical properties. Simultaneously a topographic and a chemical contrast are obtained by recording the detuning and the dissipation signal caused by the tip-surface interaction. Using FM-TR-AFM spectroscopically, we investigated frequency shift versus distance curves on the homopolymer polystyrene (PS). Depending on the molecular weight, the frequency detuning curve displayed two distinct regions. Firstly, a rather compliant surface layer was probed; secondly, the less mobile bulk of the polymer was sensed by the oscillatory motion of the tip. The high sensitivity of this technique to mechanical in-plane properties suggests that it can be used to discriminate different chemical properties (e.g. wetting) of the material by simultaneously measuring energy dissipation and surface topography.

Contents

1. Introduction	8
2. The Atomic Force Microscope	11
2.1. Principle of the atomic force microscope.....	11
2.1.1. Imaging Modes.....	11
2.2. Tip-surface interaction forces.....	15
2.2.1. Long-range attractive interactions.....	15
2.2.2. Contact forces.....	16
2.3. Frequency modulation atomic force microscopy.....	19
2.4. Lateral modulation methods.....	22
3. Torsional Resonance Mode AFM	25
3.1. Theory of the torsional resonance mode.....	29
3.2. Numerical simulation (FEM).....	31
3.3. Simulation Results.....	35
4. Experimental Results (Abstracts of the Manuscripts)	37
4.1. Frequency modulated torsional resonance mode AFM.....	37
4.2. Response of a laterally vibrating nanotip to surface forces.....	39
4.3. Frequency modulation torsional resonance mode AFM on chlorite	40
4.4. Frequency modulated torsional resonance mode atomic force microscopy on polymers.....	43
4.5. Acoustical force nanolithography of thin polymer films.....	46
4.6. Torsional mode atomic force microscopy and image processing for the analysis of protein-DNA complex binding site.....	48
4.7. Amplitude modulation torsional resonance mode AFM (TR-mode) on Graphite	50
5. Conclusion	52

References	54
Appendix	57
1. Manuscripts.....	57
2. Acknowledgements	100
3. CV.....	102

List of Abbreviations

AFM	Atomic Force Microscope
TR-AFM	Torsional Resonance Mode AFM
TM-Mode	Tapping Mode
IC-AFM	Intermittent Contact Mode AFM
FM-TR-AFM	Frequency Modulated Torsional Resonance Mode AFM
UHV	Ultra High Vacuum
LFM	Lateral Force Microscopy
nc-AFM	Non-Contact AFM
FM	Frequency Modulation
FFM	Friction Force Microscopy
HOPG	Highly Oriented Pyrolytic Graphite
CE-Mode	Constant Excitation Mode
CA-Mode	Constant Amplitude Mode
KPM	Kelvin Probe Microscopy
SCM	Scanning Capacitance Microscopy
PS	Polystyrene
AGC	Automatic Gain Control
PSD	Position-Sensitive Photo Detector
PI	Proportional Integral
RMS	Root Mean Square

1. Introduction

The Atomic force microscope (AFM) was invented as a tool for nano-, and atomic-scale surface topography imaging. In addition to topographic imaging, there has been great interest in using the AFM as a nanoscale characterization tool, probing a rich variety of information related to mechanical properties of the surface such as elasticity, hardness and tribological properties. The measurement of these properties provides additional information which helps to differentiate between distinct materials. Several techniques have been developed to extract the surface mechanical properties with nanometer resolution. Typically, an AFM tip in close contact to the surface is used as a sensor to probe the tip-sample interaction. The tip-sample interaction is usually measured perpendicular to the sample surface. Conventional methods based on flexural oscillations (in vertical direction) of the AFM sensor lack information on the in-plane properties. Usually, only information in vertical direction is measured neglecting in-plane properties. However, many material properties are described by vectors (e.g. magnetization) or tensors (e.g. elasticity). Thus, surface characterization methods are needed which allow for the determination of both in-plane and out-of-plane components of the interaction between the AFM tip and the sample.

A precise measurement of the in-plane mechanical properties depends on the mode of operation. The AFM methods cover the entire range from contact over intermittent contact, to non-contact modes. Researchers have explored many effects related to in-plane surface properties by dynamic AFM. Different modulation techniques have been used such as torsional or lateral modulation AFM. The observation of force gradients on hard magnetic coatings, anisotropy of lateral stiffness and friction, are some examples for the measurement of in-plane mechanical properties. Lateral force microscopy (LFM) [1, 2] was introduced to access frictional properties. In order to measure the lateral deflection signal, several methods have been implemented to the AFM. These are for instance optical beam deflection [3], two capacitance methods [4], or a dual fiber interferometer [5]. The first friction force measurement on the atomic scale was carried out by Mate *et al.* [6] who used a tungsten tip to characterize a graphite surface. This experiment helped to explain important phenomena of friction such as the stick-slip or the dependence of friction on the normal load. In addition to LFM, other techniques have been developed where a lateral or torsional excitation of the AFM cantilever was used for the measurements. The excitation can be provided by a dither piezo on the cantilever holder (both in thickness or in shear mode) or by an ultrasonic shear wave transducer below the sample [7].

An accurate measurement of friction requires exact knowledge of the contact area between tip and sample. Unfortunately, this parameter is not directly accessible. Thus, approximate models based on continuum elasticity theories such as Hertz, Derjaguin-Muller-Toporov (DMT) [8], Johnson-Kendall-Roberts (JKR) [9], or Maguis-Dugdale (MD) [10], can be used to estimate the contact area. In particular, Pethica [11] suggested a method based on the Hertz model where the contact area can be determined from contact stiffness measurements. If the elastic properties of tip and sample are known, the contact area can be calculated. In order to increase the accuracy of the contact area determination, the lateral stiffness of the contact can be used as an additional parameter [12, 13]. Lateral stiffness measurements reveal the reduced shear modulus of the materials. In addition to elastic property measurements, also other properties of the materials can be probed by lateral excitation of the AFM cantilever. Examples are measurements of the glass transition temperature (T_g) of polymers [14], [15], of friction on nanoscale [16], and the discrimination of different chemical properties [17].

An example for the importance of in-plane properties for conventional AFM methods is the characterization of organic monolayers. The anisotropy of the in-plane elasticity is an important factor to explain the phase contrast in intermittent contact mode AFM (IC-AFM) on such structures. The phase shift in atomic force microscopy is related to the energy dissipation between tip and specimen. On organic monolayers, an in-plane anisotropy can cause an additional phase shift. Marcus et al. [18] showed that energy dissipation caused by the in-plane anisotropy accounts for 10% of the total energy dissipation [19].

Another example for the importance of lateral forces is an experiment by Pfeiffer et al. [20] who measured energy dissipation on a Cu (100) single crystal surface in UHV. Lateral forces were probed by shaking the cantilever base at the torsional resonance frequency, in non-contact AFM mode. The excitation of torsional vibrations enabled force sensitivity in the piconewton range.

Despite to the importance of the results obtained by lateral or torsional modulation AFM, the above mentioned techniques are limited in sensitivity for several reasons; firstly, the excitation of the cantilever in lateral oscillation is also coupled to flexural vibrations. Thus, the lateral deflection channel includes several resonances which are not torsional vibrations. Secondly some of the mentioned techniques can only be used in ultra high vacuum (UHV) which is not suitable for biological applications. To overcome these limitations an accurate measurement of surface properties requires the measurement of forces in perpendicular and in lateral direction simultaneously. Towards this end, a special cantilever holder was introduced recently, which allows for the direct excitation of torsional resonances in a standard AFM

setup under ambient conditions. In the so-called torsional resonance mode (TR-mode), the torsional resonance of the cantilever is excited by two piezoelectric elements which are driven out of phase in thickness mode. This excitation forces the tip into an oscillatory motion parallel to the sample surface with a minimum of vertical movement. This technique increases the signal level in ambient air and decreases coupling or cross talk between torsional and flexural vibrations.

In this thesis, our main contribution is to understand the principle dynamics of the TR-Mode AFM in amplitude and frequency modulation feedback. The goal is to improve the sensitivity of in-plane measurements as they are needed for the characterization of nano-materials. Application examples include biological objects (DNA protein interaction), mineralogical specimen (surface heterogeneity of chlorite) and polymers. First, the response of the torsionally vibrated cantilever to the surface forces is investigated and the resulting insight is used to experimentally implement the first demonstrator of a frequency modulation torsional resonance mode AFM (FM-TR-AFM). Understanding the manner in which the feedback mechanisms of this novel mode are related to the dynamics of the cantilever is crucial to extend the current capabilities of AFM used in nanotribology. In contrast to other lateral modulation techniques, this novel method measures conservative and dissipative interaction forces simultaneously with the surface topography.

The thesis is organized into 5 chapters. Chapter 1 provides an introduction to the background and the motivation of this work. Chapter 2 reviews the principle of atomic force microscopy and provides a brief explanation of the different methods used to model the tip-sample interaction in AFM. Also the frequency modulation technique (FM) is discussed. Chapter 3 describes torsional resonance mode atomic force microscopy (TR-mode) and its dynamics in the case of visco-elastic interaction. Additionally the setup of the frequency modulation torsional resonance mode AFM is described. Chapter 4 presents a short summary of the published papers. Conclusions and an outlook to future work are presented in Chapter 5.

2. The atomic force microscope (AFM)

In this chapter, the basic principles of the atomic force microscopy will be introduced. First, we start with various modes of operation of the AFM for surface imaging and spectroscopic applications. Then, a short review of the tip-sample interaction force and contact mechanical theories used in atomic force microscopy will briefly be described. Finally, frequency modulation techniques (FM), and lateral modulation methods in atomic force microscopy (AFM) are presented.

2.1. Principle of the atomic force microscope (AFM)

2.1.1. Imaging modes

The atomic force microscope [21] is a surface analysis tool for characterizing surface topography with nanometer resolution. Since its invention in 1986, the atomic force microscope (AFM) has been used as an essential tool for different branches of science such as in material science, physics, chemistry and biology. It is a powerful tool used for high resolution imaging, manipulating and characterization of a wide range of materials such as metals, polymers, ceramics, semiconductors, and biomolecules [22-24]. In addition to high-resolution topography imaging, there has been a great deal of interest in using AFM as a tool to probe hardness and elastic properties of surfaces at the nanoscale. Imaging of elastic and frictional properties [17, 25] enables detection of variations in chemical composition [26] across the surface, characterization of thin films [15], and studies of nanomechanical structures [27].

The basic principle of AFM is the measurement of the interaction force between a high aspect ratio tip and the sample surface. The tip is integrated at the end of a soft cantilever beam which is usually microfabricated from silicon or silicon nitride in a rectangular geometry. The tip at the end of the cantilever is generally of conical or pyramidal shape and has a tip radius of curvature in the order of a few nanometers [28]. In order to acquire an image of a surface profile, an atomically sharp tip is scanned over the surface of the material with a feedback system that adjusts the piezo-scanner level to maintain the tip at a constant force between tip and surface. By recording the feedback signal, the topography image of the surface is obtained. When the tip is approached into the proximity of a sample surface, force gradients (from different surface forces) induce a deflection of the cantilever. The bending of the cantilever (in contact mode) or the damping of its oscillation amplitude (in tapping mode) due

to the response of the attractive or the repulsive force gradient is monitored by an optical lever system [29, 30]. The laser beam of a laser diode (LD) is focused on the back side of the microfabricated cantilever, and the reflected beam is projected onto the position-sensitive photo detector (PSD). For optical sensing of the cantilever motion, the back side of the cantilever is coated with a metallic film to increase the reflectivity. The channels in the quadrant-photodiode are arranged to detect the bending and the torsion signal of the cantilever beam (Fig.1a). The signal changes on the photodetector are monitored by a feedback system and the output is displayed on the computer, which gives quantitative topographical and frictional information of the surface. The detector used to sense the movement of the cantilever deflection is a crucial component for determining the performance of the microscope. There are various other methods to sense the cantilever deflection signal such as capacitance sensor and interferometry with fiber optics as described in [4, 31-33]. AFMs can be operated in a variety of modes, such as contact mode (quasi-static), flexural or tapping mode and non-contact mode (nc-AFM) (dynamically).

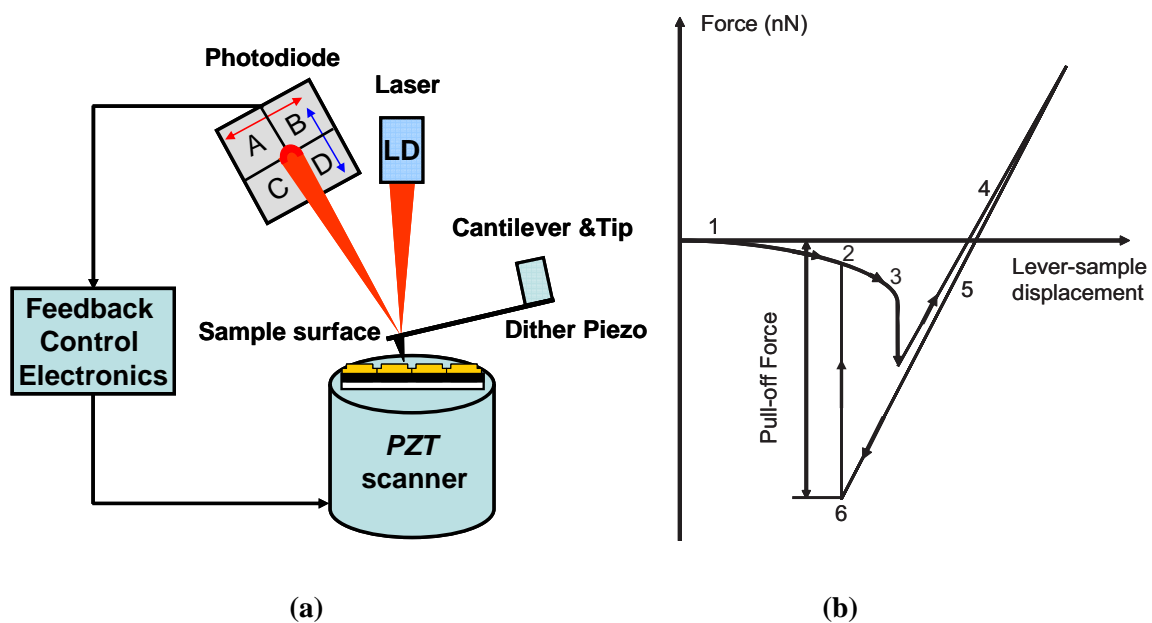


Figure 1: (a) AFM setup with an optical beam deflection system. (b) Typical AFM force-distance curve. At large distance to the sample surface, there is no force between tip and sample (1). The AFM tip is approached to the surface (2). Then the tip is being pushed to the surface resulting in a bending to the cantilever in downward direction. The jump into contact occurs due to attraction of the van der Waals force (3). Approaching more closely to the surface, the tip is in repulsive contact to the sample surface; then the cantilever is bent in upward direction (4). Retraction part of the force-distance curve (5) the motion of the tip is reversed. (6) the cantilever stiffness overcomes the pull-off force and the tip snaps out of contact (Figure 1 (b) adapted from reference [34]).

In contact mode operation, the tip stays in close contact with the sample surface (i.e., the repulsive interaction regime in the force-distance curve) during the entire imaging process. The vertical deflection of the cantilever, which is related to the tip loading force on the sample surface by the cantilever-tip system, is used as a control signal in the feedback loop. The feedback moves either the sample or the probe assembly vertically to the surface of the sample in response to the cantilever deflection, as it is sensed by the deflection system while the probe is scanned across the surface. By recording the change of the z-level of the piezo-scanner, a surface topography image is obtained. The contact mode AFM is usually preferred if high-speed scanning capabilities are required. However, the high tip-to-sample force is an important issue in contact mode AFM imaging. The presence of the lateral forces leads to a mechanical deformation of the surface. Undesired material modification can occur for a soft material such as biological materials or compliant samples. Therefore, very soft cantilevers are employed to reduce the tip and surface damage [35]. Most of the contact mode levers have a spring constant of less than 1 N/m.

The needs to avoid surface deformation and to probe surface properties dynamically were the main motivations for the development of other techniques in atomic force microscopy. One advanced technique is tapping mode [32] also known as intermittent contact mode AFM (IC-AFM). In tapping mode AFM, the cantilever is excited mechanically to oscillate at its fundamental flexural resonant frequency. The excitation of a dither piezo causes the cantilever to oscillate with an amplitude of typically 20 nm which is used as the control signal in feedback circuitry and is kept constant during imaging. Therefore, it is also called amplitude modulation AFM (AM-AFM). The oscillating tip is approached close to the surface until it starts to lightly touch or tap the surface at a small portion of its oscillation period. As the vibrating cantilever starts to periodically contact the surface, the cantilever oscillation amplitude, frequency, and the phase are changed due to the tip-sample interaction. These changes in the amplitude and the phase with respect to the reference values provide information about surface elastic and frictional properties. The oscillation amplitude is reduced due to damping and energy dissipation caused by the tip-surface interaction. The phase shift between the driving signal and the cantilever beam gives additional information about the material properties. Imaging of a large range of soft materials, especially biological samples [36], became possible by the advent of the tapping mode AFM.

Another important method in dynamic force microscopy is non-contact AFM (nc-AFM) [32]. In this mode, the system is operated in the attractive force region. In order to maintain stable imaging in the attractive regime, usually a frequency modulation feedback is used. Similar to amplitude modulation in tapping mode AFM, the atomic force microscope can be operated in non-contact in ambient air. However, in ambient conditions, water molecules adsorb to hydrophilic surfaces and a water layer forms. This water layer creates a capillary force between tip and surface. This force also prevents the tip from coming close enough in order to measure the short range repulsive forces. In such a case, the AFM tip usually snaps into contact with the sample surface. The short range repulsive force, which occurs when the electron orbitals of the tip and sample overlap, is the main source of the atomic resolution contrast in nc-AFM. In order to get the atomic resolution, the long range part of the tip-sample interaction force has to be filtered out. For this reason, the non-contact mode operation is usually employed in an ultrahigh vacuum environment (UHV) for true atomic resolution imaging [37]. Due to the increased quality factor of the oscillation of the cantilever in UHV, the sensitivity of the force measurement is increased significantly. However, the scanning speed is reduced compared to the normal operation in ambient air. The time constant in amplitude modulation is proportional to the quality factor of the cantilever where a higher quality factor cantilever has a longer time constant. To overcome this deficiency Albrecht [38] used the frequency modulation detection technique (FM) to increase the scan speed in ultrahigh vacuum (UHV). With this approach, the response time of the frequency change is shortened. By taking advantage of this increased sensitivity the FM technique allows for the measurement of much weaker force gradients. Since 1995, the non-contact atomic force microscope (nc-AFM) has achieved remarkable progress especially in imaging with true atomic resolution [39], manipulation of atoms [23] and in the creation of artificial atomic structures on surfaces [40]. More detailed information on the frequency modulation detection system will be given in section 3.3.

As we can see in Figure 1 (b) the force-distance dependence of the interaction between an AFM tip and a sample surface typically shows an attractive and a repulsive part. While the tip is far away from the sample, the tip deflection remains on an almost constant level (1). Approaching further, the attractive tip-sample force pulls the cantilever downward (2). Finally, the tip-sample contact occurs where the tip is in repulsive regime (3) and the cantilever is deflected to the upward direction (4). During the retract part of the force-distance curve, the cantilever deflection is reduced until the tip is separated from the surface. When the gradient of the restoring force of the cantilever exceed the attractive force gradient, the tip

will snap-out of the surface contact (6). The attractive or the adhesive force of the cantilever is calculated by multiplying the spring constant of the cantilever with the downward deflection. The meniscus force can be eliminated by controlling the humidity, such as imaging in a dry environment, in ultra high vacuum (UHV) or working in liquids.

2.2. Tip-surface interaction forces

There are many types of forces between the atoms at the tip and the sample in close proximity to each other [41-43] with different properties and distance dependencies. The atomic force microscopes (AFM) typically respond to three types of force, namely, attractive, repulsive, and adhesion. These forces can be classified into attractive and repulsive forces. Van der Waals interactions, short-range repulsive interactions, chemical, adhesion, electrostatic and capillary forces are the dominant interactions in an atomic force microscope experiment in ambient air. In order to interpret AFM force curves and to understand the mechanism of the contrast formation in atomic resolution imaging, researchers try to model the tip-sample interaction by using several approximations [42]. The analysis of the force curves incorporate many valuable information regarding surface chemical, mechanical and adhesive properties. Here, we will follow some of these most widely used approximations in tip-sample interaction modelling.

2.2.1. Long-range attractive interactions

The most important long-range interaction is the van der Waals (*vdW*) force that affects the tip motion when the tip is approached to the sample surface. The van der Waals force represents the electromagnetic field fluctuation of the dipoles in the atoms of the tip and the sample surface. Charge fluctuations in the tip or the surface induce dipoles in the other component generating a force between both. The van der Waals force originates from three different forces with the same distance dependencies; **(i)** dipole-dipole interaction (orientation), **(ii)** dipole-induced dipole force, **(iii)** dispersion forces (dipole-instantaneous dipole interaction). The dispersion force is the dominant component in the van der Waals interaction. Here we will be concerned about the van der Waals force between the probing tip and a surface. The *vdw* forces for a sphere (tip) with a radius R and a flat geometry (sample) can be obtained

from the Derjaguin, Müller, and Toporov (DMT) approximation as a function of the tip-sample distance d ,

$$F_{vdW} = -\frac{HR}{6d^2}, \quad (1)$$

where H is the Hamaker constant, R the tip radius. Parameter a_0 is an intermolecular distance which is introduced to avoid the divergence of F_{vdW} for $d \rightarrow 0$. The Hamaker constant is depending on the physical properties of the materials such as density of the tip and the sample, and the charge polarizability. The van der Waals forces are significant in the range between a few Ångstroms and a several hundreds of Ångstroms. Depending on the choice of the medium and the type of material between the interacting bodies, generally the van der Waals interaction has three important properties: (i) the vdW forces measured in vacuum are always attractive; (ii) the forces are always attractive if probe and sample consist of the same material, while between two different material they can be attractive or repulsive; (iii) the van der Waals forces are nonadditive properties. These properties can be used to control the resolution of the AFM images.

2.2.2. Contact forces

The atomic force microscope is the most useful tool for the measurement of surface mechanical properties on the nanoscale. The imaging of surfaces in the repulsive regime and probing the surface mechanical properties such as the elastic or the frictional properties require an understanding of the short range tip-surface interaction force. Especially an accurate prediction of the contact area is necessary for the analysis of tribological surface properties. Thus, the appropriate use of these theoretical models will be relevant in the experimental investigation. The response of two elastically interacting bodies under load is described by the continuum elastic mechanics. Here a short review is given on the approximations of relevant tip-sample interactions which are most widely used in continuum mechanics. When the surfaces of two objects are in mechanical contact with each other, their surfaces are deformed by the compressing force due to the applied load (see figure.2). Neglecting the plastic deformation, continuum models describe the contact area and the adhesion between the bodies under this external load. There are several different elastic-adhesive contact theories that provide an analytical relation between the applied force and the indentation depth.

The simplest approach to model the contact between a single asperity and a surface is the Hertz theory which describes the deformation mechanics of the sphere-flat geometry without adhesion force [41]. However, the adhesion force plays a significant role for the small length scale which is the case in the contact mechanics of a nano-tip and a surface. In the Hertz theory, the adhesive forces between the contacting asperities are neglected, whereas AFM experiments show adhesion effects, such as the snap-into contact of the tip to the surface (see Figure 1 (b)). The theories that describe the contact mechanics of the two interacting bodies are based on the following assumptions [44]. (i) The deformation of the surface is assumed small and purely in the elastic regime, (ii) under the applied load, the Young's modulus E and the Poisson's ratio ν are not changed, (iii) the radius of the contact zone a is small compared to the radius R of the cantilever probe (i.e. sphere), (iv) continuum theories neglect atomic structures of the two bodies, and (v) the bodies are elastically isotropic.

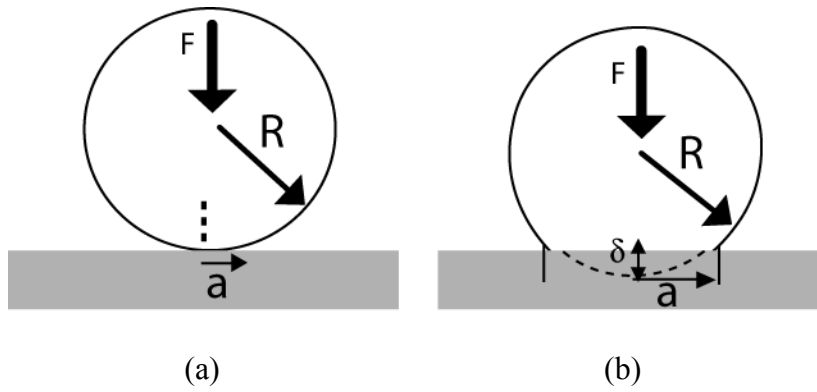


Figure 2: (a) Schematic representation of the Hertz model under external load. (b) Formation of a neck due to the adhesive interaction in JKR model. The parameters which are used to determine the visco-elastic contact of the surface are shown on the pictures. a : radius of the contact, δ : deformation depth, F : applied load, R : radius of the probe.

In order to account for the adhesion force between two interacting bodies, more advanced theories that include adhesion force were developed. Theories where the adhesion is taken into account include those of Derjaguin, Müller, and Toporov (DMT), of Johnson, Kendall, and Roberts (JKR), and of Maugis-Dugdale (MD). In the DMT model [8], the effect of the surface energy on the contact deformation was taken into account outside of the contact zone. For sphere-plane geometry, the load is related to the indentation depth by

$$F_{DMT}(d) = \frac{4E^* \sqrt{R}}{3} d^{3/2} - 4\pi RW \ ,$$

with

$$E^* = \left(\frac{1-\nu_t^2}{E_t} + \frac{1-\nu_s^2}{E_s} \right)^{-1},$$

where E^* is the reduced Young's modulus. In most text books and research papers which cover the simulation of the tip-sample interaction in AFM, the adhesion force is equated to the van der Waals (*vdW*) forces at the point of contact where the tip-sample distance is equal to the intermolecular distance,

$$F_{ts} = \begin{cases} \frac{-HR}{6\delta^2}, & \delta > a_0 \\ \frac{-HR}{6a_0^2} + \frac{4}{3}E^*\sqrt{R}(a_0 - \delta)^{3/2}, & \delta \leq a_0 \end{cases}.$$

This model is appropriate for tip-surface combinations where the elastic modulus is high and the radius of curvature and the surface energies are small.

The model of the JKR [9] theory is based on the assumption that the attractive surface forces cause additional elastic deformation on the surface. In this theory, an adhesive force is included inside the contact area (Fig. 2 (b)). The JKR model is more suitable for soft samples with low elastic modulus, and with a large tip radius as used in AFM experiments. The MD [10] theory provides an interpolation between the DMT and the JKR contact mechanical limits. The relation between the penetration depth and the contact radius for different contact mechanic models are summarized in Table 1.

	Hertz	DMT	JKR
a	$\sqrt[3]{\frac{RF}{E^*}}$	$a = \sqrt[3]{\frac{R}{E^*}(F + 2\pi RW)}$	$a = \sqrt[3]{\frac{R}{E^*}(F + 3WFR) + \sqrt{6WFR + (3WFR)^2}}$
δ	$\frac{a^2}{R}$	$\delta = \frac{a^2}{R} = \left(\frac{F + 2\pi RW}{\sqrt[3]{R(E^*)^2}} \right)^{2/3}$	$\delta = \frac{a^2}{R} - \frac{2}{3} \sqrt{\frac{6\pi Wa}{E^*}}$
F_{adh}	0	$2\pi RW$	$\frac{3WFR}{2}$

Table1: Summary of the different theories for the radius of the contact zone a , the sample deformation depth δ , and the adhesion force F_{adh} for a sphere-flat geometry (Adapted from reference [41]).

2.3. Frequency modulation atomic force microscopy (FM-AFM)

The frequency modulation (FM) mode was first implemented by Albrecht et al.[38]. It leads to an increased sensitivity through a higher Q -value. It is classified as a non-contact mode atomic force microscopy (nc-AFM) technique. The bandwidth of the AFM is described by the inverse of the time constant (i.e. $1/\tau = \omega_0/2Q$). Typically, in vacuum environment, the quality factor of the cantilever Q is increased up to $\sim 10^5$ and the corresponding bandwidth will be <1 Hz. The long time constant problem in amplitude modulation (AM-AFM) is overcome by the frequency detection system. Hence, the scan speed, which is the main issue in non-contact atomic force microscopy (nc-AFM), is significantly increased.

In FM-AFM, the force acting on the tip perturbs the cantilever oscillation only weakly, giving rise to a small shift Δf of the resonant frequency. In comparison to the amplitude modulation (AM) mode, the cantilever is kept oscillating at its current resonant frequency (f) with a constant amplitude, A_0 . The driving signal of the cantilever excitation is generated through a feedback loop. If the frequency of the driving voltage is close to the cantilever resonance frequency, the cantilever will be excited to oscillate. The photodiode signal, sensing the cantilever movement, produces an ac-signal which is amplified with some gain factor. After the proper phase adjustment thorough a phase shifter, the output signal is used as an excitation signal (see the block-diagram of the oscillator control amplifier in Figure 3). The frequency shift is used as a feedback parameter to control the tip-sample gap or to measure the conservative force interaction between the tip and sample. There are two different submodes of this technique which are employed in the FM-AFM. The constant excitation mode (CE-mode) [45, 46] keeps the driving amplitude of the lever constant and therefore results in a variable oscillation amplitude. The other mode involves a change of the amplitude of the driving piezo to keep the oscillation amplitude constant and is known as constant amplitude mode (CA-mode) [47, 48]. Basically the FM-technique has two different feedback loops, the amplitude control feedback loop and the distance control feedback loop.

The proportional and integral gains of the Phase-Locked-Loop (PLL) allow tracking the resonant frequency while an automatic gain control (AGC) keeps the oscillation amplitude constant (CA-Mode). The automatic gain control (AGC) circuit keeps the vibration amplitude

at a constant level by variation of the gain of the variable gain amplifier (see the block diagram of the oscillator control amplifier in FM-AFM detection system in Figure 3).

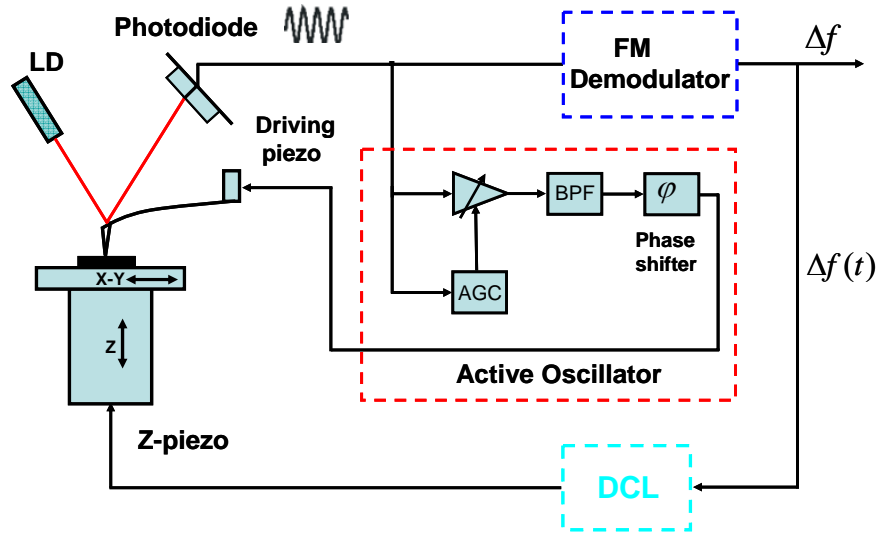


Figure 3: Schematic representation of the FM-AFM. The commercial AFM component, automatic gain control (AGC) (that keeps the oscillation amplitude in constant value), FM demodulator (PLL) (used in order to determine the frequency shift), and the distance control loop (DCL) (maintain the resonance frequency shift induced by the tip-sample interaction at a preset value Δf_{set}).

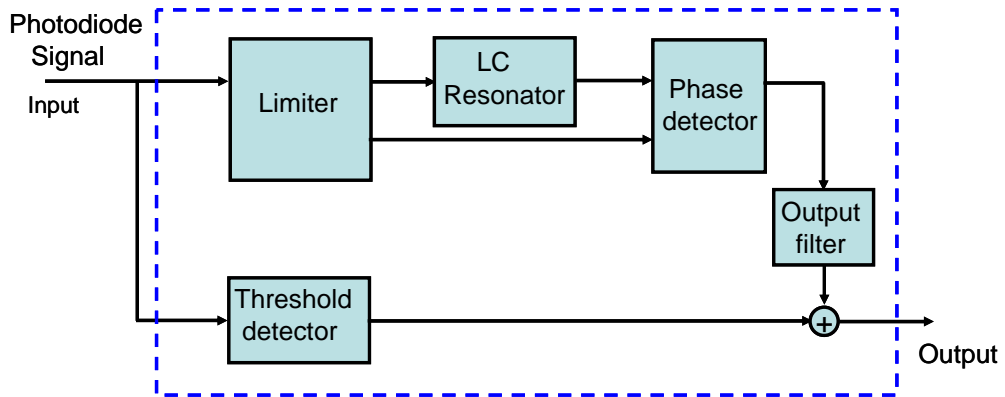


Figure 4: Scheme of the frequency demodulator (Adapted from[38]).

This feedback loop is known as amplitude control feedback loop. The amplification in the amplitude control loop is adjusted by a PI controller to keep the oscillation amplitude constant. The tip-sample gap is regulated by the distance control loop (DCL) through the PI controller in the AFM control electronics. The frequency shift caused by the conservative tip-sample interaction is detected by an frequency modulation (FM) demodulator proposed by Albrecht [38]. In our measurements, we used a Nanosurf Phase-Lock-Loop controller/detector

(PLL)¹, which offers a resolution of 4 mHz with 120Hz bandwidth to regulate the AFM in an FM detection scheme. The cantilever resonance frequency detuning Δf is detected by a FM demodulator and is used as an input for the distance control loop where the error signal of this Δf feedback loop yields the topography Z . It is worth to mention that the spatial dependence of the frequency shift in tip-sample interaction force is the source of the image contrast in FM-AFM. If the tip-sample distance regulation feedback is working properly, the tip-sample distance will be varied in order to keep the frequency shift value to the set value.

In frequency modulation atomic force microscopy, two different operation modes can be used for the z- feedback regulation depending on the scanning speed and the feedback loop gain. If the scanning speed is low and the loop gain high, the change in the frequency shift is very small and the tip follows the topography of the surface in a stable way in feedback loop. The images generated by the frequency shift show only very small changes at surface steps and a uniform contrast on surface terraces (only the derivative picture of the topography is obtained), whereas, the topography images contain the useful information regarding the tip-sample interaction. However, if the loop gains decreases and the scan speed increases, the tip is no longer capable of following the surface structure due to the faster response of the detuning change in the feedback loop. This scanning mode is called constant height mode [49]. In this case, the detuning images incorporate all useful information which comes from the tip-sample elastic interaction. The imaging of the surface with constant height mode increases the image contrast significantly with a well defined lateral structure.

Non-contact atomic force microscopy (nc-AFM) using the frequency modulation detection method [38] has been one of the most powerful methods for investigating different types of sample surface in true atomic resolution even on insulating [20] surfaces as well as on conductive surfaces [50]. Besides providing true atomic resolution, it is also very powerful tool to measure the tip-sample interaction accurately. Apart from the topographical measurement, FM-NC-AFM additionally allows for energy dissipation measurements to probe local surface properties, since the energy dissipation is strongly related with the mechanical and chemical properties of the surface.

The FM-AFM technique can also distinguish between conservative and dissipative interaction [51]. The conservative tip-sample interaction results in a distance dependent frequency shift of the cantilever resonance, without loss of vibration energy. On the other hand, the

¹ EasyPLL Digital FM Detectors and Controller made by Nanosurf AG, Liestal, Switzerland CH-8804

dissipative force interaction results in loss of the cantilever vibration energy. In order to compensate the reduction in oscillation amplitude, the power on the excitation piezo has to be increased. This leads to an increase in the excitation amplitude. The information about the dissipative interaction (i.e., energy dissipation) can be extracted from the AGC feedback signal, which shows the ratio A_d/A . [48]

2.4. Lateral modulation in atomic force microscopy

Several approaches have been demonstrated in order to achieve a lateral modulation of the AFM cantilever to measure the in-plane surface properties. Friction force microscopy (FFM) is widely used for tribological measurement of the surfaces at the atomic scale. It is a modification of the atomic force microscope that measures both the normal force as well as the lateral force simultaneously in contact mode. As the probe is scanned perpendicular to the long axis of the cantilever across the surface, the friction force between the tip and the surface causes the cantilever to bend or twist in lateral direction. The cantilever twisting angle (i.e., torsional amplitude) is a measure of the lateral force acting on the tip. By recording the lateral deflection signal of the cantilever twist during a trace-retrace loop, a characteristic friction loop of the investigated material can be obtained as plotted in Figure 5.

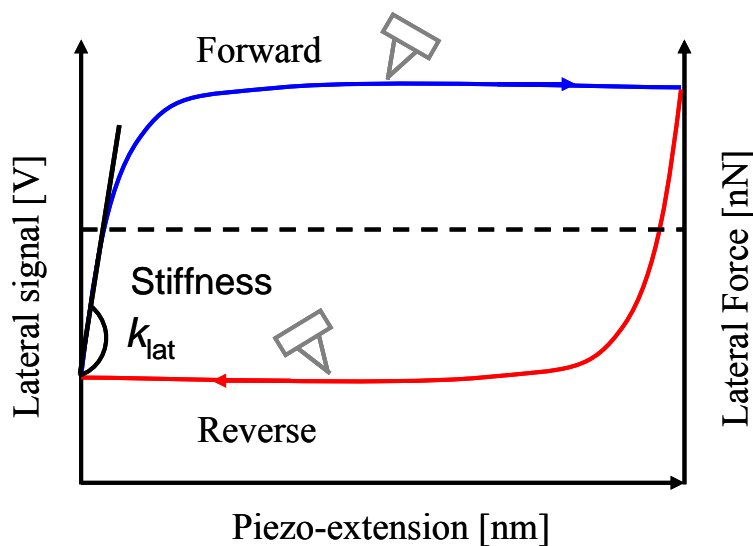


Figure 5. Schematic representation of a friction loop as measured in friction force microscopy (FFM). The cantilever twists versus the lateral position of the cantilever. The slope of the friction loop is a measure of the total stiffness. Adapted from reference [7].

At the beginning of the motion, the bending force in the cantilever is not strong enough to overcome stiction. This is represented as a linear increase of the lateral signal in the friction loop. Once the restoring force in the cantilever becomes strong enough, the tip starts to slip over the surface, resulting in a constant lateral signal in the friction loop, due to the effect of the friction. If the elastic deformations of tip and sample are sufficiently small without sliding friction contact movement, the slope of the linear part in the friction loop can be used to measure the surface elastic properties such as lateral contact stiffness and the compliance of the materials (see Figure 5). The friction loop provides the most convenient method for acquisition of quantitative data from the FFM. However, the contrast of the frictional image may include contributions from material properties as well as from topography induced effects [52, 53]. In order to reduce topography induced effects in the measurement of the frictional properties, several distinct excitation methods have been developed for the modulation of the cantilever in lateral or torsional oscillation.

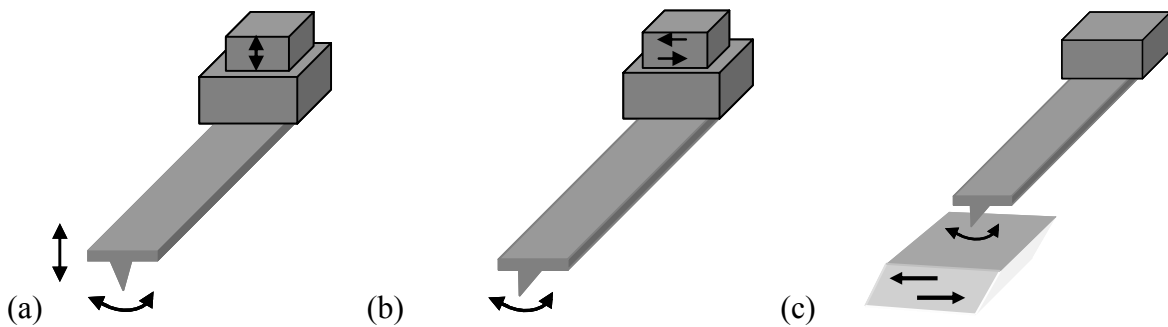


Figure 6: Different methods to achieve a lateral modulation. (a) Excitation of the cantilever by a piezo electric tube in thickness mode attached to the cantilever holder. (b) Shear-mode piezo attached to the cantilever suspension. (c) Shear wave transducer mounted below the cantilever.

The main mechanism of these techniques is based on the excitation of the cantilever by a dither piezo at the base of the cantilever on the cantilever holder (both in thickness mode (Fig. 6 (a)) and in shear polarized mode (Fig. 6 (b))) or by using a shear-wave piezoelectric transducer mounted below the sample [54]. As seen in Figure 6 (a), by using the piezo tube scanner (PZT) in thickness-mode, the flexural vibration of the cantilever can be excited as in tapping mode AFM. But, due to the asymmetry of the cantilever shape or mass distribution, the torsional vibration can also be excited at the same time with vertical bending excitation. Using a piezoelectric tube scanner which is implemented to the sample or the cantilever, Maivald et al. [55] performed a lateral modulation experiment. In this technique, a modulation voltage is applied to the x-axis electrode of the scanner without any interference with the

conventional imaging system. Several groups used similar techniques to measure frictional or elastic properties on the nanoscale. The glass transition temperature (T_g) of monodispersed polystyrene (PS) thin films was investigated by Ge et al. [15] using shear modulation force microscopy (SFMM). The results obtained by the modulation of the cantilever in lateral or torsional vibration by using a piezo mounted to the cantilever holder or below the specimen, explained the frictional or the mechanical properties of the surface at some level. However, due to coupling of the torsional and the flexural vibration in this type of excitation [56], the frictional images generated by these measurement system consist of superimposed material and topography induced effects. Furthermore, some of these techniques have limitations concerning the modulation frequency restricting it to only several kHz. To overcome this limitation, external sources have been introduced for the torsional or the lateral modulation. Shear waves in the specimen induced by a piezoelectric transducer may be used as an excitation source [57, 58]. In this measurement mode, the transducer is oriented perpendicular to the long-axis of the cantilever. Acoustic waves are transmitted through the air to the tip, so that the lateral force couple into the tip-cantilever system and excite torsional vibrations in the cantilever. With this measurement technique, Reinstadtler et al. [58] presented a new approach for the investigation of the stick-slip phenomena by analyzing the torsional amplitude and the phase signals.

3. Torsional resonance mode AFM (AM-TR-AFM)

Tapping mode imaging as described in chapter 2.1.1. is one of the most widely used modes in atomic force microscopy. As already mentioned in chapter 1, the effects of a structural in-plane anisotropy on the phase image, which corresponds to a map of energy loss, were investigated by Marcus *et al.* [59] on a thin polymer film. Since in most AFMs the tip is tilted with respect to the horizontal plane by an angle of about 11° , also in-plane properties contribute to the image contrast. This effect allowed researchers to study the effect of the in-plane anisotropy of a poly (di-acetylene) (PDA) monolayer on the phase contrast measurement. This experiment shows that the anisotropy of the in-plane elasticity is an important factor to explain the phase contrast in tapping mode AFM on organic monolayers. On such specimen, the in-plane anisotropy may cause an additional energy dissipation of about 10% of the total energy dissipation [19]. Although this experiment demonstrates that in-plane properties contribute to the conventional image contrast it is difficult to separate the vertical and the in-plane contributions quantitatively. An AFM which is operated in flexural vibration, probes the surface force mostly in vertical direction, contributions from in-plane properties are rather small. Thus, a cantilever oscillating in a flexural mode is not sensitive to shear forces. However, dissipative shear forces (i.e., friction) and lateral contact stiffness (i.e. the gradient of the shear force) are essential parameters characterizing elastic and frictional surface properties. Thus, an accurate measurement of these surface properties requires both the measurement of the force in vertical and in lateral direction to the specimen.

The results obtained by tapping mode, may reveal insufficient information about the surface properties. For instance, imaging of a magnetic recording disc with different recording area densities shows that if the flexural vibration is used for the imaging, only the force gradient perpendicular to the surface can be measured². On the other hand, torsional resonance (TR) mode images show that when the sample is rotated, a different in-plane force gradient is observed. These in-plane characteristics are not quantitatively accessible by tapping mode. Similarly, electrostatic force imaging with a probe oscillating in flexural vibration cannot detect in-plane electrostatic forces at a surface boundary or at a sloped surface, as they may occur on self assembled monolayers (SAM).

In order to overcome these limitations of a vertically oscillating probe, several torsional modulation techniques were introduced allowing one to differentiate chemical properties and

² Veeco Metrology Inc. AFMs/SPMs 112 Robin Hill Road, Santa Barbara, CA 93117

to map friction and topography simultaneously. In contact mode, the excitation and analysis of torsional resonances of AFM cantilevers allows the experimentalist to characterize in-plane properties of metals or semiconductors. For example, Drobek *et al.* [60] measured the relation between lateral sample stiffness and load using torsional overtone microscopy. The tip was in contact with the sample surface without external excitation. In their technique, the thermomechanical noise spectra of the surface coupled cantilever were analyzed. By using the finite element method (FEM), an empirical relation between the frequency shift of the first eigenmode and the shear stiffness was derived. The resonance frequency shifts were measured from the power spectral density of the photodiode signal, and used to measure the lateral contact stiffness of the sample. By using the Johnson-Kendall-Roberts theory (JKR) [9], they extracted a reduced shear modulus from the lateral stiffness versus load curve. In this way, the shear modulus of different samples such as metal and semiconductor surfaces was measured. A similar concept is used in atomic force acoustic microscopy (AFAM). In this mode the cantilever is actively vibrated in torsional oscillation by an ultrasonic transducer attached under the sample [61] [57, 58]. By analyzing the resonance spectra, the lateral contact stiffness could be measured from detuning of the torsional resonance due to the tip-sample contact.

By combining vertical and horizontal oscillations, i.e. by shaking the cantilever at the torsional resonant frequency during non-contact AFM imaging Pfeiffer *et al.* [20], measured frequency shift (elastic interaction) and frictional energy dissipation on a Cu (100) surface in UHV. The excitation of a torsional vibration enabled a lateral force sensitivity in the piconewton range for the measurement of the friction force between the tip and a sulphur impurity. In a similar approach, Jarvis *et al.* [62], used a magnetically actuated force sensor, to measure lateral forces independently from vertical forces. These results demonstrate that it is possible to measure the lateral force between an AFM tip and atoms on the surface accurately. The precise determination of lateral forces is essential to understand nanomanipulation experiments. In nanomanipulation experiments, a mechanical lateral force is used to move atoms, molecules, and nanostructures on the surface using atomic force microscopy (AFM) [63].

Besides the methods mentioned above, several other methods based on different force sensors were invented in order to achieve a laterally oscillating nanotip. In order to achieve high-resolution non-contact imaging in shear force mode, an STM tip [64, 65] or an AFM sensor [66] can be mounted to the prong of a tuning fork. However, all these techniques require

special modifications of the cantilever sensors or a special transducer (mounted below the sample or the cantilever support) to excite the lateral motion.

Mode coupling between the torsional and the flexural vibration can occur due to small asymmetries of conventional AFM sensors. Especially if the horizontal force is parallel to the axis of the cantilever, the mode coupling is enhanced. Mode coupling due to an asymmetry of the force distribution on the cantilever can lead to additional resonances. This coupling complicates the analysis of the image contrast regarding the surface frictional properties in dynamic AFM measurements. To reduce topography induced effects in dynamic friction measurements the torsional vibration should be perfectly aligned to the surface. This alignment eliminates surface slope effects in the friction force measurement. Especially, for an unambiguous determination of in-plane properties (i.e. friction, heterogeneity) a pure torsional or lateral vibration mode is needed.

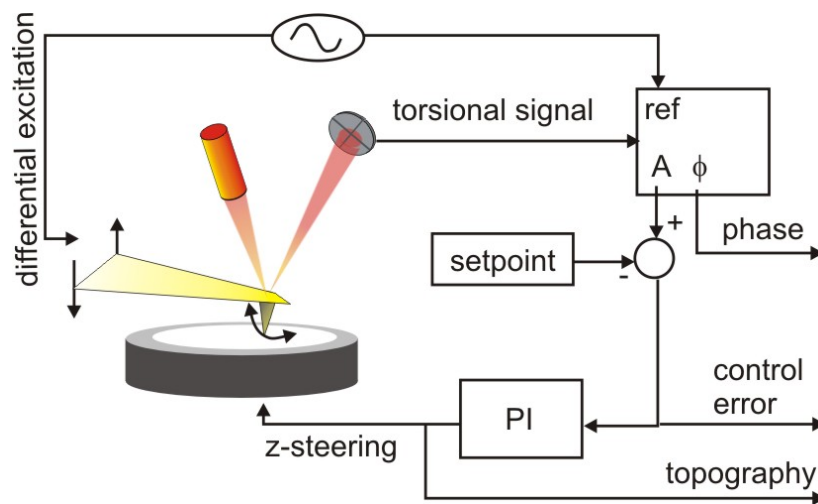


Figure 7: Experimental setup of the TR mode imaging system. The two piezos oscillating out of phase are necessary to promote a torsional vibration of the tip. The lateral deflection of the cantilever is detected by a high bandwidth optical deflection detection system. The feedback loop electronics in the controller work together with the Z piezo in the scanner to maintain constant TR amplitude or phase while the tip scans over the sample surface.

To reduce mode coupling and other difficulties described above, the torsional resonance mode (TR mode) was introduced recently, which allows for shear force microscopy with standard cantilevers [67]. In this mode, the cantilever is driven near its fundamental torsional resonance frequency by a split piezo actuator, typically in the range of 1MHz (Figure 7). In

order to generate a torsional oscillation in the cantilever probe system, experimentalists usually create an asymmetry in the cantilever-tip (i.e., putting the tip at an offset position relative to the cantilever axis) or in the transducer which is used to excite the cantilever.

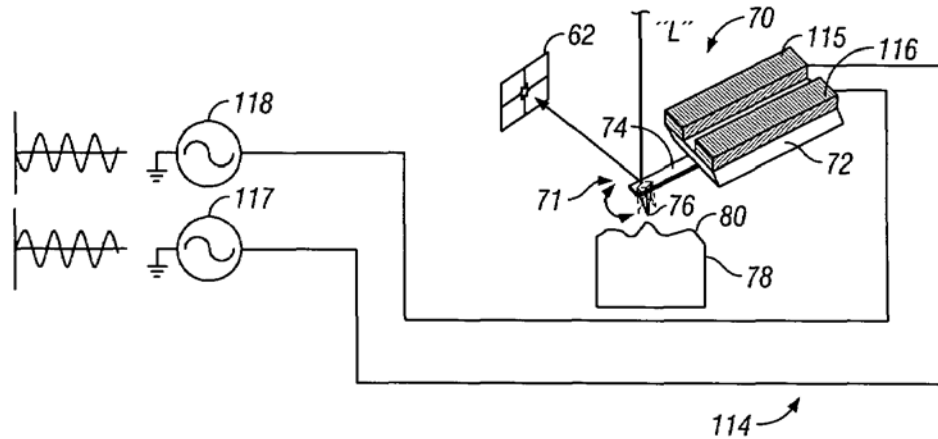


Figure 8: The original design of the setup³. Transducer 114 includes 2 piezo electric elements 115, 116 that are symmetrically attached to the base of the probe assembly 72. Two drive signals 117, 118 are 180 degrees out of phase with respect to each other. Therefore, as one of the piezo expands the other one contracts. As a result of this motion, with high frequency, the cantilever 74 and, hence the tip start to oscillate as a pendulum like motion.

In the original design of the torsional mode probe holder, the asymmetry was created by applying two signal sources with different polarity to the symmetrically attached piezoelectric elements as shown in Figure 8. As one of the piezos starts to oscillate in vertical direction (i.e., extension) the other one start to oscillate in opposite direction (i.e., contraction). This design of the cantilever holder leads to a direct excitation of the cantilever in torsion oscillation and also improves the signal to noise level and reduces possible cross talk between flexural and torsional vibrations in ambient air. Both piezoelectric elements drive the cantilever to a small torsional oscillation with a high Q-factor ($Q > 1000$). The torsion along the cantilever long axis promotes a small pendulum-like oscillation of the tip apex (typically 0.2 to 2.0 nm rms). Since the tip moves along the width axis of the cantilever beam, in TR mode the amplitude and phase of the vibration can only be affected by the force and its gradient in that particular direction. As a result, the phase and amplitude changes which are detected by the AFM, reflect the tribologic properties of the sample.

³ US patent no:6,945,099 B1(2005)

3.1. Theory of the torsional resonance mode (TR-mode)

The equation of motion of a rectangular cantilever corresponds to that of a beam which is clamped on one side and free on the other side. The cantilever has different types of vibrational modes such as flexural, torsional, and lateral vibrations. The resonance characteristics of each mode depend on the material properties, i.e. Young's modulus, Poisson ratio, density, shear modulus, and the dimension of the cantilever beam. By means of continuum elasticity theory, the frequency response of the cantilever beam can be calculated. We assume that the cantilever is oriented along the x-axis and the z-axis is the out-of-plane component. The boundary conditions are set to accordingly for the point where the cantilever is actuated by a sinusoidal displacement (Figure 10). The equation of motion in torsional resonance mode is governed by the following partial differential equation

$$GJ \frac{\partial^2 \theta(x,t)}{\partial x^2} = \rho I_p \frac{\partial^2 \theta(x,t)}{\partial t^2} + \gamma_{air} \frac{\partial \theta(x,t)}{\partial t} . \quad (1)$$

Here, θ is the twist angle of the torsion, G is the shear modulus, ρ is the mass density, I_p is the polar area moment of inertia, and γ_{air} is the viscous damping coefficient of the surrounding air. Since the cantilever is harmonically vibrated by a chip under the holder, we assume that $\theta(x,t) = \Theta(x) \exp(i\Omega t)$. Putting this into equation (1) leads to [68]

$$\frac{d^2 \Theta(x)}{dx^2} + (\rho I_p \Omega^2 / (GJ) - i \gamma_{air} \Omega / (GJ)) \Theta(x) = 0 . \quad (2)$$

Due to the lateral visco-elastic force at the end of the sensor tip, the boundary condition can be written as,

$$\begin{aligned} \Theta(x) \Big|_{x=0} &= \theta_0 \\ \Theta(x)' \Big|_{x=L} &= -(k_{lat} + i\eta_{lat} \omega \Omega) l^2 \Theta(x) \end{aligned} \quad (3)$$

Using the boundary conditions of equation (3), we can solve equation (2) in order to calculate the torsional angle of the cantilever by using the frequency response function of the cantilever at the end of the cantilever where the tip is located

$$\Theta(x=L) = H(\Omega)\theta_0 \quad (4)$$

$$H(\omega) = \frac{2\sqrt{-\alpha^2 + i\beta} \exp(\sqrt{-\alpha^2 + i\beta}L)GJ}{\sqrt{-\alpha^2 + i\beta}(1 + \exp(2\sqrt{-\alpha^2 + i\beta}L))GJ + (-1 + \exp(2\sqrt{-\alpha^2 + i\beta}L))l^2(k_{lat} + i\eta_{lat}\omega)}$$

where $\alpha^2 = \rho I_p \Omega^2 / (GJ)$ and $\beta = \gamma_{air} \Omega / (GJ)$.

The torsional amplitude and phase of the cantilever are given as [68]

$$A = |H_h| \theta_0 \quad \text{and} \quad \varphi = \text{Argument}[H(\Omega)].$$

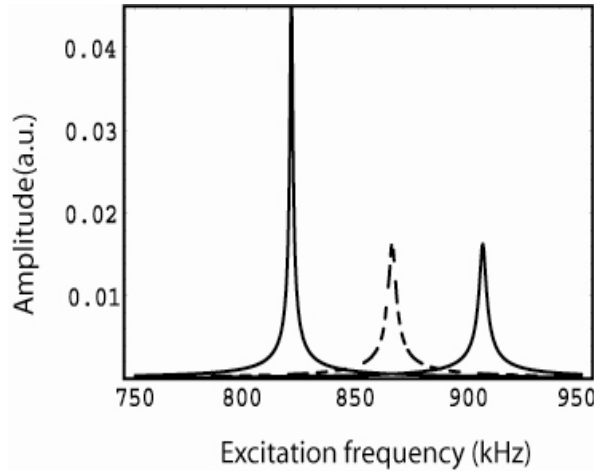


Figure 9: The calculated amplitude of the torsional oscillation for the free and surface coupled interaction for $k_{lat}=60N/m, 120N/m$ with $\eta_{lat}=2.5e^{-7} Ns/m$.

Dynamic atomic force microscopy utilizes changes of the cantilever frequency response (oscillation amplitude, resonance frequency, and phase) to reveal surface properties. Therefore, numerical simulations and analytical calculations are needed to interpret the measured surface properties quantitatively.

Figure 9 shows the calculated amplitude of the torsional vibration for the free and the surface coupled case. The amplitude of the torsional vibration decreases with an increase of the lateral stiffness of the tip-sample contact (i.e. stiffer interaction). A large in-plane stiffness leads to a large frequency shift. In order to extract in-plane surface mechanical properties such as lateral contact stiffness, the resonance shift can be used as an experimental parameter. However, in

the analytical formulae discussed in this section, the torsion axis has been assumed to be constant. The effect of the shift of the torsional axis due to surface coupling has not been included. Nevertheless, the parametric calculation of the frequency response of the cantilever in torsional vibration gives us a quantitative understanding of the dynamics and the changes due to the tip-surface interaction. In the next section, we model the system by a finite element method (FEM) to calculate the frequency response in a more accurate way.

3.2. Numerical Simulations

In order to account for the real cantilever shape and the distributed force used to excite the vibration, we employed a numerical model. To evaluate the torsional frequency response of the cantilever, a finite element (FE) model of a typical cantilever was implemented using tetrahedral mesh elements (COMSOL 3.2 / FemLab 3.2 (FEMLAB GmbH, Göttingen, Germany) with the parameters: length $L=250\mu m$, with $b=40\mu m$, thickness $h = 3\mu m$, tip length $l=15\mu m$, Young's modulus $E_T=169 GPa$, Poisson's ratio $\nu_t = 28$, and density $\rho = 2330kg/m^3$.

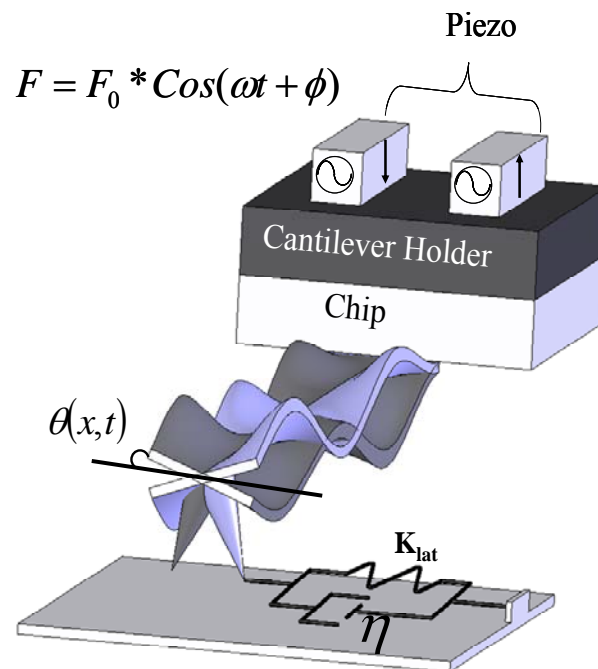


Figure.10: Schematic diagram of the torsionally excited cantilever in visco-elastic interaction. Two piezo actuators oscillating out of phase are necessary to promote a torsional vibration of the tip. The torsional movement of the piezos are transferred into the cantilever by the chip below the holder.

A rectangular cross section of the beam was assumed. The rectangular flexure of the cantilever ends in a triangle at the very end of the cantilever, which resembles the actual shape of the cantilever used in experiments. The conical tip was located at the connection of the rectangular beam and the triangular end (at $L=220 \mu m$). A mesh refinement was performed in order to check the convergence of the solution. The interaction related parameters of the silicon tip and the graphite sample are: $H=2.96 \times 10^{-19} J$, $Re(G^*)=4.2 GPa$, $Re(E^*)=10.2 GPa$, $\eta = 8 \times 10^{-7} Ns/m$ and $a_0=0.38 nm$. The beam was assumed to be under a forced interaction at the probe end and clamped at the other end (see Figure 10). Dynamic frequency response analyses were performed in the frequency range $1 < f < 7$ MHz to obtain the relation between the TR excitation frequency and the displacement amplitude in transverse and perpendicular direction. In order to make the model more realistic, Rayleigh damping is used for the modal analysis which includes mass-proportional and stiffness-proportional viscous damping. The matrix of the Rayleigh damping is given as

$$C = \eta M + \delta K .$$

In the mode superposition analysis the damping matrix should have following properties in order to lead to uncoupled modes:

$$2\omega_n \xi_n = \varphi_n^T C \varphi_n \quad , \quad 2\omega_n \xi_n = \eta + \delta \omega_n^2 .$$

Due to the orthogonality of the mass and stiffness matrices, this equation can be written as

$$\begin{bmatrix} \frac{1}{2\omega_1} & \frac{\omega_1}{2} \\ \frac{1}{2\omega_2} & \frac{\omega_2}{2} \end{bmatrix} \begin{bmatrix} \eta \\ \delta \end{bmatrix} = \begin{bmatrix} \xi_1 \\ \xi_2 \end{bmatrix} .$$

Only two frequencies are necessary in order to solve the equation for η and δ . We choose two frequencies around each eigenmode for the frequency response simulation of the cantilever (as shown in Figure 11).

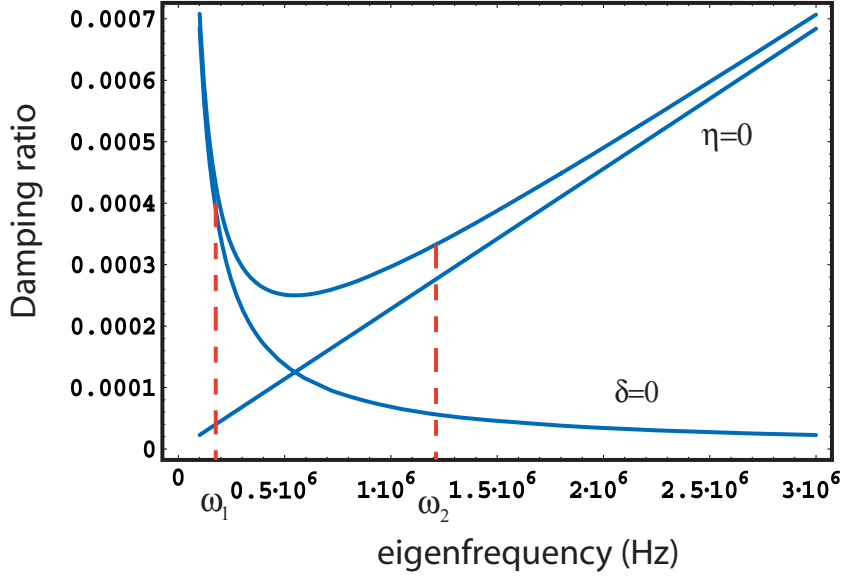


Figure 11: Damping ratio for different eigenmodes. For small eigenmode stiffness proportional damping is dominant, whereas for larger frequencies mass-proportional damping is important.

As shown in Figure 10, the two piezo actuators which are attached to the cantilever holder vibrate out of phase to excite the torsional vibration. Thus, the driving force was simulated by a distributed load along the long edge of the cantilever in the FE model. If the tip is coupled with a surface, the stiffness of the specimen and the damping between tip and sample affect the motion of the probe at the boundary [69]. Thus, the lateral interaction force between the cantilever tip and sample surface can be modelled by the Kelvin-Voigt model, which is a combination of a spring in parallel with a Newtonian dashpot. Thus, the visco-elastic interaction between probe and sample can be formulated along the vertical and lateral dimension using the DMT model

$$F_n = \begin{cases} \frac{-HR}{6\delta^2}, & \delta > a_0 \\ \frac{-HR}{6a_0^2} + \frac{4}{3}E^*\sqrt{R}(a_0 - \delta)^{3/2} - \beta_n \dot{\delta}, & \delta \leq a_0 \end{cases}$$

where β is the damping of the tip-sample contact in vertical direction. For the lateral force we assume no interaction before contact and a linear elastic interaction as derived from a Hertz model and viscous interaction. When the lateral force acting on the contact is small, then the

contact lateral stiffness can be approximated as [12, 13] $k_{lat} = 8aG^*$, where a is the contact radius, and G^* is the effective shear modulus. This equation is independent of the nature of the tip-sample interaction forces and is valid for different continuum elasticity models. This is a reasonable approximation, since the contact area does not change with the lateral force for a constant normal load. In the lateral direction, a modified damping model can be employed to account for the energy dissipation due to the lateral tip-sample interaction

$$F_{lat} = \begin{cases} 0, & \delta > a_0 \\ -8G^* \sqrt{R\delta} (\Delta_{lat}) - \beta_{lat} \dot{\Delta}_{lat}, & \delta \leq a_0 \end{cases}$$

with $G^* = [(2-\nu_t)/G_t + (2-\nu_s)/G_s]^{-1}$. Here, G_t and G_s are the shear moduli of tip and sample, respectively. The lateral interaction force is a nonlinear function of the normal contact force [68]. In the linearized approximation, where the tip is oscillating about an equilibrium position above the sample surface, the interaction force can be written as

$$F_n = -k_n \Delta_n - \beta_n \dot{\Delta}_n, \quad F_{lat} = -k_{lat} \Delta_{lat} - \beta_{lat} \dot{\Delta}_{lat}.$$

The dissipative tip-sample force is modelled by considering the damping of the medium and the indentation rate (or strain rate in lateral motion) as used in Ref. [70]. In the attractive ($\delta_0 > a_0$) and the repulsive ($\delta_0 < a_0$) regimes, the normal, and the lateral contact stiffness are derived as

$$k_n = -\left. \frac{\partial f_n}{\partial \delta} \right|_{\delta=\delta_0} = \begin{cases} \frac{-HR}{3\delta_0^3}, & \delta_0 > a_0 \\ 2E^* \sqrt{R(a_0 - \delta_0)}, & \delta_0 \leq a_0 \end{cases}$$

and

$$k_{lat} = -\left. \frac{\partial F_{lat}}{\partial \delta} \right|_{\delta=\delta_0} = \begin{cases} 0 & \delta_0 > a_0 \\ 8G^* \sqrt{R\delta_0} & \delta_0 \leq a_0 \end{cases}.$$

3.3. Simulation Results

The results of the finite element simulation shown in Figure 12 reveals that in contrast to the other imaging modes, such as vertical bending mode AFM, the neutral axis of the cantilever is mainly parallel to the sample surface. This means that the vertical tip-sample distance remains constant during the torsional oscillation cycle. The non-linear tip-sample interaction has no significant effect on the torsional oscillation of the cantilever. Therefore, torsion mode AFM is highly sensitive to the in-plane surface properties.

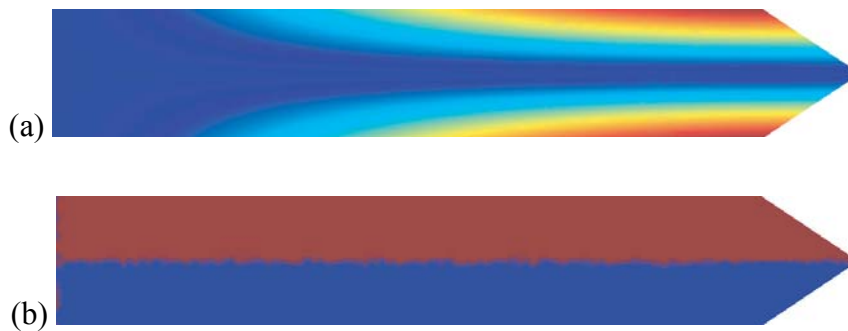


Figure 12: Finite element simulation of the amplitude (a) and the phase (b) distribution of the first eigenmode of a rectangular cantilever beam in torsional oscillation. The finite-element simulations were carried out for a rectangular cantilever with a thickness of $3\mu\text{m}$ and a length of $250\mu\text{m}$. The first torsional resonance frequency is 1.178 MHz. The colours correspond to the displacement amplitude. The finite-element simulations were processed with FemLab3.2 by using approximately 7600 tetrahedral mesh elements.

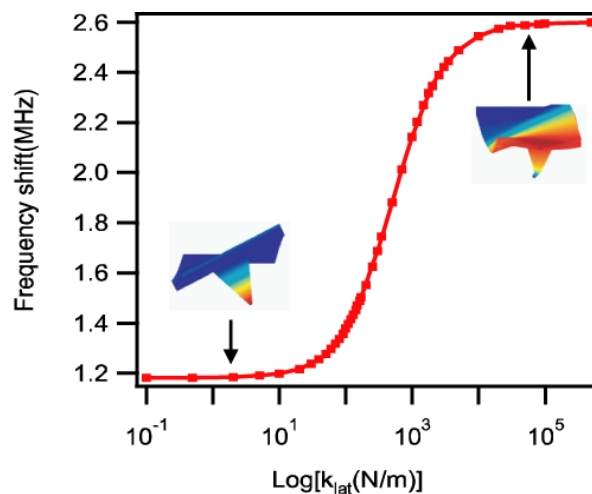


Figure 13: Simulated resonant frequency of the first torsional vibration mode versus the lateral spring constant of the tip-surface contact. The inset shows the motion of the cantilever-tip system for the weak and strong interaction region.

In order to investigate the sensitivity of the torsional mode AFM to the in-plane elasticity, we plot the resonance of the first torsional eigenmode of the cantilever as a function of the shear stiffness k_{lat} (Figure 13). A change in tip-sample stiffness leads to a shift of the resonant frequency together with a change in oscillation amplitude. In the case of a weak interaction (i.e. small k_{lat}), the tip can be assumed as freely vibrating. In the range of $k_{\text{lat}} = 10 \text{ N/m}$ to 10^4 N/m the eigenfrequency of the lateral vibration is highly sensitive (slope of the curve increases) to the shear stiffness. The resonant frequency of the first mode shows an increase in the range $k_{\text{lat}} = 10 \text{ N/m}$ to 10^4 N/m . Consequently, the resonant frequency of the first mode is useful for characterizing samples with $k_{\text{lat}} = 10 \text{ N/m}$ to 10^4 N/m . By increasing the tip-sample stiffness to a higher value, the tip of the cantilever is increasingly pinned to the sample surface. Here, the tip of the cantilever cannot move anymore, and the cantilever has to laterally bend back and forth. The frequency shift can be used to image the elastic properties of the sample surface [71]. Thus, in order to measure this frequency shift caused by conservative tip-sample interaction, we operate the torsional resonance mode in frequency modulation feedback.

4. Experimental Results

In chapters 4.2, 4.3, 4.4, and 4.5 results that have already been published are briefly described. Chapters 4.6 and 4.7 show recent results which have been submitted to peer reviewed journals together with additional data which could not be included in the papers. The complete manuscripts are attached in appendix 1.

4.1. Frequency modulated torsional resonance mode AFM (FM-TR-AFM)

In this section, we demonstrate the implementation of a frequency modulation feedback to a torsional resonance mode AFM. A Dimension 3100 atomic force microscope with a NanoScope IV controller was used for the experiments. The instrument was equipped with a cantilever holder for torsional resonance mode (Veeco Metrology Inc., Santa Barbara, CA). A TR-mode cantilever holder contains two dither piezos driven out of phase in order to induce torsional oscillations of the cantilever. Using an external phase-locked-loop unit (Easy PLL plus detector and controller, Nanosurf AG, Liestal, Switzerland) through a signal access module (SAM), a frequency modulation feedback was realized. All functionality of the FM-detector is controlled through the easyPLL plus software, which is installed on a PC. The FM unit was connected to the microscope controller via a signal access module (SAM), as shown in Figure 14 and Figure 15. The microscope controller was set to ‘contact mode’ operation, while the excitation of the cantilever and the feedback signal were provided by the external electronics. Tracking of the resonant frequency was achieved by the PLL unit, while an automatic gain control (AGC) kept the oscillation amplitude constant (CA-Mode). The frequency shift was used as control signal for the z-feedback loop in constant frequency shift mode. Using the FM technique, both frequency shift and energy dissipation can be mapped to topographic surface features under ambient conditions. Typically, in FM AFM, the oscillation amplitude of the cantilever is maintained by an automatic gain control (AGC). The shift in resonance frequency is used for topographic feedback regulation, while the output of the AGC provides a measure for energy dissipation. Silicon cantilevers with a flexural resonance frequency of 117 kHz were used for the measurements (ZEIHR Nanosensors, Neuchatel, Switzerland). The spring constant obtained by standard calibration procedures was 19 N/m [72]. The resonance frequency of the first torsional eigenmode was typically around 910 kHz.

Due to the limited bandwidth of the controller, only cantilevers with a torsional resonant frequency smaller than 1MHz can be used with this set up.

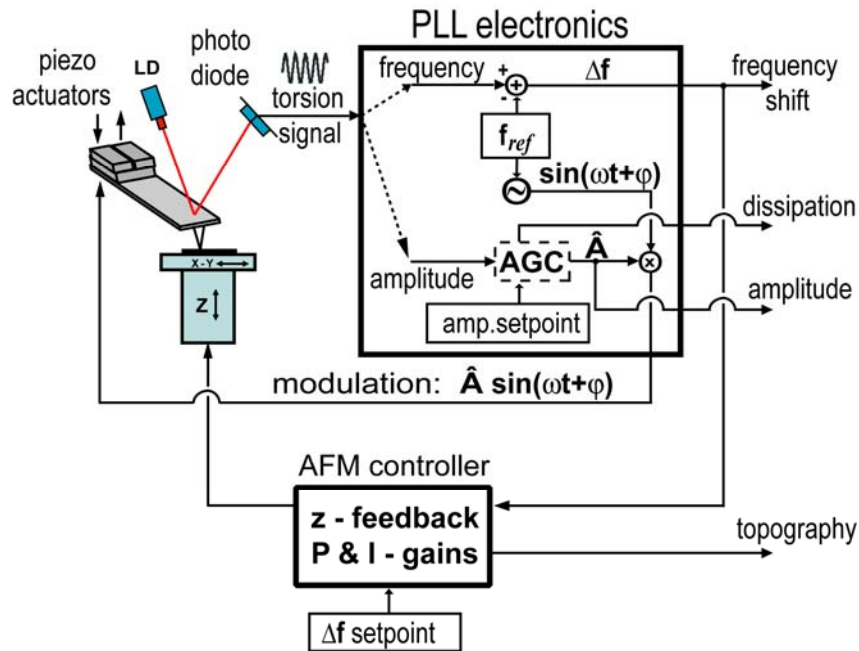


Figure 14: Scheme of the feedback circuit for torsional resonance mode in frequency modulation. The torsional vibration of the cantilever was measured as the lateral deflection signal of the segmented photodiode. The signal was amplified, phase shifted, and connected to the dither piezos for positive feedback. The frequency shift – mainly induced by conservative tip-sample interaction – is used for distance regulation. An automatic gain control (AGC) keeps the oscillation amplitude constant. Thus, the AGC error output corresponds to the local energy dissipation.

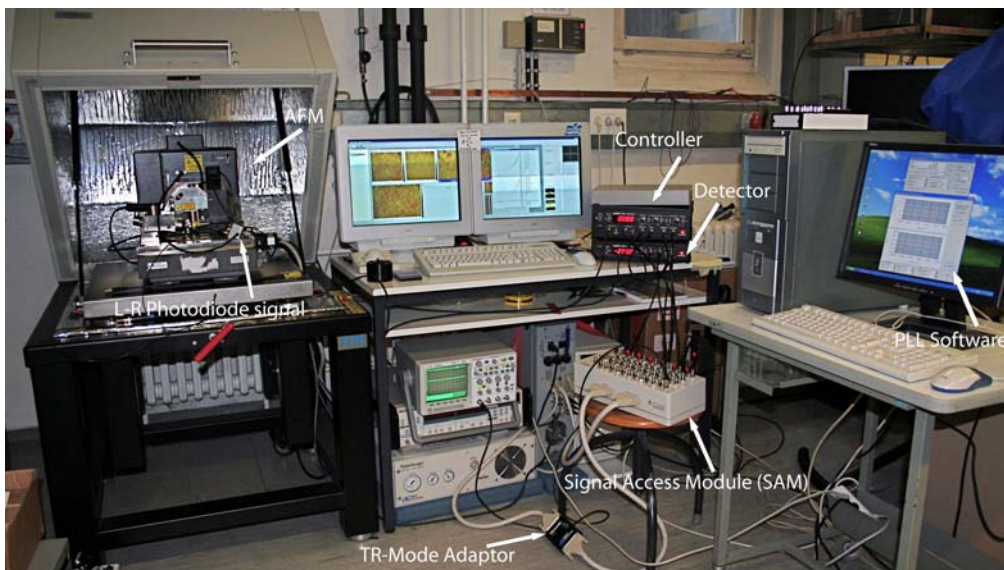


Figure 15: The laboratory pictures of the frequency modulated torsional resonance mode AFM. The instruments used in the experimental setup are shown.

4.2. Response of a laterally vibrating nanotip to surface forces⁴

In this work we try to understand the frequency response of the laterally vibrating nanotip to visco-elastic interaction forces at the surface. We studied the effect of viscosity and lateral contact stiffness on the detuning (frequency shift), amplitude, and phase response numerically. Figure 16 shows the calculated frequency response of the amplitude of a freely oscillating AFM cantilever. For small oscillations, the amplitude is proportional to the twist angle. The phase shift remains in the range between 0° and 360° . A lateral bending mode can also be excited (asterisk). Due to symmetry breaking by the tip, the torsional vibration of the cantilever can be coupled to the bending mode. To verify the theoretical considerations, a torsion mode AFM was operated in frequency modulation feedback scheme. We perform an experiment to measure the correlation of the surface tilt-angle with the detuning of the torsional oscillation. Depending on the tilt angle between the specimen and the torsional oscillation plane, the approach and the retract cycles reveal a negative detuning of the torsional resonant frequency at close approach to the surface. The numerical simulation based on the finite element method (FEM) together with the experimental results explain the fundamental mechanism of the z feedback in frequency modulated torsional resonance mode AFM (FM-TR-Mode).

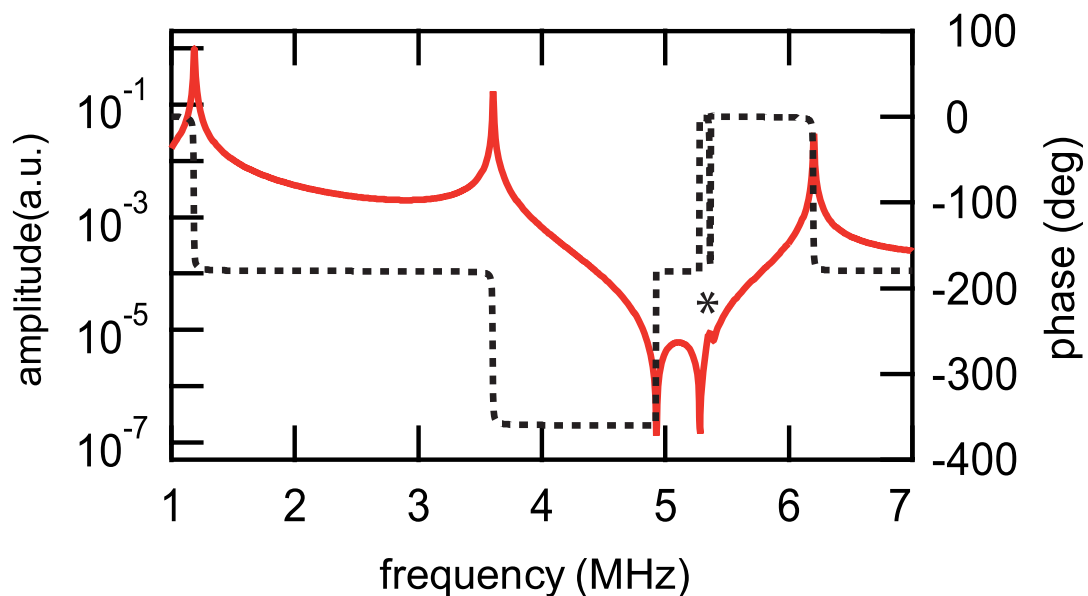


Figure 16: Frequency response of the torsionally vibrated rectangular cantilever beam. Torsional frequency response of the freely vibrating cantilever as obtained by finite element analysis. Amplitude response (red, solid) and phase response (black, dash). The asterisk indicates the lateral bending resonance.

⁴ A. Yurtsever *et al.*, *Applied Physics Letters (APL)*, 91, 253120 (2007)

The topography feedback regulates the AFM depending on the detuning of the resonant oscillation. If tip and sample are properly aligned, only positive detuning occurs due to elastic coupling between tip and sample. This detuning is accompanied by an amplitude reduction due to energy dissipation through the frictional contact. If specimen and oscillator are tilted, additional repulsive as well as attractive forces may occur due to mixing of in-plane and out of plane properties (see Fig. 17).

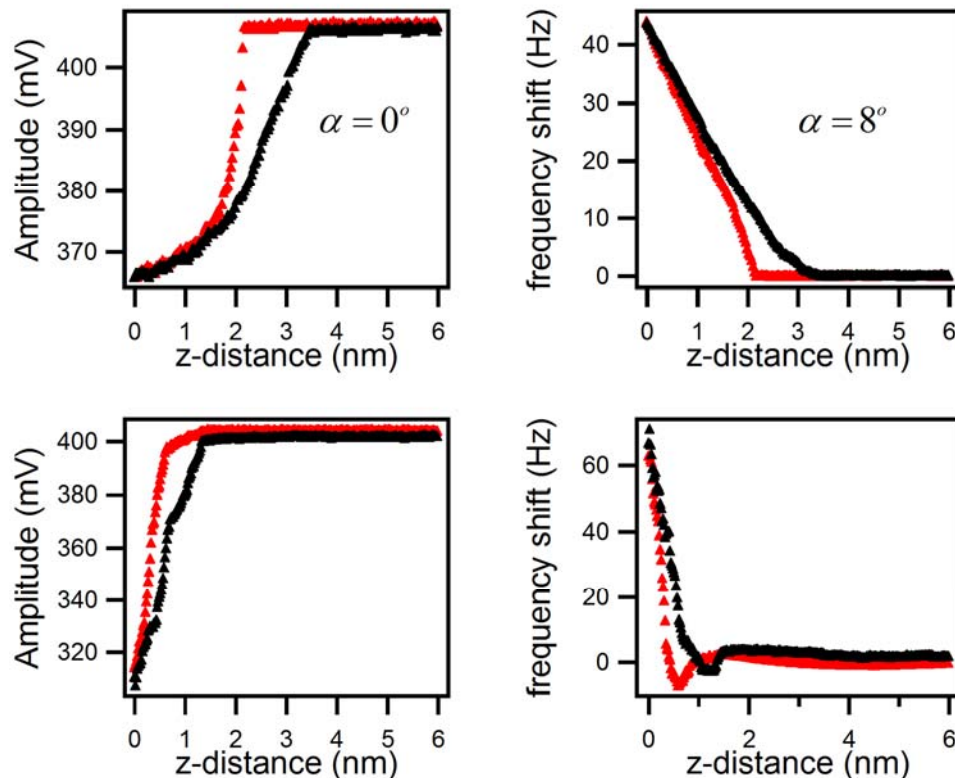


Figure 17: The effect of the sample tilt-angle on frequency shift curve of the torsionally vibrated cantilever in CE mode. Amplitude and frequency shift measured during an approach (red) and retract (black) cycle on an untilted ($\alpha = 0^\circ$) and a tilted ($\alpha = 8^\circ$) graphite surface. Torsional resonant frequency, quality factor, and amplitude were 900 kHz, 1300, 405 mV, respectively.

4.3. Frequency modulation torsional resonance mode AFM on chlorite⁵

In this work we presented the torsional resonance mode AFM (TR-Mode) in frequency modulation feedback scheme (FM-TR-AFM) (shown in figure 14) under ambient conditions. The measurements

⁵ A. Yurtsever et al., *Journal of Physics*, 100, 052033 (2007)

in frequency modulation allow the characterization of both dissipative (frictional) and elastic (conservative) properties of the specimen. In order to test the capabilities of the system a clinocllore (pennine) specimen $(\text{Mg,Fe}^{2+})_5\text{Al}[(\text{OH})_8|\text{AlSi}_3\text{O}_{10}]$ from Rimpfischwäng, Zermatt, Switzerland (Sample #17984 of the Bavarian Mineralogical State Collection, Munich) was cleaved for the investigation. The mineral belongs to the chlorite group of phyllosilicates. It consists of alternating T-O-T (tetrahedral-octahedral-tetrahedral) and brucite-like layers. The T-O-T layer corresponds to phlogopite mica. The brucite-like surface exhibits OH groups and is slightly positively charged as compared to the mica-like layer which presents oxygen at the surface. The step height is 0.5 nm for a brucite-like layer and 1 nm for a T-O-T layer.

This structure was investigated in order to demonstrate the dissipation measurement capabilities of the frequency modulation feedback in torsional mode AFM. The frequency shift provides information on the conservative interaction, while the dissipation signal also contains information on energy loss. Figure 18 displays the simultaneously measured maps of (a) topography, (b) frequency shift, and (c) energy dissipation as measured with the AGC feedback signal of the PLL on the chlorite surface. The experimental data were obtained in a constant amplitude (CA-Mode) operation mode of the FM-TR-AFM. A cross-section of the topographic data shows that the triangular shapes are brucite flakes with a typical step-height of 0.5nm. As control parameter, the frequency shift has been used. Thus, image (b) only reveals a uniform contrast with only small changes of the detuning at the surface steps. The excitation signal of the piezo represents the energy needed to keep the torsional amplitude constant and, thus, gives a measure for the dissipated energy. The dissipation signal leads to a clear contrast of the different domains on the chlorite surface. In addition to the different mechanical properties of the brucite and T-O-T layers of the crystal, these are also charged differently.

The combination of atomic force microscopy and the Kelvin probe force microscopy (KPFM) [73] is a useful tool to obtain a high resolution map of the electrical surface potential. The measurements of surface potential distribution show a clear chemical contrast for the region of the chlorite surface which has a different charge density (see the image of the surface potential in Figure 19 (b)). This surface charge density also influences the interaction between the tip and the surface due to the corresponding change in surface potential.

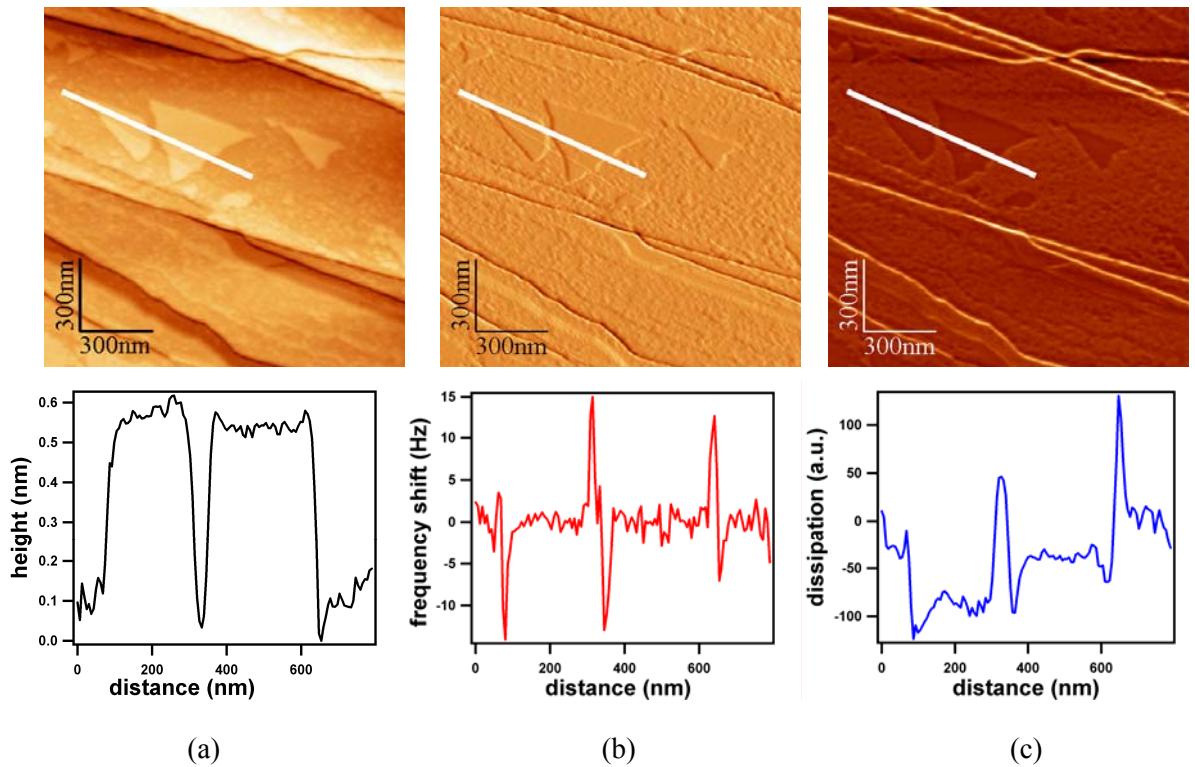


Figure 18: (a) A topographic image acquired using the frequency shift detuning feedback loop for the z-control. Image (b) shows the frequency shift. Image (c) shows the lateral mapping of the excitation amplitude of the piezo which measured simultaneously with topography on a chlorite surface in ambient air. Below the images, cross sections extracted from the images along the line drawn on the images are shown.

From the dissipation line trace, it is obvious that the oscillator loses more energy on the brucite flakes than on the T-O-T layer. This dissipative contrast might be due to different wetting properties of the respective surfaces or due to differences in the elemental friction processes at the atomic scale. The experimental results show that surfaces with different chemical properties or different surface charge densities can be discriminated in the dissipation signal while measuring the surface topography under ambient conditions.

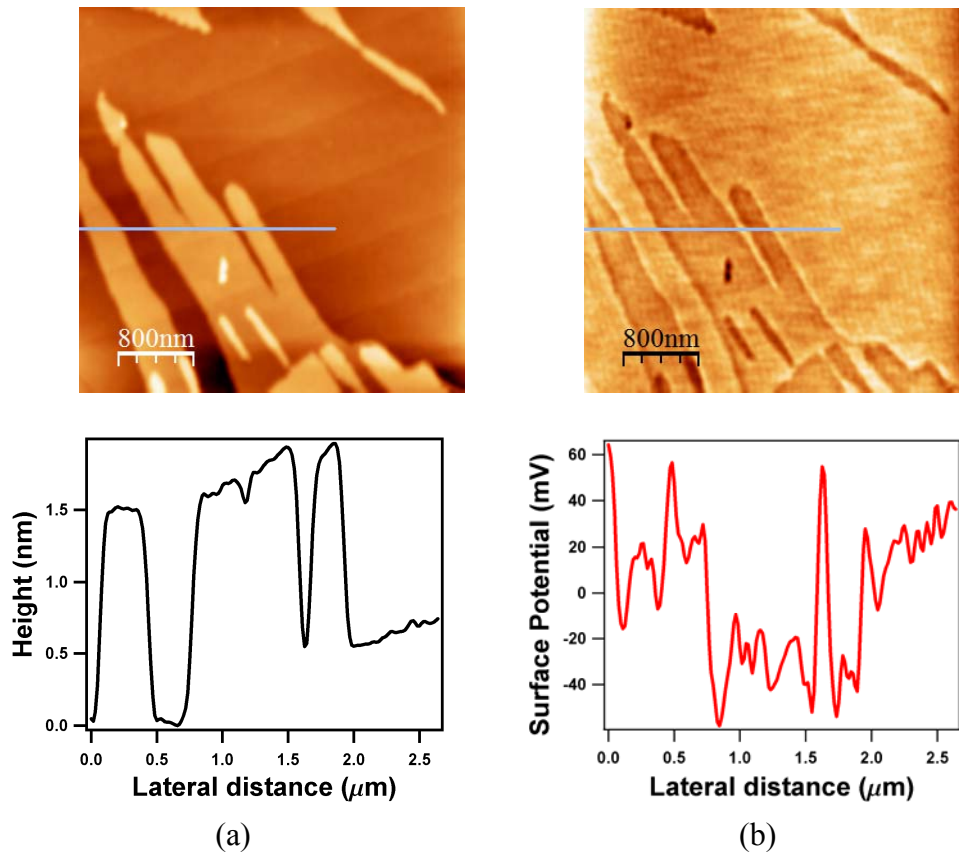


Figure 19: (a) The topography of the chlorite surface in Kelvin probe force microscopy (KPFM). (b) The surface potential image of the same surface. Corresponding profiles of the line drawn on the images are shown below the corresponding image.

4.4. Frequency modulated torsional resonance mode AFM on polymers⁶

Polymers are very important materials and have many applications, especially as protective coatings, for lubrication, or as biocompatible materials. Thermal properties of the polymer thin films such as the glass transition temperature (T_g), and the visco-elastic behaviour of the interface are the main parameters determining functionality and performance of such surfaces. Since structural properties of interfaces and surfaces determine the functionality of polymer films, the investigation of surface and bulk mechanical properties is of great importance. Hence, one needs to understand precisely how the surface differs from the bulk, both structurally and dynamically.

Here, we apply the FM-TR-mode AFM to study the surface nanomechanics of thin polymer films using displacement curves in AFM spectroscopy. In contrast to classical resonant

⁶A. Yurtsever *et al.*, *Applied Physics Letters (APL)*, **92**, 143103 (2008)

imaging such as intermitted contact or non-contact mode, the tip is oscillating parallel (instead of vertical) to the sample surface which minimizes possible sample indentation. Torsional resonance imaging resembles a shear force experiment which is strongly linked to the tribological properties of surfaces. In other words, this experiment corresponds to a shallow nanoindentation experiment where a small lateral dither is applied to the indenter.

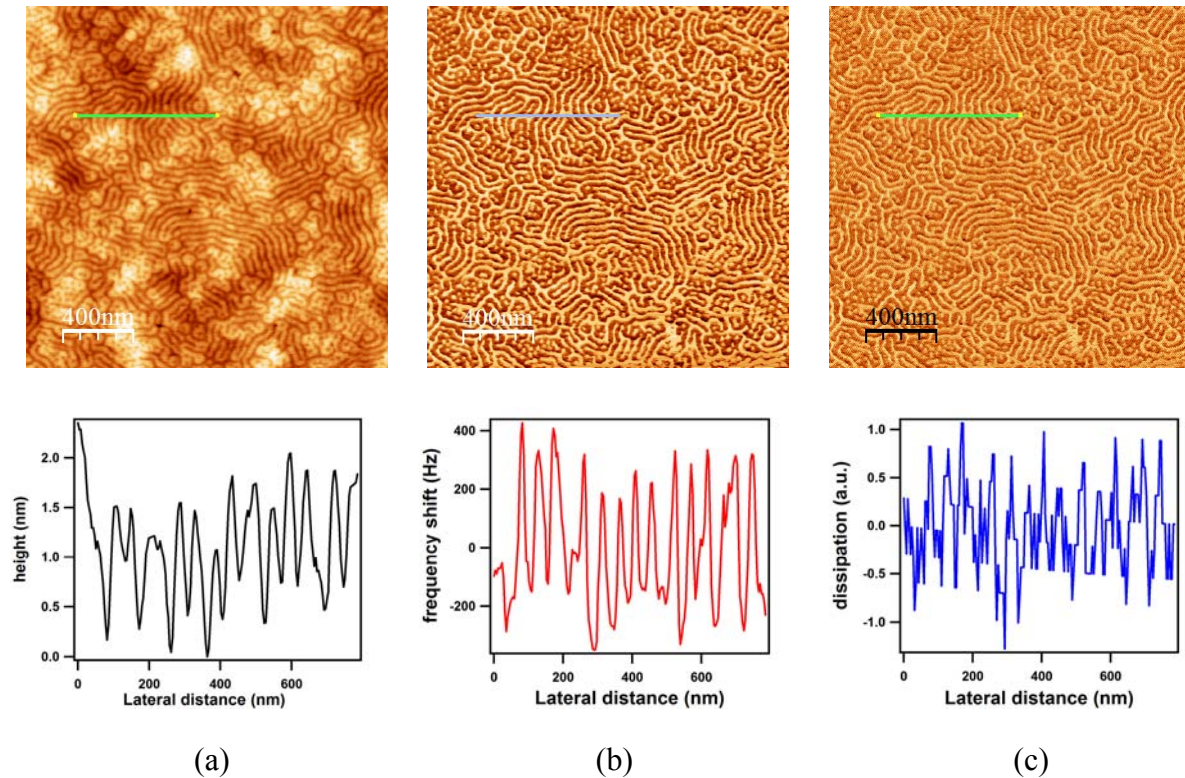


Figure 20: Constant amplitude imaging: (a) A topographic image with the constant height mode (intermediate level) feedback loop for the z-control. Image (b) shows the frequency shift (error signal). Image (c) shows the energy dissipation by the diblock copolymer surface in ambient air.

The experiment also demonstrates the feasibility of the frequency modulation technique in TR-Mode AFM for the measurement of visco-elastic properties of a compliant material. We imaged a thin film of a polystyrene-*block*-polybutadiene diblock copolymer. Diblock copolymers consist of two different types of polymer chains connected to each other with a covalent bond [74, 75]. This polymer shows a clear contrast between the blocks of polystyrene and polybutadiene due to their different local mechanical properties and different viscoelastic behaviour [76].

The frequency shift data corresponds to the conservative interaction while the energy dissipation image corresponds to the damping behaviour of the sample. Figure 20 shows

simultaneously measured maps of (a) topography, (b) frequency shift, and (c) energy dissipation on the diblock copolymer surface. Data were obtained in a constant amplitude (CA-mode) operation of the setup with a small loop gain (constant height mode), so that the frequency shift image also gives information for the surface properties. Measurements of the frequency shift and energy dissipation for compliant samples such as the diblock copolymer reveal highly detailed contrast between the different polymer phases. Since the cantilever is oscillating with a small amplitude (below 2 nm), a parallel motion above the surface is a reasonable assumption. Thus, the map of energy dissipation is directly related with the in-plane frictional properties. Since the polystyrene (PS) part of the diblock copolymer is the stiffer segment compared to the polybutadiene block, it appears higher in the topography image. In the dissipation image the contrast is inverted with respect to the topography images. Since the PBd block is more viscoelastic compared to the PS block, more mechanic deformation energy is turned into heat. Thus, the PBd domains appear brighter in this image.

In order to assess the nature of the tip-surface interaction and effect of the polymer chain length, distance curves were measured for different PS homopolymers ($M_w = 34.3$ kg/mol, 119.6 kg/mol, and 354.0 kg/mol) as shown in Fig. 21. For all specimens, two regimes were observed in the displacement curves: Firstly, a rather compliant surface layer was probed; secondly, the less mobile bulk of the polymer was sensed by the oscillatory motion of the tip. The position of the kink between the two regimes strongly correlates with the molecular weight of the homopolymer.

We investigated frequency shift versus distance curves on polystyrene, which revealed two different interaction regimes. Depending on the molecular weight, we observed a distinct change in the signature of the distance curves. Hence, we propose a stratified structure due to the segregation of shorter chains and, thus, the resulting two layer behavior. Our findings show that FM-TR-mode spectroscopy enables discerning of polymer samples by their different molecular weight. Frequency modulation in torsional resonance mode atomic force microscopy (FM-TR-AFM) is a powerful tool for imaging polymeric samples with spatially varying mechanical properties. The indentation experiments clearly show that the tip is oscillating within the motile top layer of the polymer surface even for detuning on the order of ten Hertz. For the diblock copolymer, this means that while imaging in FM-TR-AFM the tip is also compressing the different polymer blocks according to their compliance.

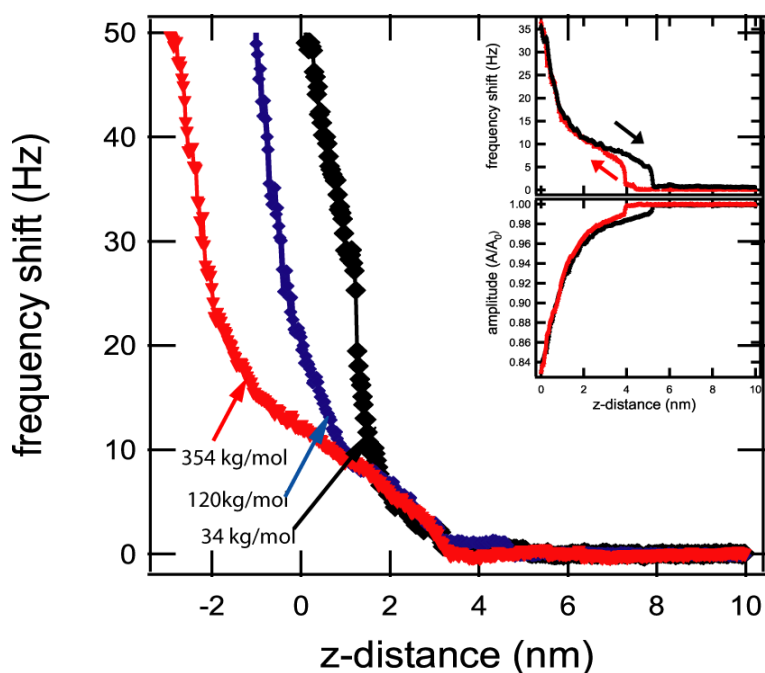


Figure 21: Detuning versus distance plots of the torsional oscillation acquired in CE-mode on PS homopolymers with $M_w = 34.3$ kg/mol (black), 119.6 kg/mol (blue), and 354.0 kg/mol (red). The inset shows a typical displacement curve on PS (119.6 kg/mol) with frequency shift and amplitude of the lateral oscillation as a function of z-actuator displacement. Approach (red) and retract (black) are also indicated by the arrows.

4.5. Acoustical force nanolithography of thin polymer films⁷

In this work, we discuss ‘acoustic force lithography’, a surface machining method based on the AFM. Nanomachining of thin polymer films with an atomic force microscope (AFM) is a promising route for the fabrication of nanoscale devices. In order to enhance the controllability of the nanomachining process an in-plane acoustic wave is coupled to the sample support. Thus, in this experiment the sample is excited to a lateral vibration while the tip remains fixed. This technique enhances the force exerted by the AFM tip. A precise control can be achieved by tuning the excitation frequency and amplitude of the excitation acoustic wave. The feasibility of the method along with the characterization of the main parameters was illustrated by lithography of a thin resist film.

⁷ Rubio-Sierra, FJ; Yurtsever, A; Hennemeyer, M, et al., *PHYSICA STATUS SOLIDI A*, 203, 1481 (2006)

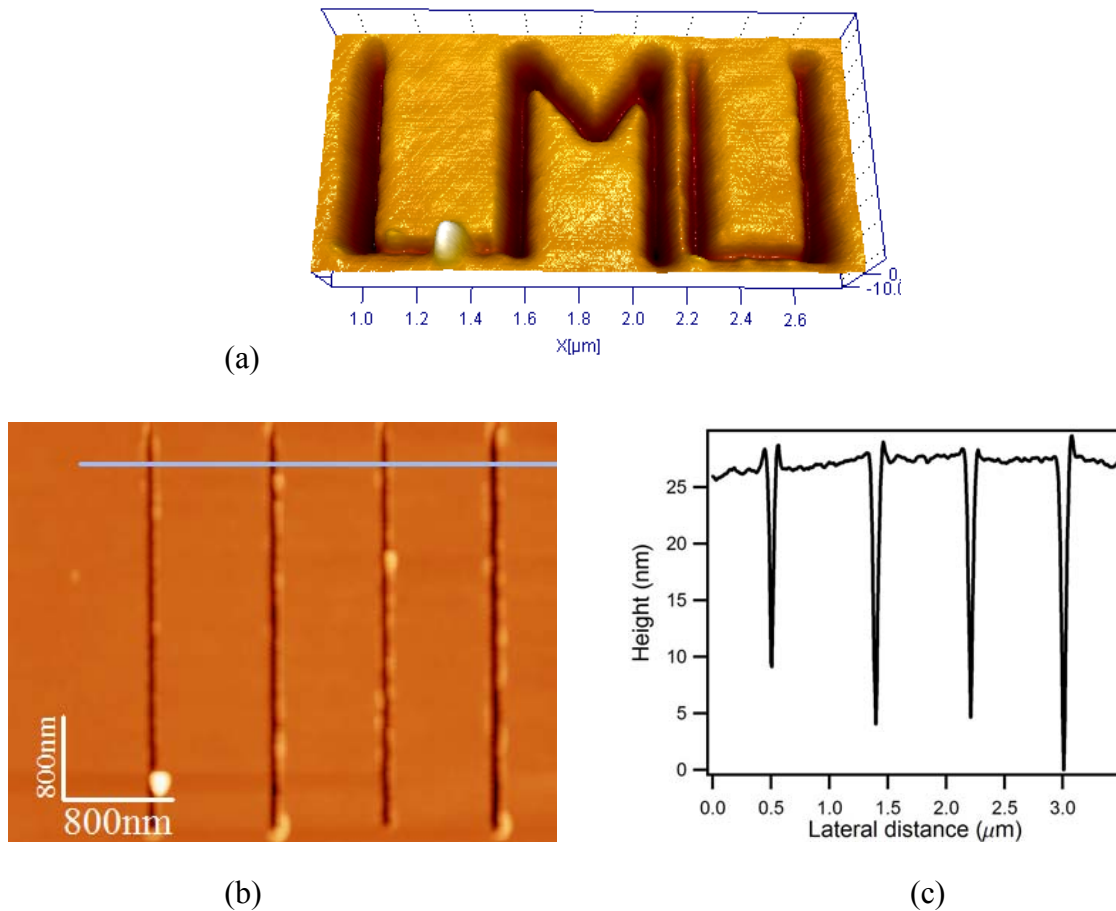


Figure 22: Nanostructures generated by acoustical force nanolithography: (a) lithographed emblem of the Ludwig-Maximilians-Universität. (b) AFM image of four 4 μm long lines lithographed using a signal amplitude of 0.5 V at a frequency of 740 kHz for acoustic wave generation, with an average tip-sample distance of 12.7 nm. Image size (4x4 μm) and z range of 55.6 nm. (c) Line profile along the line in panel b.

Due to the reduced physical dimensions of the AFM tip and precise positioning and force control provided by acoustic force nanolithography, lateral dimensions of the lithographed traces are reduced even beyond light diffraction limit. Here, the influences of the main parameters are studied in detail in acoustic force nanolithography. Figure 22 shows two lithographed structures demonstrating the feasibility of the method for the generation of nanostructures. Fig. 22 (a) shows the lithographed emblem of the Ludwig-Maximilians-Universität. Fig. 22 (b) and (c) show the AFM image and height profile of four lithographed lines with a length of 4 μm . The average line width at FWHM was 50 nm. The parameters were chosen to reach a line depth greater than 20 nm. Using an in-plane acoustic wave coupled to the sample surface decreases the debris on the pattern of the lithographed structures.

4.6. Torsion mode atomic force microscopy and image processing for the analysis of protein-DNA complex binding site⁸

In order to demonstrate the ability of the TR-mode AFM for imaging very soft materials, we imaged DNA as well as a DNA-protein complex in ambient air. Precise mapping of protein-binding sites on DNA is an important application of the atomic force microscope in nanobiotechnology. Here, we used TR-mode AFM as a complementary tool to the classical biochemical techniques for identifying DNA-protein interaction sites on DNA fragments of about 1254 base length. As a test sample (see Figure 23), complexes of the LexA repressor protein from the *Escherichia coli* SOS system and DNA fragments containing a specific LexA binding site (*recA* operator) were imaged by torsional resonance mode (TR-mode).



Figure 23: The model of the DNA-protein interaction. The protein-DNA complexes were formed between LexA protein and DNA fragments containing a specific LexA binding site, which is a 20 bp sequence within the *recA* gene regulatory region (200bp).

For a reliable measurement of distances on curved molecules, an adequate image analysis is required which extracts the DNA contour from the topographic AFM data. Here, we developed an image processing tool to determine the DNA length together with the protein binding position. This algorithm enables an efficient mapping of single or multiple protein-binding sites on DNA. The algorithm was designed to determine the axial line of DNA molecules together with the height profile along this line. These profiles were then used to detect the position of bound proteins. Protein recognition of specific DNA sequences can involve changes in the local structure and conformation of the binding partners, including curvature [77], bending, and flexing of DNA at the protein binding site [78]. The image processing algorithm can calculate a DNA bending angle from the DNA line axis by fitting a straight line before and after the protein location. The measured angle was approximately 74° as shown in Fig. 24 (a). Any protein bound to DNA is easily detected by a height peak at this profile (Fig. 24 (b)). The total length of the molecule and the position of the protein have to be determined manually using the placement of graphic cursors at the profile.

⁸ *Submitted (2008)*

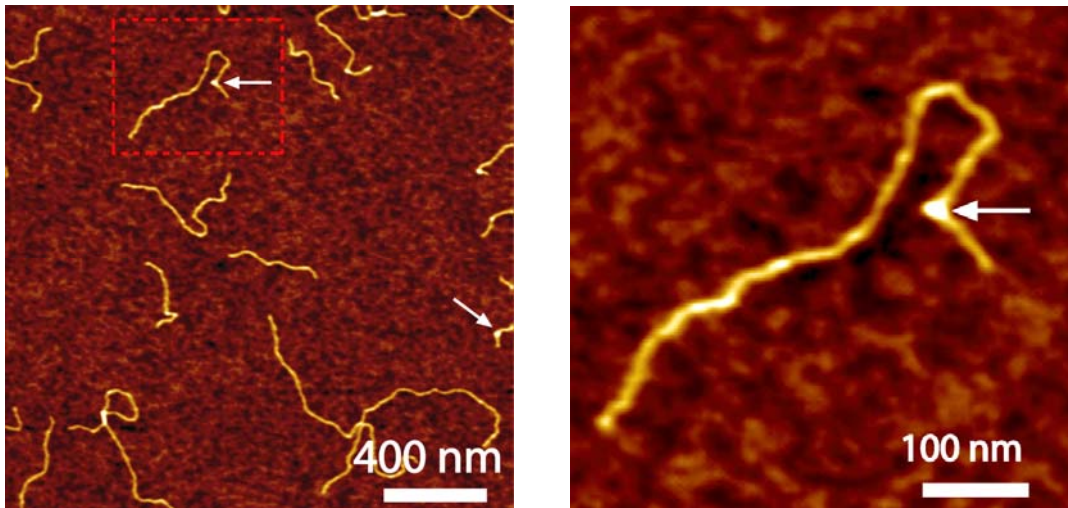


Figure 24: Topographic images of protein-DNA complexes obtained by TR-mode (Full scale: 1.2 nm). (a) Overview. (b) The arrow indicates a LexA protein dimer bound to DNA. The cross represents the initial custom chosen location which defines the molecule of interest

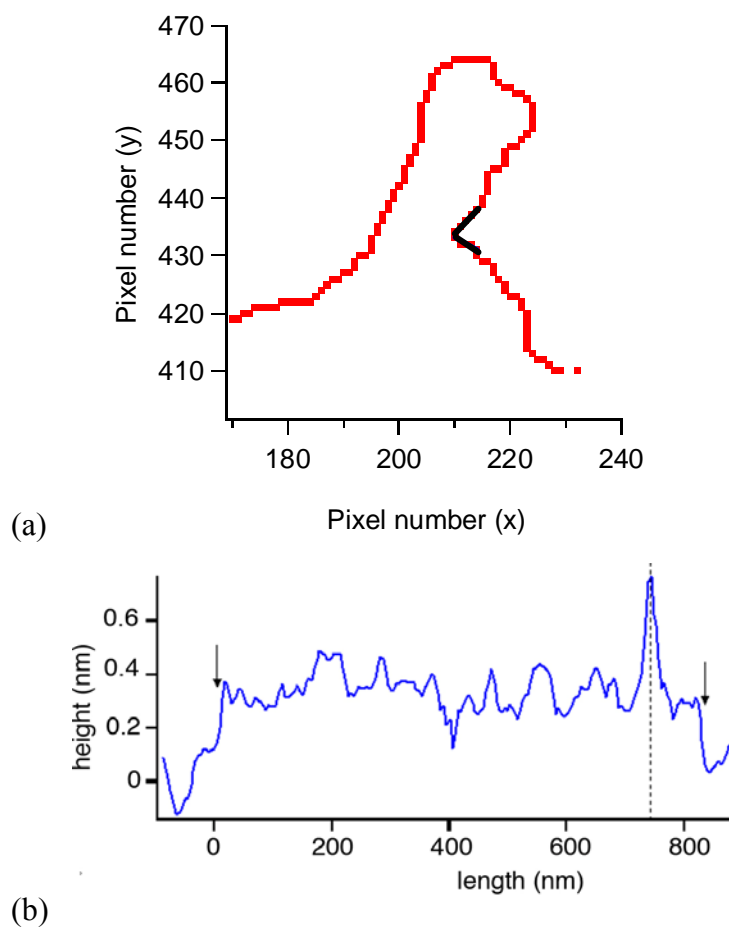


Figure 25: Analysis of the DNA in Fig. 24 (b) (a) The bending angle at the protein binding site is calculated by fitting a line at the protein location (74°). (b) Height profile along the axis. The arrow delimits the molecule and the dashed line defines the protein at 721 nm.

For the molecule shown in Fig. 24, the total length was 812 nm and the protein binding site is located at 93 nm from the nearest end. Although, the relation between operating conditions and measured topographic height of DNA remains to be clarified we have proven that the contrast makes shear force imaging a valuable tool for protein-DNA complex studies

4.7. Amplitude modulation torsional resonance mode AFM (TR-mode) on Graphite

In order to evaluate the capabilities of an amplitude modulation feedback in torsional resonance mode AFM (TR-mode) for surface topography imaging and to determine the sensitivity of phase measurements, we used freshly cleaved highly oriented pyrolytic graphite (HOPG) surfaces [79-82]. In Fig. 26, the images of topography (a) and TR phase (b) on a HOPG surface are shown. The HOPG terrace and step structures can be resolved clearly in the height and phase images. Due to environmental humidity, a water layer can condense on material surfaces. Atomic step edges are generally covered by contaminants or the adsorbed water layer [79, 83-85]. In the shear force experiment, the damping forces involved in tip-sample interaction are strongly depending of the surface and the probe wetting properties [83]. When an AFM probe is approached close to the sample surface, capillary condensation can occur and a liquid neck can be formed between tip and surface. The strong decrease in the lateral oscillation amplitude of the cantilever indicates the effects of this thin water layer. Confinement of the water layer between an AFM tip and the substrate reveals a solid-like behaviour. Thus, the high phase contrast in TR phase image may be attributed to the effect of the condensed water on the atomic steps. The additional damping due to the water meniscus may lead to a higher dissipation and a higher phase contrast in amplitude modulated torsional mode AFM. This result demonstrates that the torsional resonance amplitude can be used as a feedback signal to image the low energy HOPG surface in a stable manner and to investigate edge effects. Especially, for an edge-enhanced surface imaging, TR-mode AFM can be employed.

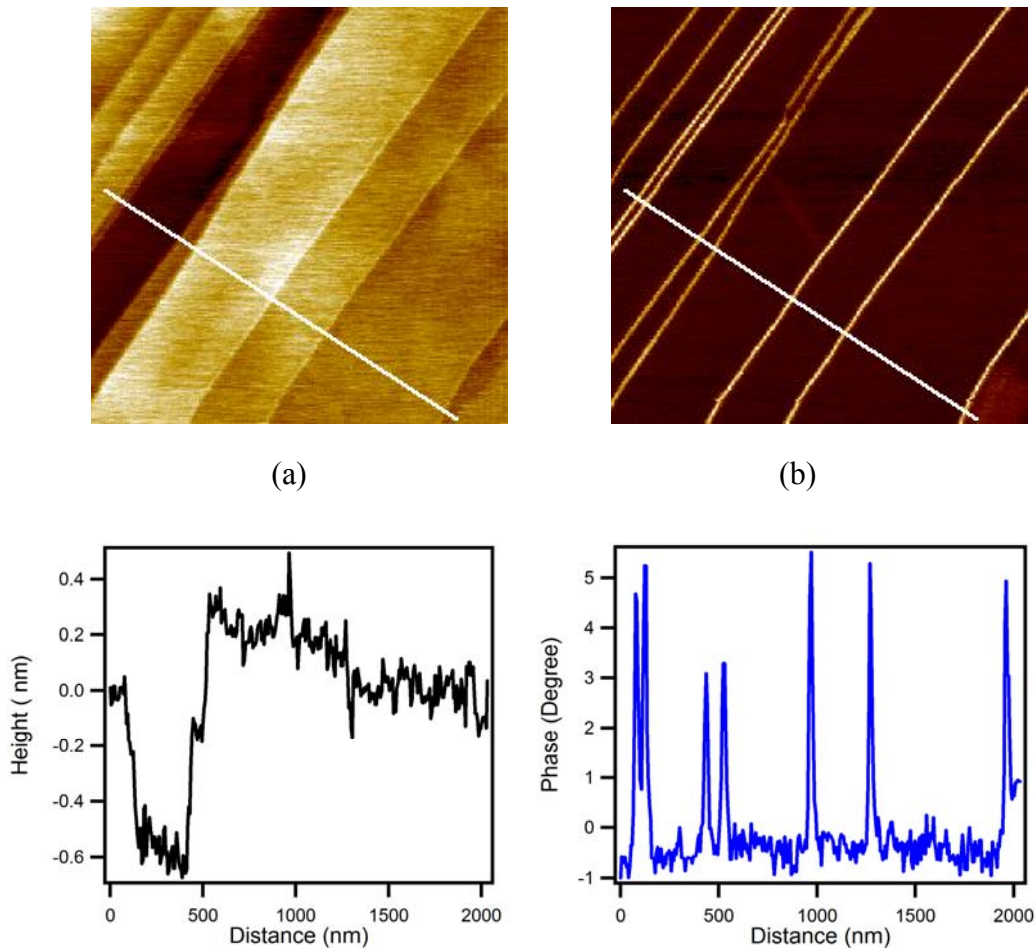


Figure 26: (a) TR mode height image of the freshly cleaved HOPG surface. (b) Phase image. The cross sections along the line drawn on images shown below the each image. The scan size is $2\mu\text{m}$ with a scan rate of 0.6 Hz.

5. Conclusions and Future Work

The torsional eigenmodes of atomic force microscope (AFM) cantilevers are highly sensitive to the in-plane material properties of the sample. Frequency modulation feedback in torsional resonance mode AFM has significantly enhanced the experimental capabilities to probe the in-plane mechanical properties. With this method, information on lateral chemical heterogeneities (e.g. different mechanical properties) and visco-elastic dynamics, which result in different friction coefficients and the dissipative interaction, can be measured and recorded at the same time with sample topography.

In this thesis, the dynamics of a torsionally vibrated cantilever under a surface coupled visco-elastic interaction was investigated. The frequency response (i.e., vibration amplitude, frequency shift, and phase shift) of the system was calculated by employing a finite element numerical model (FEM). The model includes attractive forces (adhesion), repulsive forces (elasticity), and damping. The results of these calculations imply that the torsional vibration amplitude of the cantilever is coupled to the lateral bending mode due to the symmetry breaking of the cantilever-tip system. This coupling in the cantilever motion complicates the derivation of the analytical solution for the cantilever frequency response function. The amplitude of the torsional vibration decreases in a dissipative interaction due to damping of the system. However, the response of the amplitude shows an increase with the increase in tip-sample contact stiffness in a purely elastic medium. This result reveals a different behaviour as compared to a simple harmonic oscillator where the oscillation amplitude decreases with stiffness. Actually, the variation of the amplitude depends on the measurement location on the cantilever. Detecting the spectrum at the end of the cantilever edge as in an optical lever detection system, the amplitude increases due to the shift in torsional vibration axis (i.e. the slope of the cantilever increases). The amplitude enhancement of the torsional vibration can be utilized to map the surface elastic properties both in imaging and spectroscopic application.

To corroborate the numerical findings experimentally, we implement a frequency modulation feedback to the torsional resonance mode AFM. Hereafter, we call it frequency modulated torsional resonance mode AFM (FM-TR-AFM). This mode of operation allows for the measurement of the frequency shift due to conservative tip-sample interaction and energy dissipation (i.e. damping behaviour) due to the inelastic interaction, simultaneously. The frequency shift induced by the conservative tip-sample interaction was utilized as a feedback

parameter to control the tip-sample distance. To increase the signal to noise ratio and to decrease coupling between different modes in ambient, a specially designed cantilever holder was used to excite the cantilever in a pendulum like motion in ambient air with amplitudes in the order of 1 nm. At such small amplitudes the motion of the cantilever can be considered to be perfectly parallel to the sample surface. Therefore, the torsional mode AFM is particularly suitable for probing the surface lateral or in-plane mechanical properties such as friction, elasticity, and anisotropy under ambient condition. In order to elucidate the effects of the cantilever oscillation plane on the feedback mechanism of the frequency modulated torsional resonance mode AFM, approach and retract curves (i.e. displacement curves) were recorded on a highly oriented pyrolytic graphite surface (HOPG). By operating the system in constant excitation mode (CE-Mode), the correlation between the frequency shift (detuning) and tilt angle between the torsional oscillation plane and the specimen is investigated. Clearly, the tilt between the torsional oscillation plane and specimen leads to an additional negative detuning. This means that the analysis of the frequency shift and the dissipation images in (FM-TR-AFM) requires considering the effects of the surface slope or the alignment of the torsional vibration axis.

The results of the measurement on a compliant material such as diblock copolymer pointed out that the dissipation signal clearly resolves the different polymer phases due to their different mechanical properties. A freshly cleaved chlorite surface was investigated to examine the effects of the surface charge distribution on the dissipation process. The measurement of the energy dissipation revealed a slight contrast between the brucite-like and talc-like surfaces. These experimental results show that surfaces with different surface properties (i.e. friction, stiffness) can be discriminated in the dissipation signal while measuring the surface topography in ambient.

In summary, the frequency modulated torsional resonance mode AFM is a powerful technique to investigate in-plane conservative and non-conservative interaction forces simultaneously. To improve imaging capabilities further, the bandwidth of the frequency detection system needs to be extended above 1 MHz. To increase the sensitivity in spectroscopic applications, specially designed AFM cantilevers such as torsional harmonic cantilever (THC) [86] or special excitation mechanism should be used. Combining the FM-TR-AFM with a Kelvin probe microscopy (KPM), could provide a tool to characterize the surface in both ways mechanically and electrostatically. Such a combined measurement of surface potential and friction would allow us to characterize the surface chemistry of functionalized surfaces.

References

- [1] G. Meyer, and N. M. Amer, *Applied Physics Letters* **57**, 2089 (1990).
- [2] L. Howald *et al.*, *Applied Physics Letters* **63**, 117 (1993).
- [3] O. Marti, J. Colchero, and J. Mlynek *Nanotechnology* **1**, 141 (1990).
- [4] G. Neubauer *et al.*, *Review of Scientific Instruments* **61**, 2296 (1990).
- [5] D. Rugar, H. J. Mamin, and P. Guethner, *Applied Physics Letters* **55**, 2588 (1989).
- [6] C. M. Mate *et al.*, *Physical Review Letters* **59**, 1942 (1987).
- [7] B. Bhushan, H. Fuchs, and S. Hosaka, *Book, Applied Scanning Probe Methods*, 75 (2002).
- [8] B. V. Derjaguin, V. M. Muller, and Y. P. Toporov, *Journal of Colloid and Interface Science* **53**, 314 (1975).
- [9] K. L. Johnson, K. Kendall, and A. D. Roberts, *Proceedings of the Royal Society of London Series a-Mathematical and Physical Sciences* **324**, 301 (1971).
- [10] D. Maugis, *Journal of Colloid and Interface Science* **150**, 243 (1992).
- [11] S. P. Jarvis *et al.*, *Review of Scientific Instruments* **64**, 3515 (1993).
- [12] R. W. Carpick, D. F. Ogletree, and M. Salmeron, *Applied Physics Letters* **70**, 1548 (1997).
- [13] M. A. Lantz *et al.*, *Applied Physics Letters* **70**, 970 (1997).
- [14] Y. Pu *et al.*, *Langmuir* **17**, 5865 (2001).
- [15] K. B. Crozier *et al.*, *Applied Physics Letters* **76**, 1950 (2000).
- [16] J. Colchero, M. Luna, and A. M. Baro, *Applied Physics Letters* **68**, 2896 (1996).
- [17] R. M. Overney. *et al.*, *Nature* **359**, 133 (1992).
- [18] M. S. Marcus *et al.*, *Physical Review Letters* **88** (2002).
- [19] M. S. Marcus *et al.*, *Ultramicroscopy* **97**, 145 (2003).
- [20] O. Pfeiffer *et al.*, *Physical Review B* **65** (2002).
- [21] G. Binnig, C. F. Quate, and C. Gerber, *Physical Review Letters* **56**, 930 (1986).
- [22] S. A. C. Gould *et al.*, *Journal of Vacuum Science & Technology a-Vacuum Surfaces and Films* **8**, 369 (1990).
- [23] N. Oyabu *et al.*, *Physical Review Letters* **90** (2003).
- [24] D. Fotiadis *et al.*, *Micron* **33**, 385 (2002).
- [25] S. Amelio *et al.*, *Thin Solid Films* **392**, 75 (2001).
- [26] R. Garcia, R. Magerle, and R. Perez, *Nature Materials* **6**, 405 (2007).
- [27] C. D. Mao *et al.*, *Nature* **397**, 144 (1999).
- [28] T. R. Albrecht *et al.*, *Journal of Vacuum Science & Technology a-Vacuum Surfaces and Films* **8**, 3386 (1990).
- [29] G. Meyer, and N. M. Amer, *Applied Physics Letters* **53**, 1045 (1988).
- [30] S. Alexander *et al.*, *Journal of Applied Physics* **65**, 164 (1989).
- [31] T. R. Albrecht, and C. F. Quate, *Journal of Vacuum Science & Technology a-Vacuum Surfaces and Films* **6**, 271 (1988).
- [32] Y. Martin, C. C. Williams, and H. K. Wickramasinghe, *Journal of Applied Physics* **61**, 4723 (1987).
- [33] R. Erlandsson *et al.*, *Journal of Vacuum Science & Technology a-Vacuum Surfaces and Films* **6**, 266 (1988).
- [34] G. V. Dedkov, *Physica Status Solidi a-Applied Research* **179**, 3 (2000).
- [35] M. Radmacher, M. Fritz, and P. K. Hansma, *Biophysical Journal* **69**, 264 (1995).
- [36] P. K. Hansma *et al.*, *Applied Physics Letters* **64**, 1738 (1994).
- [37] F. J. Giessibl, *Science* **267**, 68 (1995).
- [38] T. R. Albrecht *et al.*, in *Journal of Applied Physics* (1991), pp. 668.
- [39] F. J. Giessibl, and C. F. Quate, *Physics Today* **59**, 44 (2006).

- [40] Y. Sugimoto *et al.*, *Nature Materials* **4**, 156 (2005).
- [41] H. J. Butt, B. Cappella, and M. Kappl, *Surface Science Reports* **59**, 1 (2005).
- [42] R. Garcia, and R. Perez, *Surface Science Reports* **47**, 197 (2002).
- [43] R. J. Colton, *Journal of Vacuum Science & Technology B* **22**, 1609 (2004).
- [44] U. D. Schwarz, *Journal of Colloid and Interface Science* **261**, 99 (2003).
- [45] S. Kitamura, and M. Iwatsuki, *Japanese Journal of Applied Physics Part 2-Letters* **34**, L145 (1995).
- [46] H. Ueyama, Y. Sugawara, and S. Morita, *Applied Physics a-Materials Science & Processing* **66**, S295 (1998).
- [47] Y. Sugawara *et al.*, *Science* **270**, 1646 (1995).
- [48] U. Durig, O. Zuger, and A. Stalder, *Journal of Applied Physics* **72**, 1778 (1992).
- [49] C. Barth *et al.*, *Nanotechnology* **17**, S128 (2006).
- [50] F. J. Giessibl, *Reviews of Modern Physics* **75**, 949 (2003).
- [51] A. A. Farrell *et al.*, *Physical Review B* **72** (2005).
- [52] S. Grafstrom *et al.*, *Nanotechnology* **4**, 143 (1993).
- [53] C. Ascoli *et al.*, *Journal of Vacuum Science & Technology B* **12**, 1642 (1994).
- [54] V. Scherer, W. Arnold, and B. Bhushan, *Surface and Interface Analysis* **27**, 578 (1999).
- [55] P. Maivald, H J Butt, S A C Gould, C B Prater, B Drake, J A Guriey, V B Eiings and P K Hansma, *Nanotechnology* **2**, 103 (1991).
- [56] M. Reinstaedtler *et al.*, *Surface Science* **532**, 1152 (2003).
- [57] H. U. Krottil, T. Stifter, and O. Marti, *Applied Physics Letters* **77**, 3857 (2000).
- [58] M. Reinstadtler *et al.*, *Applied Physics Letters* **82**, 2604 (2003).
- [59] M. J. D'Amato *et al.*, *Applied Physics Letters* **85**, 4738 (2004).
- [60] T. Drobek, R. W. Stark, and W. M. Heckl, *Physical Review B* **6404** (2001).
- [61] A. Caron *et al.*, *Applied Physics Letters* **85**, 6398 (2004).
- [62] S. P. Jarvis *et al.*, *Applied Surface Science* **157**, 314 (2000).
- [63] M. F. Crommie, C. P. Lutz, and D. M. Eigler, *Science* **262**, 218 (1993).
- [64] K. Karrai, and R. D. Grober, *Applied Physics Letters* **66**, 1842 (1995).
- [65] K. Karrai, and I. Tiemann, *Physical Review B* **62**, 13174 (2000).
- [66] H. Gottlich *et al.*, *Review of Scientific Instruments* **71**, 3104 (2000).
- [67] L. Huang, and C. M. Su, *Ultramicroscopy* **100**, 277 (2004).
- [68] Y. X. Song, and B. Bhushan, *Journal of Applied Physics* **99** (2006).
- [69] T. Drobek *et al.*, *NEW JOURNAL OF PHYSICS* **1**, 15.1 (1999).
- [70] B. Gotsmann *et al.*, *Physical Review B* **60**, 11051 (1999).
- [71] M. Reinstadtler *et al.*, *Journal of Physics D-Applied Physics* **38**, R269 (2005).
- [72] J. E. Sader, J. W. M. Chon, and P. Mulvaney, *Review of Scientific Instruments* **70**, 3967 (1999).
- [73] M. Nonnenmacher, M. P. Oboyle, and H. K. Wickramasinghe, *Applied Physics Letters* **58**, 2921 (1991).
- [74] F. S. Bates, *Science* **251**, 898 (1991).
- [75] F. S. Bates, and G. H. Fredrickson, *Annual Review of Physical Chemistry* **41**, 525 (1990).
- [76] F. Dubourg *et al.*, *European Physical Journal E* **6**, 387 (2001).
- [77] J. A. H. Cognet *et al.*, *Journal of Molecular Biology* **285**, 997 (1999).
- [78] M. A. Dyer *et al.*
- [79] S. Davy, M. Spajer, and D. Courjon, *Applied Physics Letters* **73**, 2594 (1998).
- [80] R. Brunner, O. Marti, and O. Hollricher, *Journal of Applied Physics* **86**, 7100 (1999).
- [81] P. J. James *et al.*, *Langmuir* **17**, 349 (2001).
- [82] A. Spychalski-Merle *et al.*, *Applied Physics Letters* **77**, 501 (2000).
- [83] L. Vaccaro *et al.*, *Applied Physics Letters* **77**, 3110 (2000).

- [84] L. Vaccaro *et al.*, *Journal of Microscopy-Oxford* **202**, 439 (2001).
- [85] M. Antognozzi, A. D. L. Humphris, and M. J. Miles, *Applied Physics Letters* **78**, 300 (2001).
- [86] O. Sahin *et al.*, *Nature Nanotechnology* **2**, 507 (2007).

Appendix

1. Manuscripts

Response of a laterally vibrating nanotip to surface forces

Applied Physics Letters (APL), 91, 253120 (2007)

Ayhan Yurtsever, Alexander M. Gigler, Eduardo Macias, and Robert W. Stark

Response of a laterally vibrating nanotip to surface forces

Ayhan Yurtsever, Alexander M. Gigler, Eduardo Macias, and Robert W. Stark^{a)}
 Center for NanoScience (CeNS) and Department of Earth and Environmental Sciences,
 Ludwig-Maximilians-Universität München, Theresienstrasse 41, 80333 Munich, Germany

(Received 28 August 2007; accepted 29 November 2007; published online 20 December 2007)

The torsional eigenmodes of atomic force microscope (AFM) cantilevers are highly sensitive toward in-plane material properties of the sample. We studied the effect of viscosity and lateral contact stiffness on the detuning, amplitude, and phase response numerically. To verify the theoretical considerations, a torsion mode AFM was operated in frequency modulation. During approach and retract cycles, we observed a negative detuning of the torsional resonant frequency close to the sample surface depending on the tilt angle between the tip and the sample. Thus, the tilt has a significant effect on the imaging process in torsional resonance mode. © 2007 American Institute of Physics. [DOI: 10.1063/1.2826285]

The tribological characterization of nanomaterials requires friction measurements with very high sensitivity and resolution as can be provided by an atomic force microscope (AFM). To this end, scanning shear force microscopy¹ is a very valuable tool. Several shear force microscopes for measurements with AFM cantilevers but different excitation mechanisms have been reported such as overtone microscopy,² combined dynamic mode,³ ultrasonic torsional contact resonance spectroscopy,⁴ or torsional resonance mode using amplitude modulation.⁵ The common idea is to measure changes in the response of the torsional cantilever resonance. In torsional resonance mode, a split piezoactuator drives the cantilever at its torsional resonance, typically in the range of 1–2 MHz. This technical approach greatly facilitates shear force microscopy with standard cantilevers. However, coupling of torsional and flexural modes complicates an analytic treatment of torsional cantilever vibrations. Thus, finite element analysis is advantageous for the investigation of the system dynamics. A three dimensional simulation of the torsional resonances clearly showed that flexural bending and torsional oscillations are coupled due to tip-sample interaction.⁶

In the following, we investigate the frequency response of the torsionally vibrating AFM cantilever in order to clarify the role of the tilt between specimen and plane of oscillation. Understanding the influence of the tip-sample interaction on frequency response is essential for a quantitative interpretation of data obtained in torsional resonance mode. The calculations are corroborated by an experiment under ambient conditions, demonstrating the influence of the tilt angle.

For a vertically oscillating tip, the attractive surface potential and viscoelastic sample properties determine the interaction forces. van der Waals forces dominate the interaction in the attractive regime ($\delta < 0$). In the repulsive regime ($\delta \geq 0$), forces can be calculated using a Derjaguin-Muller-Toporov model.⁷ Thus, the vertical tip-sample forces are given by

$$F_{\perp}(\delta) = \begin{cases} -HR/[6(\delta - a_0)^2], & \delta < 0 \\ -HR/(6a_0^2) + \frac{4}{3}E^*\sqrt{R}\delta^{3/2}, & \delta \geq 0. \end{cases} \quad (1)$$

Parameter H is the Hamaker constant, R is the tip radius, δ is the indentation depth into the sample, and a_0 is a typical interatomic distance. Distance parameters are defined in Fig. 1(a). The elastic modulus of the tip-sample contact is given by

$$E^* = [(1 - \nu_t^2)/E_t + (1 - \nu_s^2)/E_s]^{-1}, \quad (2)$$

where E_t and E_s are the elastic moduli and ν_t and ν_s are the Poisson ratios of tip and sample, respectively. Linearization

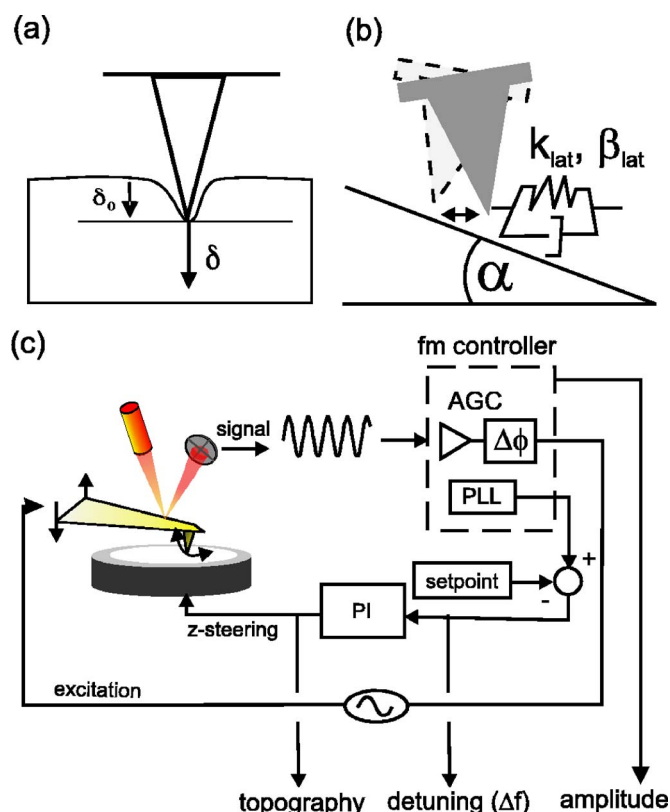


FIG. 1. (Color online) (a) Parameters used to describe the indentation. (b) A laterally vibrating tip interacting with a tilted specimen. (c) Experimental setup of a frequency modulation torsion mode AFM.

^{a)} Author to whom correspondence should be addressed. Electronic mail: stark@lrz.uni-muenchen.de. Tel./FAX: +49 89 2180-4329/-4334.

for very small vertical oscillations at a given indentation δ_0 leads to the effective tip-sample stiffness

$$k_{\perp} = - \left. \frac{\partial F_{\perp}}{\partial \delta} \right|_{\delta=\delta_0} = \begin{cases} -HR/[3(\delta_0 - a_0)^3], & \delta_0 < 0 \\ 2E^* \sqrt{R\delta_0}, & \delta_0 \geq 0. \end{cases} \quad (3)$$

For the lateral force, we assume no interaction before contact ($\delta < 0$). Within the repulsive regime, we use an elastic interaction as derived from the Hertz model.⁸ Thus, we obtain

$$k_{\parallel} = \begin{cases} 0, & \delta_0 < 0 \\ 8G^* \sqrt{R\delta_0}, & \delta_0 \geq 0 \end{cases} \quad (4)$$

for the linearized in-plane stiffness. The shear stiffness is $G^* = [(2 - \nu_t^2)/G_t + (2 - \nu_s^2)/G_s]^{-1}$, where G_t and G_s are the shear moduli and ν_{\parallel} denotes an in-plane velocity due to lateral oscillations. We assume that the lateral viscous damping force is dependent on the strain rate and the damping coefficient β in the dissipation process ($F = \beta \dot{\delta}$). In the model, we have neglected friction in the noncontact regime which, for example, can be caused by a liquid neck due to capillary condensation.

If the lateral oscillations occur with respect to a tilted specimen, the in-plane and out-of plane components both contribute to the interaction, as illustrated in Fig. 1(b)

$$k_{\text{lat}} = k_{\parallel} \cos(\alpha) + k_{\perp} \sin(\alpha),$$

$$k_{\text{norm}} = k_{\parallel} \sin(\alpha) + k_{\perp} \cos(\alpha). \quad (5)$$

For small angles α , the effective lateral force is given by

$$k_{\text{lat}} = k_{\parallel} + \alpha k_{\perp}. \quad (6)$$

Notably, an attractive elastic interaction may be introduced to the in-plane component, whereas a dissipative component is added to the normal component due to interfacial friction. Additionally, the elastic contact stiffens. In other words, increasing the tilt angle leads to a transition from a purely frictional (rubbing the surface) to a vibroimpact (tapping and sliding on the surface) regime.

In order to evaluate the response of the cantilever to in-plane surface properties, a finite element (FE) model of a typical cantilever was implemented in COMSOL 3.2/FEMLAB 3.2 (FEMLAB GmbH, Göttingen, Germany), as illustrated in Fig. 2(a). Tetrahedral mesh elements and the following geometry parameters were used: length $L=250 \mu\text{m}$, width $b=40 \mu\text{m}$, thickness $t=3 \mu\text{m}$, Young's modulus $E_t=169 \text{ GPa}$, Poisson's ratio $\nu_t=0.28$, and density $\rho=2330 \text{ kg/m}^3$. A rectangular cross section of the beam was assumed. The beam ends in a triangle, which resembles the actual shape of such a cantilever. The conical tip was located at $L=220 \mu\text{m}$ (cone base diameter $d=12 \mu\text{m}$, height $h=15 \mu\text{m}$, semiangle $\alpha=21.8^\circ$). Mesh refinement was performed in order to check the convergence of the modal solution. Interaction related parameters of the silicon tip and the graphite sample were $H=2.96 \times 10^{-19} \text{ J}$, $G^*=4.2 \text{ GPa}$, $E^*=10.2 \text{ GPa}$, $\beta=8 \times 10^{-7} \text{ N s/m}$, and $a_0=0.38 \text{ nm}$. The boundary conditions were set according to a clamped end at the cantilever chip. At the tip end, the mechanical coupling is described by a Kelvin-Voigt model assuming a Hookian spring in parallel with a Newtonian dash pot. Since the response to vertical force gradients k_{norm} has been discussed on the basis of numerical and analytic models,⁹ we only investigate the effect

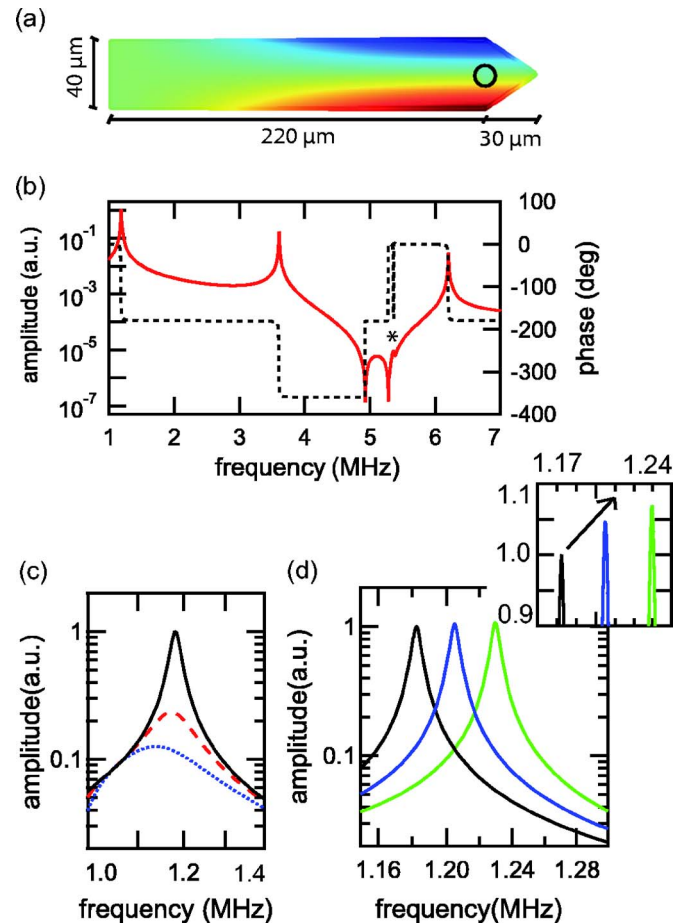


FIG. 2. (Color online) (a) Geometry of the cantilever as used for the finite element analysis. The colors show the shape of the first torsional eigenmode. The circle indicates the base of the conical tip. (b) Torsional frequency response of the freely vibrating cantilever as obtained by finite element analysis. Amplitude response (red, solid) and phase response (black, dash). The asterisk indicates the lateral bending resonance. (c) Amplitude change due to increasing damping: $\beta=8 \times 10^{-7}$, 4×10^{-6} , and $8 \times 10^{-6} \text{ N s/m}$. (d) Frequency shift caused by elastic interaction (tip-sample stiffness: $k=0$, 13, and 26 N/m). The inset illustrates amplitude increase on a linear scale.

of a lateral stiffness k_{lat} on the characteristics of the torsional oscillator.

The driving force was simulated as a distributed load at the long cantilever edge in the FE model, because, experimentally, a split piezoactuator at the cantilever holder was used to excite the torsional vibration [Fig. 1(c)]. Dynamic frequency response analyses were carried out between 1 and 7 MHz. To account for intrinsic damping, Rayleigh damping was included, assuming a mass-proportional and stiffness-proportional viscous damping.

Figure 2(b) shows the calculated frequency response of the amplitude of a freely oscillating AFM cantilever. For small oscillation amplitudes, the amplitude is proportional to the twist angle. The phase shift remains in the range between 0° and 360° . A lateral bending mode can also be excited (asterisk). Furthermore, we calculated antiresonances at 4.92 and 5.28 MHz. Figure 2(c) shows the amplitude response of the first torsional eigenmode under purely dissipative interaction. The oscillation amplitude decreases with increasing damping parameter β . Figure 2(d) shows the results of the calculation of the amplitude response of the first torsional eigenmode for different contact stiffnesses k_{lat} . With increasing tip-sample stiffness, the resonant frequency increases but

the transmission minima stay at the same frequency. Additionally, the torsion angle increase is leading to an increased amplitude measured by the light lever [inset in Fig. 2(d)]. For resonance detuning on the order of 50 kHz, the increase in amplitude is about 0.15 % / kHz. This effect is different from a harmonic oscillator where the oscillation amplitude decreases for an increased stiffness. The change in amplitude can be neglected for imaging purposes but becomes relevant in torsional spectroscopy applications, where a detuning on the order of several kilohertz can occur. The physical reason for this amplitude increase is the shift of the torsion axis due to tip-surface coupling. In the case of the free cantilever, the axis of torsion is close to the cantilever main axis. By increasing the tip-sample stiffness to higher values, the tip of the cantilever is increasingly pinned to the sample surface and the torsional axis intersects close to the pinpoint. Thus, torsion angle, as measured by the light lever, can increase (depending of the actual laser beam adjustment). Additionally, tip mass and tip-sample interactions break the twofold rotational symmetry of the cantilever beam. Such a reduced symmetry leads to coupling between closely spaced torsional and bending modes.¹⁰ Thus, geometric effects together with mode coupling can help explain the experimental observation that with increasing load onto the specimen, the power stored in a torsional resonance eigenmode due to thermomechanical excitation apparently decreases while the measured oscillation amplitude increases.¹¹

In order to verify the role of sample tilt on the frequency response experimentally, we used a combination of the Dimension 3100 setup with a NanoScope IV controller (Veeco Metrology Inc., Santa Barbara, CA) equipped with torsional resonance mode adapter and probe holder together with a phase-locked-loop Nanosurf Easy PLL (Nanosurf, Liestal, Switzerland/Schaefer Technologie GmbH, Langen, Germany) [Fig. 1(c)]. Silicon cantilevers (ZEHR, Nanosensors, Neuchâtel, Switzerland) with a typical flexural resonance frequency of 117 kHz and a nominal spring constant of 27 N/m were used for the frequency modulated torsional resonance mode AFM (FM-TR-AFM) measurements. The torsional resonance frequency was 910 kHz. The cantilever was driven using the constant excitation mode where the response time is Q limited. A goniometer (GN05/M, Thorlabs GmbH, Dachau, Germany) was used to change the angle between tip and sample.

Figure 3 shows a typical distance curve of torsional resonant frequency shift versus the z piezotravel on highly oriented pyrolytic graphite. Adjustment of the tilt angle of the sample surface to zero with respect to the cantilever oscillation (i.e., oscillation and the surface are parallel), reveals that long-range interaction forces have little effect on the torsional vibration. However, if the plane of oscillation and the surface are tilted with respect to each other, this angle leads to a mixing of in-plane sample properties with the out-of-plane interaction. In this case, van der Waals forces induce a negative frequency shift of the torsional resonance. This suggests that the negative detuning of the torsional resonance, as also observed by others,¹² is due to a slight tilt between the plane of oscillation and the local specimen surface.

The numerical results together with the experiments help explain the fundamental mechanisms of z feedback in frequency modulated torsional resonance mode AFM (Ref. 13) (FM-TR-AFM). The topography feedback regulates the AFM depending on the detuning of the resonant oscillation.

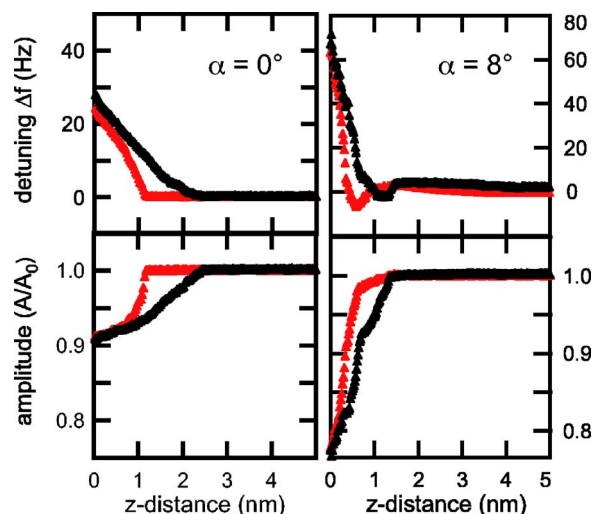


FIG. 3. (Color online) Amplitude and frequency shift measured during an approach (red) and retract (black) cycle on an untilted ($\alpha=0^\circ$) and a tilted ($\alpha=8^\circ$) graphite sample. Note that a negative frequency shift occurs due to attractive forces on the tilted specimen. In the repulsive regime, the detuning response is steeper on the tilted specimen. Free torsional resonant frequency, the quality factor, and the amplitude were 900 kHz, 1300, and 405 mV, respectively.

If tip and sample are properly aligned, positive detuning occurs due to elastic coupling between the tip and sample. This detuning is accompanied by an amplitude reduction due to energy dissipation through the frictional contact. If specimen and oscillator are tilted, additional repulsive as well as attractive forces may occur due to mixing of in-plane and out-of-plane properties.

We gratefully acknowledge financial support by the German Federal Ministry of Education and Research, grant Nanofutur 03N8706. A.Y. is supported by the Scholarship of the Elite Network of Bavaria, International Doctorate Program Nano-Bio-Technology (IDK-NBT).

¹K. Karrai and R. D. Grober, *Appl. Phys. Lett.* **66**, 1842 (1995); K. Karrai and I. Tiemann, *Phys. Rev. B* **62**, 13174 (2000); H. Göttlich, R. W. Stark, J. D. Pedarnig, and W. M. Heckl, *Rev. Sci. Instrum.* **71**, 3104 (2000); A. D. L. Humphris, M. Antognozzi, T. J. McMaster, and M. J. Miles, *Langmuir* **18**, 1729 (2002).

²T. Drobek, R. W. Stark, M. Gräber, and W. M. Heckl, *New J. Phys.* **1**, 15 (1999).

³H. U. Krottil, T. Stifter, and O. Marti, *Appl. Phys. Lett.* **77**, 3857 (2000).

⁴M. Reinstädler, U. Rabe, V. Scherer, U. Hartmann, A. Goldade, B. Bhushan, and W. Arnold, *Appl. Phys. Lett.* **82**, 2604 (2003).

⁵L. Huang and C. M. Su, *Ultramicroscopy* **100**, 277 (2004); M. Reinstädler, T. Kasai, U. Rabe, B. Bhushan, and W. Arnold, *J. Phys. D* **38**, R269 (2005).

⁶Y. X. Song and B. Bhushan, *Ultramicroscopy* **106**, 847 (2006).

⁷B. V. Derjaguin, V. M. Muller, and Yu. P. Toporov, *J. Colloid Interface Sci.* **53**, 314 (1975).

⁸R. W. Carpick, D. F. Ogletree, and M. Salmeron, *Appl. Phys. Lett.* **70**, 1548 (1997).

⁹U. Rabe, K. Janser, and W. Arnold, *Rev. Sci. Instrum.* **67**, 3281 (1996); R. Vázquez, F. J. Rubio-Sierra, and R. W. Stark, *Nanotechnology* **18**, 185504 (2007).

¹⁰M. Reinstädler, U. Rabe, V. Scherer, J. A. Turner, and W. Arnold, *Surf. Sci.* **532-535**, 1152 (2003); L. B. Sharos, A. Raman, S. Crittenden, and R. Reifenberger, *Appl. Phys. Lett.* **84**, 4638 (2004).

¹¹S. Maier, Y. Sang, T. Filleter, M. Grant, R. Bennewitz, E. Gnecco, and E. Meyer, *Phys. Rev. B* **72**, 245418 (2005).

¹²O. Pfeiffer, R. Bennewitz, A. Baratoff, E. Meyer, and P. Grütter, *Phys. Rev. B* **65**, 161403 (2002); S. Kawai, S. Kitamura, D. Kobayashi, and H. Kawakatsu, *Appl. Phys. Lett.* **87**, 173105 (2005).

¹³A. Yurtsever, A. M. Gigler, and R. W. Stark, *J. Phys.: Conf. Ser.* (in press).

Frequency modulation torsional resonance mode AFM on chlorite

Journal of Physics, 100, 052033 (2007)

Ayhan Yurtsever, Alexander M. Gigler, and Robert W. Stark

Frequency modulation torsional resonance mode AFM on chlorite (001)

Ayhan Yurtsever, Alexander M. Gigler and Robert W. Stark

Center for NanoScience (CeNS) and Dept. Earth and Environmental Sci., Ludwig-Maximilians-Universität München, Theresienstr. 41, 80333 Munich, Germany

E-mail: stark@lrz.uni-muenchen.de

Abstract. In this paper, we discuss torsional resonance mode atomic force microscopy in frequency modulation (FM-TR-AFM) under ambient conditions. Freshly cleaved chlorite (001) exhibiting brucite-like and mica-like surface areas was investigated in constant amplitude operation in order to visualize topography and frictional properties. The measurements in frequency modulation allow the characterization of dissipative effects due to changes in the lateral forces between tip and sample.

1. Introduction

Mapping in-plane surface properties by atomic force microscopy (AFM) enables the characterization of friction, shear stiffness, and other tribologically relevant properties with nanometer resolution. Torsional resonance imaging resembles an AFM shear force experiment which is strongly linked to these tribological surface properties. In contrast to classical resonant imaging such as intermittent contact or non-contact mode, the tip is oscillating parallel (instead of normal) to the sample surface reducing peak repulsive forces. Several approaches have been demonstrated in order to achieve a laterally oscillating tip. A direct excitation and analysis of torsional resonances in contact mode allows to characterize frictional properties of hard samples [1]. Atomic steps on graphite could be resolved by an AFM sensor attached to the prong of a tuning fork [2].

For standard AFM setups, a special cantilever holder was introduced, which allows for the direct excitation of torsional resonances [3]. This improves the coupling to torsional oscillations and reduces possible cross talk between flexural and torsional vibrations. Two piezoelectric elements drive the cantilever to a small torsional oscillation. Typical Q-factors are on the order of $Q = 1000$. Since the twisting angle is very small, the tip oscillates nearly parallel to the surface with typical amplitudes smaller than 1 nm. Thus, the torsional resonance mode allows for the quantitative characterization of in-plane sample properties such as friction or shear stiffness [4]. By shaking the cantilever base at the torsional resonance frequency Pfeiffer et al. [5], could measure the energy dissipation on the Cu (100) surface in UHV. Kunstmann et al. [6] used frequency-modulation for a combined flexural and torsional measurement mode. They derived additional information on dissipation from the torsional oscillation response on insulating surfaces in UHV.

Frequency modulation (FM) techniques in non-contact atomic force microscopy are powerful tools to achieve atomic resolution on a great variety of samples, including semiconducting [7] or conductive [8, 9] samples. The imaging process has been investigated extensively by theory [10-12] and

experiment [13-15]. In addition to imaging, FM techniques in AFM allow to study energy dissipation. The dissipation is strongly associated with the mechanical and chemical properties of the surface [16, 17].

In this work, we demonstrate frequency modulation [18] for torsional resonance mode AFM (FM-TR-AFM). Both, frequency shift and energy dissipation are measured under ambient conditions. The frequency shift provides information on the conservative interaction, while the dissipation signal also contains information on energy loss.

2. Materials and methods

All experiments were carried out on a Dimension 3100 atomic force microscope equipped with a NanoScope IV controller and a torsion resonance (TR) mode adapter (Veeco Metrology Inc., Santa Barbara, CA). Here, two dither piezos were driven out of phase in order to generate a torsional oscillation of the cantilever. Frequency modulation feedback was realized using an external phase-locked-loop unit (Nanosurf Easy PLL, Liestal, Switzerland) connected to the microscope controller via a signal access module, as shown in figure 1.

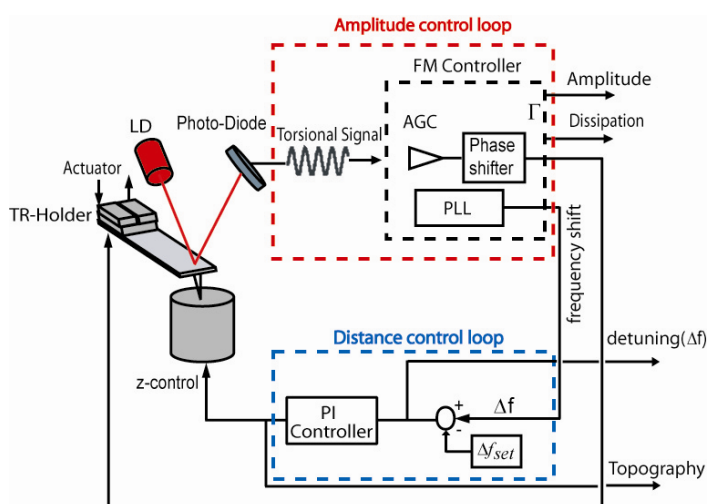


Figure 1. Scheme of the feedback circuit for torsional resonance mode in frequency modulation. The torsional vibration of the cantilever was measured as the lateral deflection signal of the segmented photodiode. The signal was amplified, phase shifted, and connected to the dither piezos for positive feedback. The frequency shift – mainly induced by conservative tip-sample interaction – is used for distance regulation. An automatic gain control (AGC) keeps the oscillation amplitude constant. Thus, the AGC error output corresponds to the local energy dissipation.

Silicon cantilevers with a flexural resonance frequency of 117 kHz and a nominal spring constant of 27 N/m were used (ZEIHR Nanosensors, Neuchatel, Switzerland). Typically, the resonant frequency of the first torsional eigenmode was 910 kHz. The torsional oscillation of the cantilever was maintained by feeding the amplified and phase shifted torsion signal to the driving piezos attached underneath the cantilever holder. The PLL proportional and integral gains allowed to track the resonant frequency while an automatic gain control (AGC) kept the oscillation amplitude constant (CA-Mode). The amplification in the amplitude control loop is adjusted by a PI controller to keep the oscillation amplitude constant. The frequency shift of the oscillation was used as a control signal for the z-feedback loop. Measurements were carried out in constant frequency shift mode, where the frequency shift of the resonant frequency of the cantilever was kept constant during FM-TR-AFM imaging. Image processing was done using WSxM [19].

A clinoclone (pennine) specimen $(\text{Mg,Fe}^{2+})_5\text{Al}[(\text{OH})_8|\text{AlSi}_3\text{O}_{10}]$ from Rimpfischwäng, Zermatt, Switzerland (Sample #17984 of the Bavarian Mineralogical State Collection, Munich) was cleaved. The mineral belongs to the chlorite group of phyllosilicates. It consists of alternating T-O-T (tetrahedral-octahedral-tetrahedral) and brucite-like layers. The T-O-T layer corresponds to phlogopite mica. The brucite-like surface exhibits OH groups and is slightly positively charged as compared to the mica-like layer which presents oxygen at the surface. The step height is 0.5 nm for a brucite-like layer and 1 nm for a T-O-T layer.

3. Results and Discussion

We imaged a freshly cleaved chlorite surface in TR-mode AFM using the frequency modulation technique with constant oscillation amplitude. The frequency shift data corresponds to the conservative interaction due to feedback errors while the energy dissipation image corresponds to the damping or frictional behavior of the sample. The information of the energy dissipation was extracted from the AGC feedback signal, which showed the variation in amplitude of the cantilever excitation signal. The power needed to keep the torsional oscillation amplitude constant is directly proportional to the power dissipated at the tip-sample contact. Figure 2 shows simultaneously measured maps of (a) topography, (b) frequency shift, and (c) energy dissipation as measured with the AGC on the mineral surface. The experimental data were obtained in a constant amplitude operation of the FM-TR-AFM. A cross-section of the topographic data shows that the triangular shapes are brucite flakes with a typical step-height of 0.5 nm.

As feedback control parameter, the frequency shift was used. Thus, image (b) only reveals the control error which results in a derivative picture of the topography. The cross-section shows that despite of edges, the frequency was maintained well. The excitation signal represents the energy needed to keep the torsional amplitude constant. Thus, it gives a direct measure for the dissipated energy, which shows a clear contrast for the different domains of the chlorite surface. In addition to the different mechanical properties of the T-O-T and brucite-like layers of the crystal, these are also charged differently. This surface charge density also influences the interaction between tip and surface due to corresponding changes in the surface potential. From the dissipation cross section, it is obvious that the oscillator loses more energy on the brucite flakes as compared to the T-O-T layer. This dissipative contrast might be due to different wetting properties of the respective surfaces or due to differences in the elemental friction processes at the atomic scale.

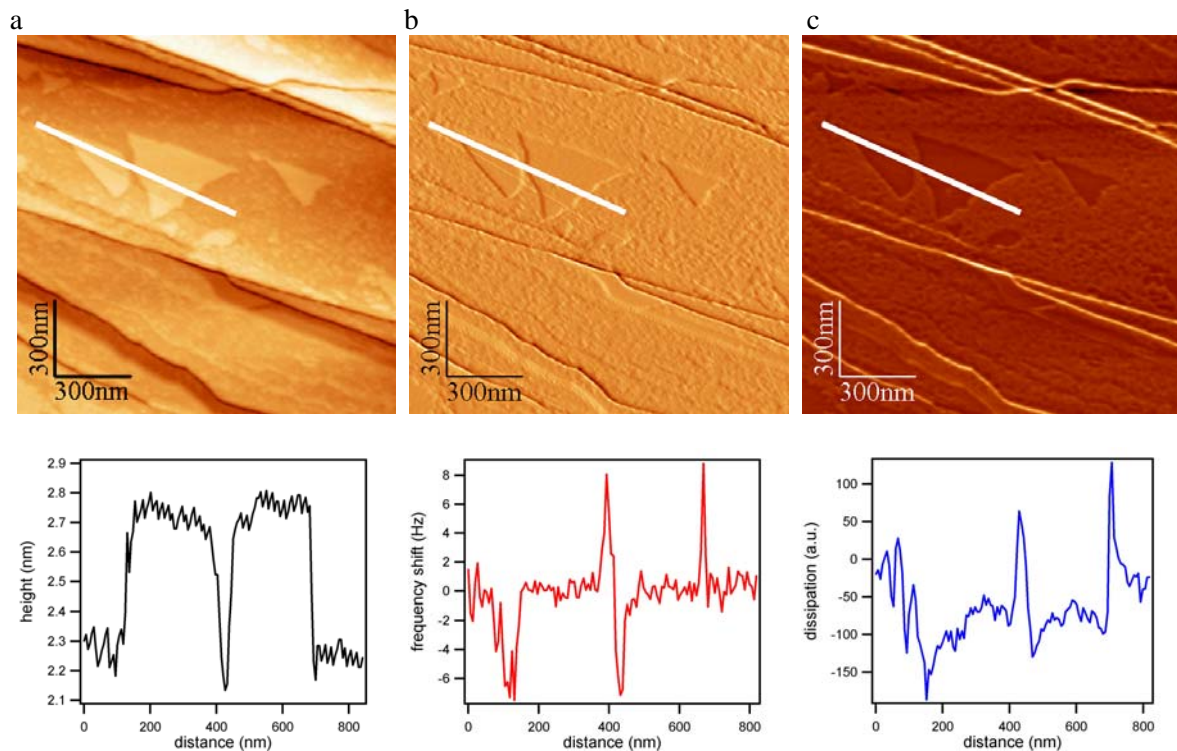


Figure 2. (a) Topographic image of the chlorite (001) surface. Image (b) shows the local detuning (z -feedback error). Image (c) shows the two dimensional mapping of the piezo excitation amplitude which was measured simultaneously with topography in ambient air. The cross sections below the respective images were extracted as indicated by the white lines.

4. Conclusions

We have demonstrated torsional resonance mode atomic force microscopy using the frequency modulation technique under ambient conditions. On a chlorite surface, image contrast between exposed T-O-T and brucite-like layers could be achieved in the dissipation signal. The fundamental mechanism of this contrast still needs to be investigated. Mapping energy dissipation in this mode opens a wide field for quantitative tribological analyses. Thus, frictional properties can be accessed, which so far have not been accessible by conventional dynamic AFM.

Acknowledgments

We gratefully acknowledge financial support by the German Federal Ministry of Education and Research (BMBF) Nanofutur grant 03N8706. AY is supported by the Scholarship of the Elite Network of Bavaria, International Doctorate Program Nano-Bio-Technology (IDK-NBT).

References

- [1] Drobek T, Stark R W, Gräber M and Heckl W M 1999 *New J. Phys.* **1** 15
- [2] Göttlich H, Stark R W, Pedarnig J D and Heckl W M 2000 *Rev. Sci. Instrum.* **71** 3104-3107
- [3] Huang L and Su C M 2004 *Ultramicroscopy* **100** 277-285
- [4] Reinstädler M, Kasai T, Rabe U, Bhushan B and Arnold W 2005 *J. Phys. D-Appl. Phys.* **38** R269-R282
- [5] Pfeiffer O, Bennewitz R, Baratoff A, Meyer E and Grutter P 2002 *Phys. Rev. B* **65**
- [6] Kunstmann T, Schlarb A, Fendrich M, Paulkowski D, Wagner T and Moller R 2006 *Appl. Phys. Lett.* **88**
- [7] Sugawara Y, Ohta M, Ueyama H and Morita S 1995 *Science* **270** 1646-1648
- [8] Giessibl F J 1995 *Science* **267** 68-71
- [9] Fukui K, Onishi H and Iwasawa Y 1997 *Phys. Rev. Lett.* **79** 4202-4205
- [10] Gauthier M and Tsukada M 2000 *Phys. Rev. Lett.* **85** 5348-5351
- [11] Gotsmann B, Anczykowski B, Seidel C and Fuchs H 1999 *Appl. Surf. Sci.* **140** 314-319
- [12] Kantorovich L N and Trevethan T 2004 *Phys. Rev. Lett.* **93** 236102
- [13] Fukuma T, Ichii T, Kobayashi K, Yamada H and Matsushige K 2004 *J. Appl. Phys.* **95** 1222-1226
- [14] Jarvis S P, Yamada H, Kobayashi K, Toda A and Tokumoto H 2000 *Appl. Surf. Sci.* **157** 314-319
- [15] Loppacher C, Bennewitz R, Pfeiffer O, Guggisberg M, Bammerlin M, Schar S, Barwich V, Baratoff A and Meyer E 2000 *Phys. Rev. B* **62** 13674-13679
- [16] Hölscher H, Gotsmann B, Allers W, Schwarz U D, Fuchs H and Wiesendanger R 2001 *Phys. Rev. B* **64** 075402
- [17] Gotsmann B and Fuchs H 2001 *Phys. Rev. Lett.* **86** 2597-2600
- [18] Albrecht T R, Grutter P, Horne D and Rugar D 1991 *J. Appl. Phys.* **69** 668-673
- [19] Horcas I, Fernandez R, Gomez-Rodriguez J M, Colchero J, Gomez-Herrero J and Baro A M 2007 *Rev. Sci. Instrum.* **78** 013705

Frequency modulated torsional resonance mode AFM on polymers

Applied Physics Letters (APL), 92, 143103 (2008)

Ayhan Yurtsever, Alexander M. Gigler, Christian Dietz, and Robert W. Stark

Frequency modulated torsional resonance mode atomic force microscopy on polymers

Ayhan Yurtsever,¹ Alexander M. Gigler,^{1,a)} Christian Dietz,² and Robert W. Stark^{1,b)}

¹Center for NanoScience (CeNS) and Department of Earth and Environmental Sciences, Ludwig-Maximilians-Universität München, Theresienstraße 41, 80333 Munich, Germany

²Chemische Physik, Technische Universität Chemnitz, Reichenhainer Str. 70, 09107 Chemnitz, Germany

(Received 26 February 2008; accepted 19 March 2008; published online 8 April 2008)

In-plane mechanics of polymers can be probed by integrating frequency modulation and torsional resonance mode atomic force microscopy. We investigated a thin film of polystyrene-*block*-polybutadiene diblock copolymer. To gain more insight into image contrast formation, we examined displacement curves on polystyrene homopolymer surfaces of different molecular weights focusing on energy dissipation and frequency shift. Data suggest that the transition from a highly motile surface layer to the bulk material depends on the molecular weight of the polymer. This, in turn, indicates that the tip is slightly oscillating within the sample surface during imaging. © 2008 American Institute of Physics. [DOI: 10.1063/1.2907498]

The atomic force microscope (AFM) has become a standard instrument for imaging and characterization of polymers with nanometer resolution. Various AFM imaging techniques allow for mapping material properties to topographic surface features. Depending on the scheme of excitation, these techniques can be categorized as nonresonant methods, such as pulsed force mode,^{1,2} or resonant methods such as phase imaging,³ frequency modulation,^{4,5} and time-resolved AFM.^{6,7} All of these techniques are based on a flexural oscillation of the cantilever sensing forces perpendicular to the surface. The probe only interacts with the sample at the lower turning point of the cantilever oscillation and, thus, is far away from the surface for most of the oscillation cycle. In order to probe the in-plane mechanical properties of materials, the tip can also be driven to a small lateral instead of vertical oscillation. Such a lateral oscillation is used in imaging modes where the specimen is characterized by shear force interactions. Shear force imaging can be realized by applying a lateral modulation to a tip or sample with an amplitude of a few nanometers either while the tip is scanned across the specimen⁸ or during approach/retract curves (displacement curves).^{9,10} Using higher excitation frequencies close to the torsional resonances (TR) of the cantilever,¹¹ in-plane conservative (elasticity under shear) as well as dissipative (friction) properties can be determined. Even without the need for active driving of the TR, in-plane elastic properties can be extracted from the thermomechanical oscillations of the force sensor in contact with the surface.¹²

In order to achieve a well-defined lateral tip oscillation, the TR mode has been introduced where two piezoelectric elements force the cantilever to a torsional oscillation.¹³ To provide high sensitivity together with stable imaging, frequency modulation techniques can be applied to TR mode.^{14,15} However, the fundamental mechanisms of image formation in this mode demand further investigation. We therefore discuss frequency modulated TR mode

AFM (FM-TR-AFM) for imaging thin polymer films in the following.

The experiment was set up using a Dimension 3100 AFM with a NanoScope IV controller equipped for TR-mode operation (Veeco Metrology Inc., Santa Barbara, CA). The control loop was extended by a phase-locked loop electronics (Easy-PLL, Nanosurf AG, Liestal, Switzerland), as shown in Fig. 1. Silicon cantilevers (ZEIHR, Nanosensors, Neuchâtel, Switzerland) with torsional resonant frequencies below 1 MHz were used (flexural resonance of 117 kHz, TR of 910 kHz, and flexural spring constant 27 N/m). A positive feedback of the lateral signal of the photodiode together with an automatic gain control was implemented for driving the cantilever into a stable torsional oscillation. The detuning (Δf) of the TR was utilized for topographic feedback. Two different modes of operation were used: constant amplitude (CA) mode for imaging and constant excitation (CE) mode for displacement curves. In CA mode, the energy needed to maintain the torsional oscillation amplitude constant pro-

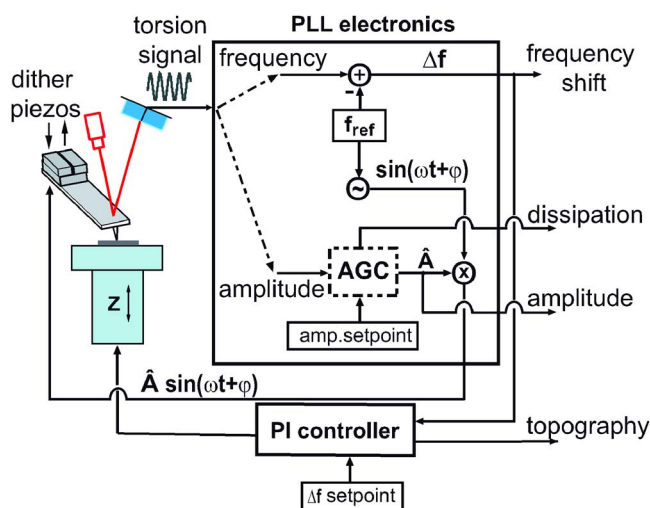


FIG. 1. (Color online) Scheme of frequency modulated torsional resonance mode AFM. A positive feedback of the photodiode signal is used to drive the dither piezos for torsional excitation. Frequency shift, energy dissipation, and oscillation amplitude can be concurrently measured with the topography.

^{a)}Author to whom correspondence should be addressed. Electronic mail: gigler@lmu.de. Tel.: +49 89 2180 4185. FAX: +49 89 2180 4334.

^{b)}Electronic mail: stark@lmu.de.

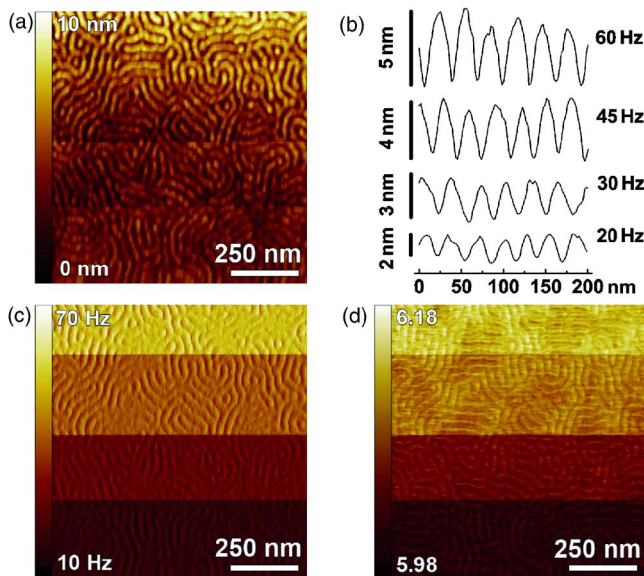


FIG. 2. (Color online) Dependence of image contrast on the detuning set point in CA mode. The detuning set point was varied in steps (20, 30, 45, and 60 Hz from bottom to top). Representative cross sections from each region are shown in (b). (c) Frequency shift (error) image and (d) energy dissipation image.

vides a direct measure for energy dissipation at the tip-sample contact.

To demonstrate the capabilities of the frequency modulation technique in TR mode AFM, we imaged a thin film of polystyrene-*block*-polybutadiene (SB) diblock copolymer (Polymer Source Inc., Dorval Montreal, Canada) with molecular weights $M_{w,PS}=13.6$ kg/mol and $M_{w,PB}=33.7$ kg/mol (PS is polystyrene and PB is polybutadiene). For sample preparation, the polymer was dissolved in toluene (concentration 30 mg/ml) and spin coated onto pieces of a silicon wafer. Prior to coating, the substrates were cleaned by sonication with acetone, ethanol, and toluene for 15 min each and dried in a stream of nitrogen afterwards. Spin coating at 1000 rpm resulted in a 150-nm-thick film of SB with a structure of cylinders of PS lying parallel to the surface. The thickness was determined by measuring the height profile of a scratch.

For imaging of SB, the CA scheme of the FM-TR mode was used. The cantilever was oscillated with small amplitude (below 2 nm) parallel to the sample surface. In order to elucidate the effect of the detuning set point on image contrast, the set point was varied stepwise from 20 to 60 Hz. Figure 2(a) shows the topography together with representative cross sections [Fig. 2(b)] for each region of interest. Since the PB block is more compliant compared to the PS block, PS appeared higher (brighter color) in the topography image. The topographic image showed the typical structure of cylinders oriented parallel to the substrate.¹⁶ The height difference between PS and PB increased from 2 nm (20 Hz set point), 3 nm (30 Hz), 4 nm (45 Hz), to 5 nm (60 Hz), since the material was increasingly compressed due to the effective average force exerted by the tip. As the frequency shift was used as a control parameter for the z -feedback loop, Fig. 2(c) reflects the feedback response only. Energy dissipation [Fig. 2(d)], however, allows discerning of the polymer blocks. It correlates with the amount energy needed to maintain the oscillation amplitude constant (CA mode). With the increase in frequency shift set point, we observed a shift to

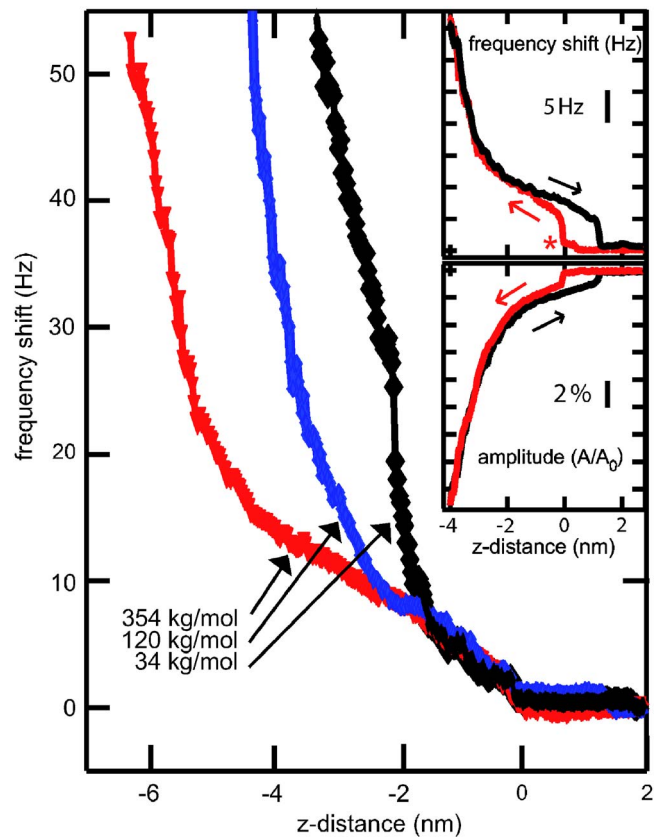


FIG. 3. (Color online) Detuning vs distance plots of the torsional oscillation acquired in CE mode on PS homopolymers with $M_w=34.3$ kg/mol (black), 119.6 kg/mol (blue), and 354.0 kg/mol (red). The inset shows a typical displacement curve on PS (119.6 kg/mol) with frequency shift and amplitude of the torsional oscillation as a function of z -actuator displacement, respectively. Approach (red) and retract (black) are also indicated by the arrows. The asterisk marks the jump of the AFM tip to contact with the sample.

higher values of dissipation, i.e., the PB domains appeared brighter in this image since more deformation energy was turned into heat.

Lacking a rigid theoretical description of the indentation process of a torsionally vibrating tip into a polymeric material, we attempted to understand the image formation from an experimental point of view. Hence, displacement curves of the torsional resonance detuning versus z position as well as torsional oscillation amplitude versus z position were conducted on PS homopolymer surfaces (Polymer Source Inc., Dorval Montreal, Canada) with different molecular weights ($M_w=34.3$, 119.6, and 354.0 kg/mol). Similar to the SB samples, the polymer samples were prepared by spin coating from a toluene solution with a concentration of 20 mg/ml onto freshly cleaned pieces of a silicon wafer, which resulted in a film thickness of 150 nm for all samples. Cleaning equaled the procedure described above.

Displacement curves (frequency shift and amplitude change versus z position recorded in CE mode), as shown in the inset of Fig. 3, revealed details of the interaction between the tip and the sample. At close proximity, the tip snapped into contact with the surface (asterisk). The snap in was accompanied by a sharp change in amplitude and detuning. Over the next 2 nm, amplitude and frequency slowly varied. At a displacement of more than 3 nm, both amplitude and frequency rapidly changed. Upon retraction, a hysteresis of frequency shift and amplitude prevailed. We observed a posi-

tive frequency shift and decreased amplitude due to contact stiffening. The initial slope of the frequency shift plot was rather linear. This can be explained by mobile polymer coils close to the polymer/air interface. Indenting further, the tip penetrated through the first layer exerting shear stress on the bulk polymer. With the increasing indentation, more and more material was involved in tip-sample interaction. This led to an increased frequency shift which may be attributed to polymer entanglements,^{17,18} limiting the chain mobility in the bulk.

In order to assess this effect of the polymer chain length, displacement curves focusing on frequency shift were measured on different PS homopolymers ($M_w=34.3$, 119.6, and 354.0 kg/mol), as shown in Fig. 3. For all specimens, two regimes were observed in the displacement curves: Firstly, a rather compliant surface layer was probed; secondly, the less mobile bulk of the polymer was sensed by the oscillatory motion of the tip. The position of the kink between the two regimes strongly correlated with the molecular weight of the homopolymer.

The approach-retract response of amplitude reduction and frequency shift of the torsional oscillation can be related to the mechanical properties of the thin film. As we observed two distinct regions of different mechanical behavior in terms of periodic shear stress, a mobile thin layer followed by a more rigid bulk seems a reasonable assumption. The apparent stratification of the film may be caused by the segregation of short and long chained molecules at the interfaces of a film, since short chains (low M_w) are repelled from the bulk (higher M_w) due to entropic forces. Even purified homopolymers yet having a finite polydispersity of 1.05, such as the polymers used in our experiments, result in a superficial layer consisting of the shorter molecules.

In summary, FM-TR-AFM is a powerful tool for imaging polymeric samples with spatially varying mechanical properties. The indentation experiments clearly show that the tip is oscillating within the motile top layer of the polymer surface even for detuning on the order of 10 Hz. For the diblock copolymer, this means that while imaging in FM-TR-AFM, the tip is also compressing the different polymer blocks according to their compliance. This effect causes an apparent increase of topography with the detuning set point. Furthermore, we investigated frequency shift versus distance curves on PS, which revealed two different interaction regimes. Depending on the molecular weight, we

observed a distinct change in the signature of the distance curves. Hence, we propose a stratified structure due to the segregation of shorter chains from longer chains and, thus, a resulting two layer behavior. Our findings show that FM-TR-mode spectroscopy enables discerning of polymer samples by their different molecular weight.

We gratefully acknowledge financial support by the German Federal Ministry of Education and Research (BMBF) Grant Nanofutur 03N8706 and by the European Commission (FORCETOOL, NMP4-CT-2004-013684). The authors thank Robert Magerle for fruitful discussions. A.Y. was supported by the Doctorate Program Nano-Bio-Technology (IDK-NBT) of the Elite Network of Bavaria, International and A.M.G. was financed by the cluster of excellence "Nanosystems Initiative Munich (NIM).

¹H. U. Krottil, T. Stifter, and O. Marti, *Rev. Sci. Instrum.* **71**, 2765 (2000).

²A. Gigler, C. Gnahn, O. Marti, T. Schimmel, and S. Walheim, *J. Phys.: Conf. Ser.* **61**, 346 (2007).

³S. N. Magonov, V. Elings, and M. H. Whangbo, *Surf. Sci.* **375**, L385 (1997).

⁴F. Dubourg, G. Couturier, J. P. Aime, S. Marsaudon, P. Leclere, R. Lazzaroni, J. Salardenne, and R. Boisgard, *Modell. Simul. Mater. Sci. Eng.* **167**, 177 (2001).

⁵F. Dubourg, S. Kopp-Marsaudon, P. Leclere, R. Lazzaroni, and J. P. Aime, *Eur. Phys. J. E* **6**, 387 (2001).

⁶M. Stark, R. W. Stark, W. M. Heckl, and R. Guckenberger, *Proc. Natl. Acad. Sci. U.S.A.* **99**, 8473 (2002).

⁷O. Sahin, S. Magonov, C. Su, C. F. Quate, and O. Solgaard, *Nat. Nanotechnol.* **2**, 507 (2007).

⁸H. U. Krottil, E. Weilandt, T. Stifter, O. Marti, and S. Hild, *Surf. Interface Anal.* **27**, 341 (1999).

⁹H. U. Krottil, T. Stifter, and O. Marti, *Appl. Phys. Lett.* **77**, 3857 (2000).

¹⁰H. U. Krottil, T. Stifter, and O. Marti, *Rev. Sci. Instrum.* **72**, 150 (2001).

¹¹M. Reinstädler, U. Rabe, V. Scherer, U. Hartmann, A. Goldade, B. Bhushan, and W. Arnold, *Appl. Phys. Lett.* **82**, 2604 (2003).

¹²T. Drobek, R. W. Stark, and W. M. Heckl, *Phys. Rev. B* **64**, 045401 (2001).

¹³L. Huang and C. M. Su, *Ultramicroscopy* **100**, 277 (2004).

¹⁴A. Yurtsever, A. M. Gigler, E. Macias, and R. W. Stark, *Appl. Phys. Lett.* **91**, 253120 (2007).

¹⁵A. Yurtsever, A. M. Gigler, and R. W. Stark, *J. Phys.: Conf. Ser.* **100**, 052033 (2008).

¹⁶A. Knoll, A. Horvat, K. S. Lyakhova, G. Krausch, G. J. A. Sevink, A. V. Zvelindovsky, and R. Magerle, *Phys. Rev. Lett.* **89**, 035501 (2002).

¹⁷F. Dubourg, J. P. Aime, S. Marsaudon, G. Couturier, and R. Boisgard, *J. Phys.: Condens. Matter* **15**, 6167 (2003).

¹⁸H. R. Brown and T. P. Russell, *Macromolecules* **29**, 798 (1996).

Acoustical force nanolithography of thin polymer films

PHYSICA STATUS SOLIDI A, 203, 1481 (2006)

F. J. Rubio-Sierra, Ayhan Yurtsever, Marc Hennemeyer, Wolfgang M. Heckl,
and Robert W. Stark

Acoustical force nanolithography of thin polymer films

F. J. Rubio-Sierra¹, A. Yurtsever¹, M. Hennemeyer¹, W. M. Heckl^{1,2}, and R. W. Stark^{*,1}

¹ CeNS and Crystallography, Department of Earth and Environmental Sciences, Ludwig-Maximilians-Universität München, Theresienstr. 41, 80333 München, Germany

² Deutsches Museum, Museumsinsel 1, 80538 München, Germany

Received 30 September 2005, revised 16 December 2005, accepted 17 December 2005

Published online 4 April 2006

PACS 07.79.Lh, 68.37.Ps, 81.16.Nd

Nanomachining of thin polymer resist films with an atomic force microscope (AFM) is a promising route for the fabrication of nanoscale devices. In order to enhance the controllability of the nanomachining process an in-plane acoustic wave is coupled to the sample support. This enhances the intermittent force exerted by the AFM tip. The lateral resolution reached by this method is only limited by the physical size of the AFM tip to dimensions far below the light diffraction limit. The main process parameters are the frequency and magnitude of the acoustic wave, and the preloading force. In this work, the feasibility of acoustical force lithography and the influence of the relevant parameters are investigated.

© 2006 WILEY-VCH Verlag GmbH & Co. KGaA, Weinheim

1 Introduction

Surface patterning at the smallest scale is a key issue for the further development of technological and scientific applications that require rapid prototyping of nanostructures. Currently, optical lithography is the standard technique for the fabrication of structured surfaces. However, the lateral resolution of optical lithography is limited by diffraction. To overcome this limitation, alternative surface patterning methods have been developed during the last years, such as e-beam lithography, masked deposition, scanning probe techniques, or microcontact printing [1]. Scanning probe microscope related techniques represent the most versatile approach for rapid prototyping of lateral nanoscale structures [2, 3]. Among the members of the scanning probe family, the atomic force microscope (AFM) has experienced an impressive development for its application to lithography [4, 5]. Essentially, there are three physically different types of AFM lithography: local anodic oxidation [6], surface chemical patterning [7], and mechanical machining [8]. Mechanical machining by AFM has the main advantages of being a direct method – it is not restricted to functional materials. The resolution is only limited by the physical dimensions of the AFM tip, which is much smaller than the light diffraction limit.

Currently, two different approaches are used for mechanical machining by AFM. The quasi-static approach relies on the application of a static load on the sample to produce plastic deformation while the AFM tip moves on the surface [9]. The main drawback of the quasi-static method is the poor controllability of the process due to lateral forces [10]. In the second approach, dynamic mechanical machining, the AFM cantilever is oscillated with a small amplitude which minimizes unwanted lateral forces during the lithography process. Typically, the supporting piezo-element is used to generate cantilever oscillations by the excitation of flexural resonant modes. If the AFM tip is sufficiently close to the sample and the excitation is strong enough, nanostructures can be lithographed on the surface. This method is also found in the literature as dynamic plowing lithography [11].

* Corresponding author: e-mail: stark@nanomanipulation.de, Phone: +49 89 2180 4329, Fax: +49 89 2180 4334

The controllability of standard dynamic plowing is limited by the fact that the cantilever actuation depends strongly on the transfer characteristics of the dithering piezo-element and the cantilever: The fixed end actuation of the cantilever introduces a time-delay in the system between the actuation and the tip. This can limit the bandwidth of high-speed closed-loop control of the machining process [12]. Additionally, the non-linear tip-sample interaction produces a strong shift of the cantilever resonant frequency. Thus, a promising method for cantilever excitation is to couple a normal incidence shear acoustic wave to the cantilever tip through sample surface. The acoustic wave is generated by an acoustic transducer below the sample [13, 14].

In the following, we discuss ‘acoustical force nanolithography’, a surface machining method based on the AFM. In order to avoid the hardly controllable stick-slip oscillations of quasi-static plowing lithography, the oscillations are induced by a normal incidence shear acoustic wave. Prior to lithography, the frequency response of the cantilever is acquired to obtain the optimal frequency of operation. The influence of the main experimental parameters such as excitation frequency, amplitude, and the preloading force is investigated in detail.

2 Experimental and methods

The experiments were carried out on a Dimension 3100 Scanning Probe Microscope System (Veeco Metrology, Santa Barbara, CA). Lithography paths were programmed using the NanoMan II software of the instrument. For the process parameters characterization, a triangular cantilever with a nominal force constant of 48 N/m was used (NSC11, MikroMasch, Tallinn, Estonia). For the lithography a rectangular cantilever with a nominal force constant of 40 N/m was used (NSC16, MikroMasch, Tallinn, Estonia). As illustrated in Fig. 1, the sample was mounted on a normal incidence shear wave transducer (v153, Panametrics-NDT, Waltham, MA). For lithography a continuous sinusoidal signal was coupled to the ultrasonic transducer. To switch between imaging and lithography mode, the sample bias voltage signal of the AFM controller was used as trigger signal; this signal can be accessed through a signal access module. In this modified lithography system the sample holder is electrically isolated from the sample bias voltage signal of the controller.

Samples were prepared on silicon chips with a size of about 1 cm². Prior to coating, the chips were cleaned with acetone, isopropanol, and de-ionized water. A thin polymer film was prepared by spin coating ($\omega = 500 \text{ min}^{-1}$ for 30 s, $\omega = 5000 \text{ min}^{-1}$ for 60 s) *ma-p 1205*[®] (based on Novolak, naphthoquinone diazide, and solvents; MicroChem, Newton, MA). After spinning, the samples were dried on a hot plate at 100 °C for 40 s.

All images were acquired in standard tapping mode where the dither piezo of the cantilever holder is used for excitation. For image processing a commercial software package was used (SPIP 4.0, Image Metrology A/S, Lyngby, Denmark). In order to obtain a reliable measurement of the width of the litho-

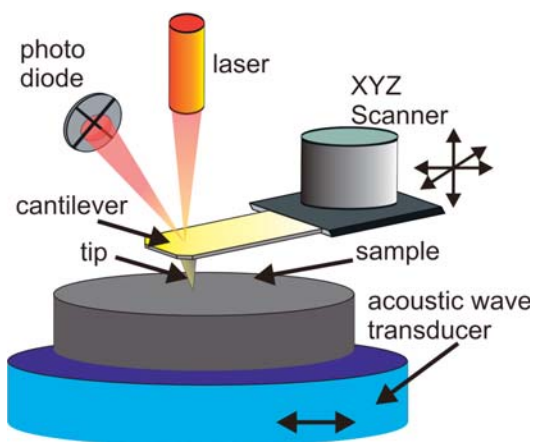


Fig. 1 (online colour at: www.pss-a.com) Schema of the experimental setup for acoustical force nanolithography. The sample holder consists on an acoustic wave transducer that is used to enhance cantilever flexural vibrations for lithography.

graphed structures, the influence of the tip-shape on the measured topography had to be considered. Due to the geometric 'convolution' of the tip shape with the surface profile the width of grooves is underestimated in the raw topographic data. Thus, the images were low-pass filtered to remove high frequency noise. Then, a worst-case tip shape was estimated employing the tip characterization procedure of the software package [15]. In order to obtain reliable upper limits for the width of the nanomachined lines, the tip shape was deconvoluted from topographic data [16].

3 Process parameters

3.1 Resonance spectra

In order to tune the excitation frequency for lithography the frequency response of the cantilever to a continuous single tone excitation of the ultrasonic transducer was analyzed. Two different types of vibration spectra were acquired: one for the free cantilever and one for the surface-coupled cantilever. The excitation frequency was swept stepwise in the frequency band from 400 kHz to 1 MHz. The vibration spectra of the AFM cantilever were measured by demodulation of the deflection signal with an external lock-in amplifier (7280, Ametek, Oak Ridge, TN). The frequency response of the free cantilever is shown in Fig. 2(a). The cantilever was placed about 2 μm over the sample surface during the measurement of the frequency response. The out-of plane oscillations of the vibrations of the ultrasonic transducer couple through the air to the cantilever. Only one resonant peak appears at a frequency of 423.4 kHz within the analyzed frequency band.

In order to acquire the resonance spectra of the surface-coupled cantilever, the vibrating AFM cantilever is brought into intermittent contact by approaching the cantilever to the surface until the AFM cantilever oscillation amplitude was reduced to 20%. Then, the microscope feedback-loop was disconnected and the vibration spectrum was acquired. Figure 2(b) shows the vibration spectrum with several resonant peaks. The main resonance peak is shifted and obscured by new resonances in the spectrum. These new resonances are caused by the strong non-linear character of the tip-sample interaction and resonances in the frequency response of the acoustic transducer [17, 18]. Six major resonant peaks are located at $f = 477.0, 598.2, 637.8, 777.2, 879.6,$ and 940.8 kHz. The response of the system close to 1 MHz is enhanced due to the frequency response of the acoustic wave transducer which is centered at this frequency.

3.2 Acoustic wave frequency

The frequency response of the surface-coupled cantilever shows that the vibration amplitude depends strongly on the excitation frequency. Four traces were lithographed at different resonant peaks of the surface-coupled cantilever frequency response in order to characterize the influence of the excitation frequency (1 Volt signal amplitude). Figure 3(a) shows the resulting traces and the height profile. All lines successfully ploughed grooves on the sample surface. Residual material from the plowing process

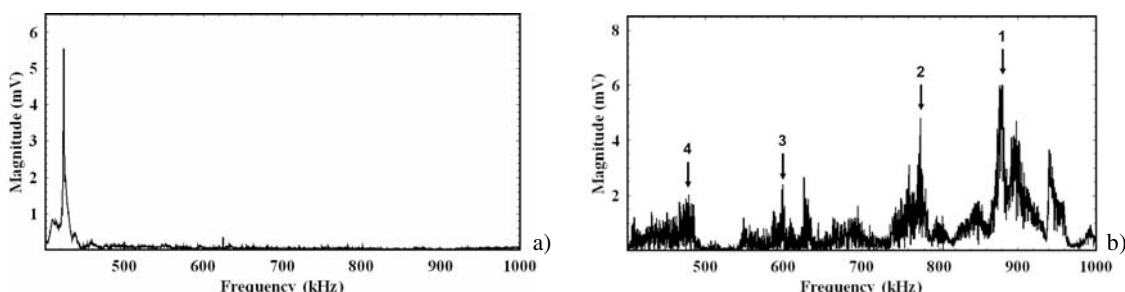


Fig. 2 Vibration spectra of: a) the freely vibrating cantilever, and b) the surface-coupled cantilever. The numbered peaks in (b) were used to characterize the influence of the frequency response in the lithography process.

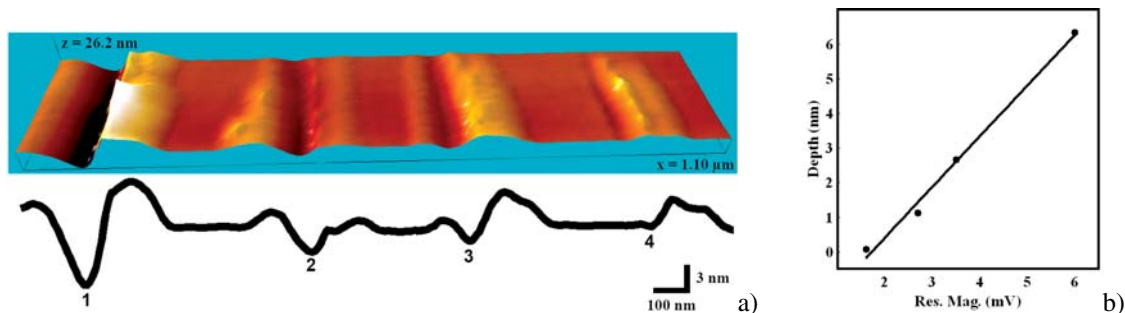


Fig. 3 (online colour at: www.pss-a.com) Variation of lithography depth with the resonant magnitude of the surface-coupled frequency response (Fig. 2). The resonant magnitudes and corresponding excitation frequencies for the four different traces were: trace 1, 6.0 mV (at 879.4 kHz); trace 2, 3.5 mV (at 774.2 kHz); trace 3, 2.7 mV (at 626 kHz); trace 4, 1.6 mV (at 479.4 kHz). a) 3D-representation and height profile of the patterned area. b) Increase of lithographed depth with the frequency response magnitude of the resonant peak. A linear fit of the experimental data is also displayed.

appears at both sides of the grooves. From the results it is clearly seen that the lithographed depth is directly related to which resonant peak is used to generate the acoustic wave. Figure 3(b) shows that the lithographed trace depth increases linearly with the magnitude of the resonant peak.

3.3 Acoustic wave amplitude

The vibration amplitude of the surface-coupled cantilever and, consequently, the applied tip-sample forces, directly depends on the magnitude of the excitation. To characterize the influence of the acoustic wave amplitude on the lithography process, six lines were lithographed using the same frequency (940.8 kHz) but at different magnitudes of the excitation signal.

The first trace was performed without acoustic wave excitation. All the lines traced with acoustic wave excitation resulted in the fabrication of grooves. Figure 4(b) shows a slight deviation from a linear relation between acoustic wave magnitude and lithographed depth. From Fig. 4(a) it is evident that the sample surface appears raised next to the groove. Raised polymer areas after quasi-static machining for loads below the yield strength of the polymer have been previously reported [9]. However, the mechanism for this material displacement is not well understood. Morphological changes induced by viscoelastic effects or localized heat have been proposed as origins of this phenomenon.

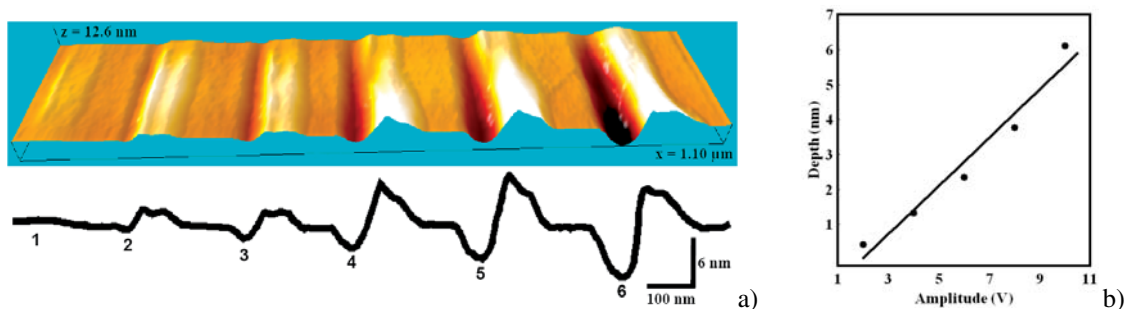


Fig. 4 (online colour at: www.pss-a.com) Increase in lithography depth with the magnitude of the excitation signal. The signal amplitudes for the five different traces were: trace #1, 0 V; trace #2, 2 V; trace #3, 4 V; trace #4, 6 V; trace #5, 8 V; trace #6, 10 V. a) 3D-representation and height profile of the patterned area. b) Relation between lithographed depth and signal magnitude. A linear fit of the experimental data is also displayed.

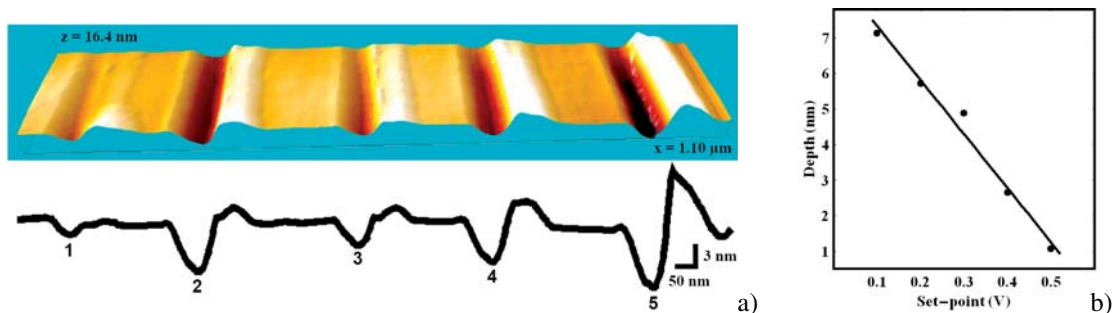


Fig. 5 (online colour at: www.pss-a.com) Variation of lithography depth with set-point of the topography feedback. The corresponding set-points were: trace 1, 0.5 V; trace 2, 0.2 V; trace 3, 0.4 V; trace 4, 0.3 V; trace 5, 0.1 V. a) 3D-representation and height profile of the patterned area. b) Decrease of lithographed depth with increasing set-point. A linear fit of the experimental data is also displayed.

3.4 Preloading force

The coupling of the acoustic wave to the AFM tip depends on the cantilever preloading force. The preloading force is determined by the set-point of the topography feedback prior to lithography. A lower set-point corresponds to a greater preloading force.

Thus, a dependency between the lithographed depth and the preloading force can be expected. To illustrate this, five lines were lithographed at different set-points while applying an excitation signal of 1 V of amplitude at the main resonant peak of the surface-coupled cantilever frequency response (at 879.4 kHz). As expected, a decrease of lithographed depth with increasing set-point is observed in Fig. 5. This dependence has a linear character within the investigated range as seen in Fig. 5(b).

Figure 6 shows two lithographed structures demonstrating the feasibility of the method for the generation of nanostructures. Figure 6(a) shows the lithographed emblem of the Ludwig Maximilians University.

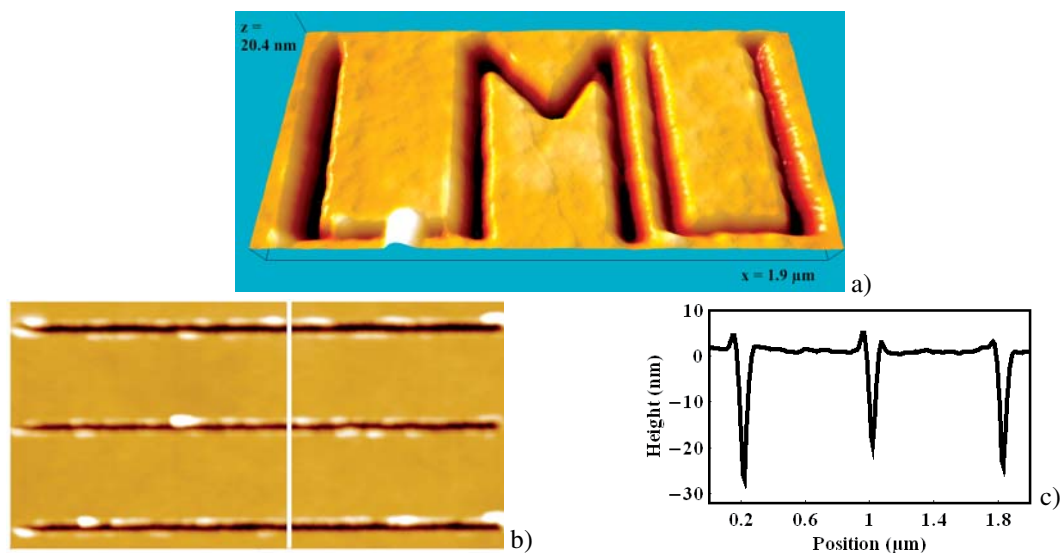


Fig. 6 (online colour at: www.pss-a.com) Nanostructures generated by acoustical force nanolithography: a) lithographed emblem of the Ludwig-Maximilians-University. b) AFM image of three 4 μm long lines lithographed using a signal amplitude of 0.5 V at a frequency of 740 kHz for acoustic wave generation, with an average tip-sample distance of 12.7 nm. Image size (4 \times 2 μm) and z-range of 55.6 nm. c) Line profile along the white line in panel b.

Figure 6(b) and (c) show the AFM image and height profile of three lithographed lines with a length of 4 μm . The average line width at FWHM was of 50 nm. The parameters were chosen to reach a line depth greater than 20 nm. This is relevant for the application of this method as first step in high resolution lift-off lithography, where thin resist layers with a thickness about 20 nm are used [19].

4 Conclusions

Acoustical force nanolithography is an AFM lithography method providing control on the machining process by actuation of AFM cantilever through the specimen by an acoustic wave. A precise control can be achieved by tuning the excitation frequency and amplitude of the excitation to purpose. The feasibility of the method along with the characterization of the main parameters was illustrated by lithography of a thin resist film. After initial tuning of the machining forces by fine tuning the excitation frequency, amplitude and set point, the nanolithography process is a reliable process.

Due to the reduced physical dimensions of the AFM tip and precise positioning and force control provided by acoustic force nanolithography, lateral dimensions of the lithographed traces are reduced far beyond light diffraction limit. The method is easy to implement in probe-scanning AFM configurations and can be used as a stand-alone method for surface modification or as complement for fine adjustment of standard mechanical machining of surfaces by AFM.

Acknowledgements Funding by the German Federal Ministry of Education and Research (BMBF) under grant 03N8706 is gratefully acknowledged. F. J. Rubio-Sierra thanks the Elite Network of Bavaria for financial support.

References

- [1] M. Geissler and Y. Xia, *Adv. Mater.* **16**, 1249 (2004).
- [2] A. A. Tseng, A. Notagiacomo, and T. P. Chen, *J. Vac. Sci. Technol. B* **23**, 877 (2005).
- [3] D. Wouters and U. S. Schubert, *Angew. Chem. Int. Ed.* **43**, 2480 (2004).
- [4] F. J. Rubio-Sierra, W. M. Heckl, and R. W. Stark, *Adv. Eng. Mater.* **7**, 193 (2005).
- [5] D. Fotiadis, S. Scheuring, S. A. Müller, A. Engel, and D. J. Müller, *Micron* **33**, 385 (2002).
- [6] R. Garcia, M. Calleja, and H. Rohrer, *J. Appl. Phys.* **86**, 1898 (1999).
- [7] S. Krämer, R. R. Fuierer, and C. B. Gorman, *Chem. Rev.* **103**, 4367 (2003).
- [8] T. A. Jung, A. Moser, H. J. Hug, D. Brodbeck, R. Hofer, H. R. Hidber, and U. D. Schwarz, *Ultramicroscopy* **42**, 1446 (1992).
- [9] X. Jin and W. N. Unertl, *Appl. Phys. Lett.* **61**, 657 (1992).
- [10] R. W. Stark, S. Thalhammer, J. Wienberg, and W. M. Heckl, *Appl. Phys. A* **66**, S579 (1998).
- [11] M. Heyde, K. Rademann, B. Cappella, M. Geuss, H. Sturm, T. Spangenberg, H. Niehus, *Rev. Sci. Instrum.* **72**, 136 (2001).
- [12] F. J. Rubio-Sierra, R. Vázquez, and R. W. Stark, in: *Proceedings of IMECE2005 2005, ASME International Mechanical Engineering Congress and Exposition, November 5–11, 2005, Orlando, Florida, USA.*
- [13] A. Caron, U. Rabe, M. Reinstädler, J. A. Turner, and W. Arnold, *Appl. Phys. Lett.* **85**, 6398 (2004).
- [14] C. K. Hyon, S. C. Choi, S. W. Hwang, D. Ahn, Y. Kim, and E. K. Kim, *Jpn. J. Appl. Phys.* **38**, 7257 (1999).
- [15] J. S. Villarrubia, *J. Natl. Inst. Stand. Technol.* **102**, 435 (1997).
- [16] R. W. Stark, F. J. Rubio-Sierra, S. Thalhammer, and W. M. Heckl, *Eur. Biophys. J.* **32**, 33 (2003).
- [17] U. Rabe, K. Janser, and W. Arnold, *Rev. Sci. Instrum.* **67**, 3281 (1996).
- [18] R. W. Stark, G. Schitter, M. Stark, R. Guckenberger, and A. Stemmer, *Phys. Rev. B* **69**, 085412 (2004).
- [19] C. Martin, G. Rius, X. Borrisé, and F. Pérez-Murano, *Nanotechnology* **16**, 1016 (2005).

Torsion mode atomic force microscopy and image processing for the analysis of protein-DNA complex binding site

Submitted (2008)

Gilberto Weissmüller, Ayhan Yurtsever, Lilian T. Costa, Ana B. F. Pacheco,
Paulo M. Bisch, Wolfgang M. Heckl, Robert W. Stark

Torsion mode atomic force microscopy and image processing for the analysis of protein-DNA complexes

Gilberto Weissmüller¹, Ayhan Yurtsever², Lilian T. Costa^{2,3}, Ana B. F. Pacheco¹,
Paulo M. Bisch¹, Wolfgang M. Heckl^{2,4}, Robert W. Stark²

¹ Instituto de Biofísica Carlos Chagas Filho, Universidade Federal do Rio de Janeiro, Rio de Janeiro, Brazil

² Ludwig-Maximilians-Universität München, Dept. Earth and Environmental Sciences, Theresienstr. 41, 80333 Munich, Germany

³ Materials Metrology Division-National Institute of Metrology, Normalization and Industrial Quality, Duque de Caxias, Brazil;

⁴ Deutsches Museum, Museumsinsel 1, 80538 Munich, Germany

E-mail: gilberto@ufrj.br , stark@nanobiomat.de

Abstract. Precise mapping of protein-binding sites on DNA is an important application of imaging by atomic force microscope in nanobiotechnology. For a reliable measurement of distances on curved molecules an adequate image analysis is required which extracts the DNA contour from topographic AFM data. To this end we propose an image analysis method which provides a rapid and efficient way to obtain the DNA contour together with a physical map of single and/or multiple protein binding sites. This method relies on a calculation of the height profile along the DNA fragment, which allows for the precise determination of the DNA length and the relative position of the binding site occupied by a single protein molecule. As a first test, complexes of the LexA repressor protein from the *Escherichia coli* SOS system and DNA fragments containing a specific LexA binding site (*recA* operator) were imaged by Torsional Resonance mode (TR-mode) and analysed using the specialized algorithm.

PACS: 68.37.Ps, 07.05.Pj, 87.14.Gg

Keywords: atomic force microscope, AFM, torsional resonance, image processing, DNA

1. Introduction

Mapping protein-binding sites on individual DNA molecules is one important application of AFM imaging. The analysis of highly resolved AFM data allows one to quantify the level of promoter occupancy by a regulatory protein or to study dynamic interactions in solution [1]. To this end it is necessary to find the relative location of the protein along the DNA molecule. Here, mathematical algorithms help to calculate the contour length of DNA fragments from AFM data [2].

The force sensor of the atomic force microscope (AFM) vibrates parallel to the sample surface in the shear force mode of operation. This mode allows one to image the specimen without the strongly varying contact forces that are usually associated with other dynamic AFM modes. Different force sensors haven been suggested for shear force operation. High resolution imaging in shear force mode could be achieved with modified tuning fork sensors [3]. Reliable DNA imaging was demonstrated using modified optical fibres in transverse dynamic force microscopy [4]. Recently, the torsional resonance mode (TR mode) was introduced which allows for shear force microscopy with standard AFM cantilevers [5]. In this mode, the cantilever is driven near to its fundamental torsion resonance frequency (1-2 MHz). The torsion along the cantilever long axis promotes a small pendulum-like oscillation of the tip apex with amplitudes of typically 0.2 to 2.0 nm as illustrated in figure 1.

In this work, we demonstrate the capability of torsional resonance mode for imaging of DNA protein interaction and discuss an image processing tool which determines the DNA length together with the protein binding position with minor custom intervention. This algorithm enables an efficient mapping of single or multiple protein-binding sites on DNA. The algorithm was designed to determine the axial line of DNA molecules together with the height profile along this line. These profiles are also used to detect the position of bound proteins. As a biological model system we used the complex DNA-LexA. LexA is a repressor protein which controls a complex response to DNA damage or inhibition of DNA replication, binding to the regulatory regions of approximately 30 genes in the *Escherichia coli* genome [6].

2. Materials and methods

LexA protein was overexpressed in *E. coli* strain BL21 (\square DE3) carrying the plasmid pJWL228, in which *lexA* is fused to a T7 RNA polymerase promoter (kindly supplied by J.W. Little, University of Arizona, Tucson, AZ). Bacteria cultivation, expression, and purification of LexA were performed as described previously [7]. Purified LexA protein was stored in buffer (50 mM Tris.HCl pH 7.2, 200 mM NaCl, 0.1 mM EDTA, and 5% glycerol), in liquid nitrogen.

The LexA binding site (5'-TACTGTATGCTCATACAGTA-3') located in the regulatory region of the *recA* gene of *E. coli* was inserted in the EcoRI site of plasmid pIC552 (9.3 Kb) [8]. The recombinant plasmid was digested with HindIII and PstI and DNA fragments, containing the *recA* operator were purified from agarose gel using the CONCERT Rapid Purification System (GIBCO BRL) as recommended by the manufacturer. DNA fragments (0.7 nM) and LexA (27 nM) were mixed in a buffer containing 10 mM Tris.HCl pH 8.0 and 15 mM MgCl₂, and incubated for 30 minutes at room temperature keeping a DNA:LexA dimer proportion of 10:1. A volume of 10 \square l of the binding reaction was deposited on freshly cleaved mica. After 10 min incubation at room temperature, it was rinsed with de-ionised water (18 M Ω) during a 2 min vortex, dried under vacuum and used for AFM imaging, as described below.

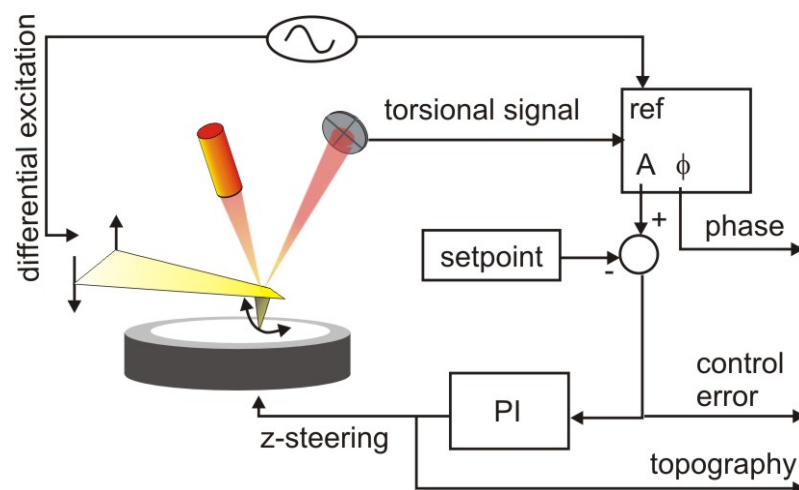


Figure 1. Scheme of the TR mode imaging system. Two piezos oscillating out of phase are used to promote a lateral vibration of the tip.

An AFM (Dimension 3100 SPM, DI-Veeco, Santa Barbara, CA) with modifications for the TR mode was used. Measurements were performed with silicon (NSC35) cantilevers with a

flexural stiffness of $k=2.5\text{N/m}$, a nominal tip radius $r<10\text{ nm}$, and a torsional vibration frequency of about 1.2 MHz. AFM images were pre-processed in SPIP and then exported to our custom software. The code for analysis of AFM images was implemented in Igor Pro 5 (WaveMetrics, Inc., Lake Oswego, OR).

3. Results and Discussion

The protein-DNA complexes were formed between LexA protein and DNA fragments containing a specific LexA binding site which is a 20 bp sequence corresponding to the *recA* gene regulatory region. The protein-DNA complex was imaged by TR-mode as shown in Fig 2. The operating conditions were adjusted to achieve “hard” imaging conditions with a set-point to amplitude ratio of 60 %. The typical height of DNA in this image was less than 0.5 nm. Remarkably, our measured DNA height is a factor of five smaller than the diameter of the DNA Watson-Crick structure of 2.4 nm [11]. This result is not surprising since in earlier shear force scanning probe experiments a DNA height of 1.6 nm was reported for optimized imaging conditions [12]. Similar discrepancies between the diameter of the Watson-Crick structure and measured DNA heights have been reported for standard imaging modes. DNA heights measured by amplitude or frequency modulation AFM critically depend on the operating conditions. It was shown that heights between 0.4 nm and 1.2 nm can be measured depending on driving frequency and amplitude set-point [13]. In the light of these earlier findings our results indicate that topography measurements on soft samples in TR-mode deserve further attention in order to clarify the relation between measured heights and operating conditions.

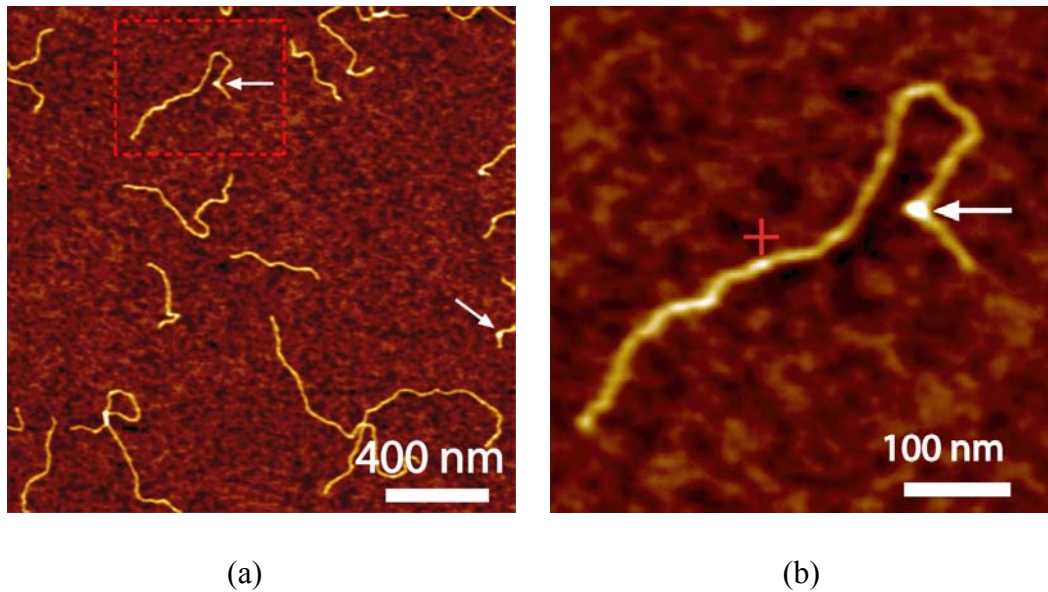


Figure 2. Topographic images of protein-DNA complexes obtained by TR-mode (color scale: 1.2 nm). (a) Overview. (b) The arrow indicates a LexA protein dimer bound to DNA. The cross represents the initial custom chosen location which defines the molecule of interest.

In order to separate the DNA molecule from the background data automatically, first the backbone of the DNA contour has to be identified. Our method to find the axial line of the molecule is based on local contrast gradient search. Therefore images have to be pre-processed to remove any non-uniform background. The AFM images were first processed by a line-wise correction algorithm. Since the small surface corrugation can be affected by the noise, this can lead to steps between subsequent scan lines. To remove the background noise and to flatten the AFM data, the image was corrected by leveling each scan line. Subtraction of a Least Median Squares (LMS) polynomial fit applied to the individual scan lines was sufficient to flatten the images. Ordinary least squares perform poorly in terms of robustness because a single, aberrant data point, or outlier, can change the fitted line way off. The smallest percentage of bad data that can cause the fitted line to explode is defined as the breakdown point. Since a single bad data point can invalidate the least squares polynomial fit, LS have a zero breakdown point. LMS has the highest possible breakdown point of 50% and, therefore, it is extremely resistant to contaminated data.

Unlike usual image filters, which transform the image to enhance particular characteristics such as lines or edges, we needed a processing algorithm to extract specific information from the image. We had first to select the molecule to be analyzed at the pre-treated image. Placing

a graphic cursor near to a horizontal segment of the DNA molecule (fig. 2), the algorithm first finds the exact vertical (y) position of the molecule to that chosen x position. Then, in a similar way to the compass edge detection [9], a set of eight height (z) mean values around that point are calculated (fig. 3). The next (x,y) point is chosen by taking the higher z mean value to the right, so that in each step, the gradient is maximized. The process continues until a custom chosen number of pixels is reached. The same procedure is taken to the left side of the graphic cursor.

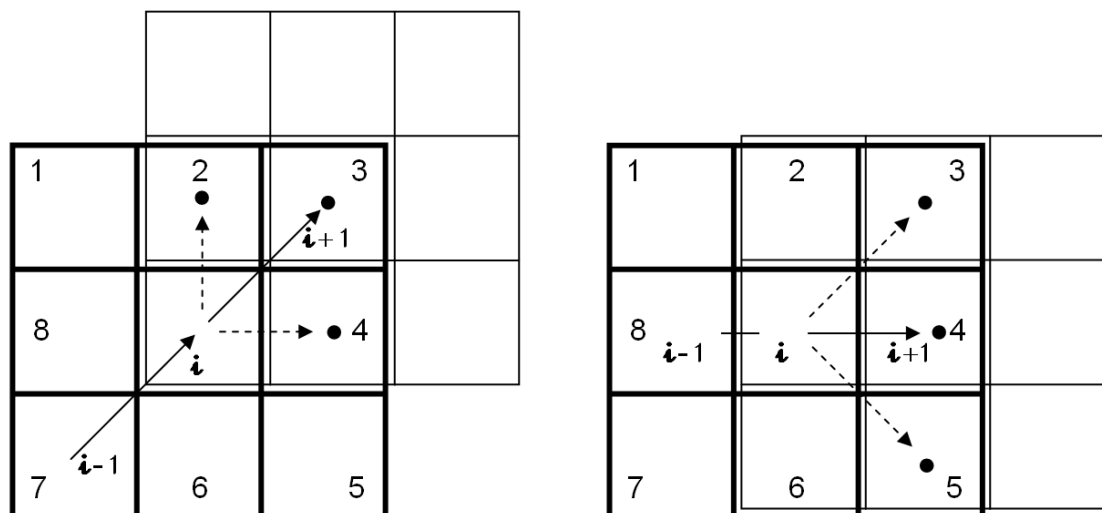


Figure 3. The search of the next pixel $i+1$, representing the DNA line axis, depends on the pixel $i-1$. The only possible candidate as the next ($i+1$) pixel, among the eight possible directions, is the pixel in the same direction or the two neighbouring pixels, which correspond to an expected slight bending of the molecule.

Noise has normally a much higher spatial frequency than the DNA molecule along its axis, which bends gradually on the surface. Therefore, as shown in Fig. 3, we can constrain the search for each next pixel, to only three pixels, depending on the last one. This procedure works like a low-pass filter, stabilizing the search method. In this way, a continuous sequence of pixels is found along the DNA line, which can be stored in an array, as shown in fig 3a. The DNA molecule height vs. length profile is automatically found by the convolution of this array with the original image (fig. 4a). Protein recognition of specific DNA sequences can involve changes in the local structure and conformation of the binding partners, including curvature, bending and flexing of DNA at the protein binding site [10]. The image processing algorithm can calculate a DNA bending angle from the DNA line axis by fitting a straight line before and after the protein location. The measured angle was approximately 74° as shown in

fig. 4 a. Any protein bound to DNA is easily detected by a height peak at this profile (fig. 4b). The total length of the molecule and the position of the protein have to be manually determined using the placement of graphic cursors at the profile. For the molecule shown in fig. 2, the total length was 812 nm and the protein binding site is located at 93 nm from the nearest end.

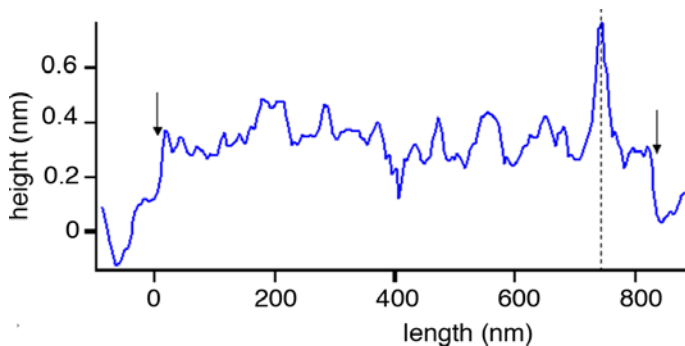
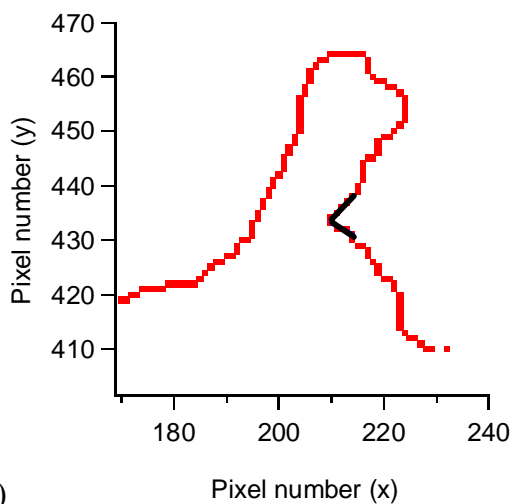


Figure 4. Analysis of the DNA in fig. 2b. (a) The bending angle at the protein binding site is calculated by fitting a line at the protein location (74°). (b) Height profile along the axis. The arrows delimits the molecule and the dashed line defines the protein at 721 nm.

4. Conclusions

Although, the relation between operating conditions and measured topographic height of DNA remains to be clarified we have proven that the contrast makes shear force imaging a valuable tool for protein-DNA complex studies. In this work we also presented an image analysis method developed to map single or multiple protein-binding sites on DNA. The algorithm applied to line-wise flattened images could find the DNA contour line in a very stable way. From the reconstructed line axis, the bending angle at kink sites can be calculated. The algorithm needs very few user interventions and represents an important step toward a fully automated analysis of DNA-protein AFM images.

Acknowledgments

We thank Dr. Ronaldo Mohana-Borges and Francisco J. R. Sousa for purification of LexA protein and also J. Guyer for Igor Pro procedures (JEG NanoLoader). This work was supported by Fundação Univ. José Bonifácio (FUJB), Conselho Nac. de Desenvolvimento Científico e Tecnológico (CNPq), Coordenação de Aperfeiçoamento de Pessoal de Nível Superior (CAPES-PROBAL) and Fundação de Amparo à Pesquisa Carlos Chagas Filho do Estado do RJ (FAPERJ). LTC was supported by Alexander von Humboldt fellowship. AY and RWS thank the German Federal Ministry BMBF for financial support (Nanofutur Grant No. 03N8706).

References

- [1] Gaczynska M., Osmulski P A, Jiang Y, Joon-Kyu Lee, Bermudez V and Hurwitz J 2004, *Proc. Natl. Acad. Sci. U.S.A.*, **101**:52.
- Jiao Y., D.I. Cherny, G. Heim, T.M. Jovin and T.E. Schäffer 2001, *J. Mol. Biol.*, **314**:233-243.
- Moreno-Horrero F., P. Herrero, J. Colchero, A.M. Baró and F. Moreno, 2001, *Biochem. Biophys. Res. Co.*, **280**:151-157 .
- Pastushenko V. Ph., R. Kaderabek, M. Sip, C. Borken, F. Kienberger and P. Hinterdorfer 2002, *Single Mol.* **3**, 111-117.
- Yokota H., D.A Nickerson., B.J. Trask, G. Van den Engh, M. Hirst, I. Sadowski and R. Aebersold 1998, *Anal. Biochem.*, **264**:158-164.
- [2] Y.Fang, T.S. Spisz, T. Wiltshire et al. 1998, *Anal.Chem.* **70**, 2123-2129.
- T.S.Spitz, Y. Fang, R.H. Reeves, C.K. Seymour, I.N. Bankman, J.H. Hoh 1998, *Med. Bio. Eng. Comput.* **36**: 667-672

- F. Jamitzky, R.W. Stark, G. Morfill, W.M. Heckl 1998, *J. Computer-Assisted Micr.* **10** (2): 57-62
- A.Sanchez-Sevilla, J. Thimonier, M. Marilley, J. Rocca-Serra, J. Barbet, 2002 *Ultramicroscopy* **92**: 151-158.
- [3] Göttlich H., R.W. Stark, J.D. Pedarnig, W.M. Heckl 2000, *Rev. Sci. Instr.*, **71**:3104-3107.
- [4] Antognozzi M, Szczelkun M D, Round A N and Miles M J 2002 *Single Mol.* **3**:105-110.
- [5] Huang L. and C. Su, A 2004, *Ultramicroscopy* **100**:277-285.
- [6] Fernandez de Henestrosa A R., Ogi T, Aoyagi S, Chafin D, Hayes J J, Ohmori H and Woodgate R 2002, *Mol. Microbiol.*, **35**:1560-1572.
- Little, J. W. and D. W. Mount 1982, *Cell*, **29**:11-22.
- [7] Little J.W., B. Kim, K.L. Roland, M.H. Smith, L.L. Lin and S.N. Slilaty 1994, *Methods Enzymol.*, **244**:266-284.
- [8] Macian F., I. Perez-Roger and M.E. Armengod 1994, *Gene*, **145**:17-24.
- [9] Gonzalez and Woods, *Digital Image Processing - 2nd Edition - Prentice Hall* (2002).
- [10] Harrington R.E., 1992, *Mol Microbiol.*, **6**(18):2549-55.
- [11] Watson J. D. and F. H. C. Crick 1953 *Nature* **171**: 737–8.
- [12] Antognozzi M., Szczelkun M. D., Round A. N. and Miles M. J. 2002 *Single Mol.* **3** 105–10
- [13] Nony L., R. Boisgard and J.-P. Aimé 2001, *Biomacromolecules* **2**: 827-835.
- Round A.N. and M. J. Miles 2004, *Nanotechnology* **15**: S176-S183.

Amplitude and Frequency Modulation Torsional Resonance Mode Atomic Force Microscopy

Submitted (2008)

Ayhan Yurtsever, Alexander M. Gigler, and Robert W. Stark

Amplitude and Frequency Modulation Torsional Resonance Mode Atomic Force Microscopy

Ayhan Yurtsever, Alexander M. Gigler, and Robert W. Stark*

Dept. of Earth and Environmental Sciences, Ludwig-Maximilians-Universität München,
Theresienstr. 41, 80333 Munich, Germany

*corresponding author Tel/Fax: +49 89 2180 4329 / 4334

E-mail: stark@lrz.uni-muenchen.de

Abstract. Scanning probe imaging in a shear force allows for the characterization of in-plane surface properties. In a standard AFM shear force imaging can be realized by the torsional resonance mode. In order to investigate the imaging conditions on mineral surfaces a torsional resonance mode atomic force microscope was operated in amplitude and frequency modulation feedback. A freshly cleaved chlorite surface was investigated which showed brucite-like and talc-like surface areas. In constant amplitude FM mode, a slight variation in the energy dissipation could be observed for both surfaces. Amplitude and frequency vs. distance curves revealed that the tip was in repulsive contact with the specimen during imaging.

PACS: 68.37.Ps, 07.05.Pj, 87.14.Gg

Keywords: atomic force microscope, AFM, torsional resonance, frequency modulation, chlorite, clinocllore

Introduction

Scanning shear force measurements with an atomic force microscope (AFM) provide access to in-plane surface properties such as friction, shear stiffness, and other tribological surface properties with nanometer resolution. In a torsional resonance mode AFM¹, the fundamental torsion mode of the force sensor is used. The excitation of a torsional oscillation is in contrast to classical resonant imaging methods that are based on flexural resonances. Provided small oscillation amplitudes, the motion of the tip is parallel to the surface². Thus, the strong nonlinearities encountered by a flexurally vibrated tip due to the vibro-impact dynamics can be avoided. This implies that the torsional resonance mode is well suited to investigate tribological surface properties.

Several technical concepts were demonstrated which help to achieve and analyze such a pendulum-like oscillation of the tip. Excitation and analysis of the torsional resonances of AFM cantilevers during contact mode experiments allow characterizing in-plane properties of metals or semiconductors³. In an inverted scheme, shear waves induced by a piezoelectric transducer and traveling through the specimen, may also be used as a source of excitation⁴. Furthermore, high-resolution imaging in shear force mode has been achieved by an STM tip⁵ or AFM sensor⁶ mounted to the prong of a tuning fork. In this case, the tuning fork serves as a detector for the tip sample interaction. For scanning near-field optical microscopy using optical fibers, the shear-force distance control is a very common method⁷. Based on a similar concept, transverse dynamic force microscopy provides high sensitivity and high resolution⁸.

Most techniques for shear force imaging require a modified force sensor, special substrates, or tailored sample shakers. To alleviate this, a special cantilever holder was introduced recently, which allows the direct excitation of torsional cantilever resonances in standard AFM setups¹. This special type of probe fixation improves the signal level while reducing possible cross talk between flexural and torsional vibrations. In particular, two piezoelectric elements mounted near the cantilever chip drive the tip to a small torsional oscillation. Typically, the tip oscillates close to parallel with the surface at amplitudes smaller than 1 nm and high Q-factors ($Q > 1000$).

Torsional cantilever resonances allow for the quantitative characterization of in-plane sample properties such as friction or shear stiffness⁹. Using the fundamental torsional resonance, Pfeiffer et al.¹⁰ could measure friction on the Cu (100) surface in UHV. Kunstmann et al.¹¹

demonstrated a combined normal and torsional measurement mode working in frequency-modulation. In general, frequency modulation (FM) techniques in atomic force microscopy¹² have proven to be powerful tools to achieve atomic resolution¹³. In order to explain the contrast mechanisms in detail, the imaging dynamics of frequency modulated AFM was investigated extensively, both in theory¹⁴ and experiment¹⁵. In spectroscopic applications, FM techniques open the door to study the local energy dissipation which can be related to mechanical and electrical surface properties¹⁶. Frequency modulation in shear force imaging was shown to enhance the performance of topographic surface profiling^{17,18}. The relation between frequency shift, distance, and amplitude has been determined for optical fibers as force sensors¹⁹.

In the following, we discuss shear force imaging of a mineral surface with a torsional resonance mode AFM operated in amplitude and frequency modulation feedback. Using the FM technique, both frequency shift and energy dissipation can be mapped to topographic surface features under ambient conditions. In order to clarify the fundamental imaging process in torsional resonance AFM frequency shift vs. distance curves help to identify the operation regime non-contact vs. contact.

Materials and methods

A Dimension 3100 atomic force microscope with a NanoScope IV controller was used for the experiments. The instrument was equipped with a cantilever holder for torsional resonance mode (Veeco Metrology Inc., Santa Barbara, CA). A torsional resonance mode cantilever holder contains two dither piezos driven out of phase in order to induce torsional oscillations of the cantilever. Silicon cantilevers with a nominal spring constant of 20 N/m were used for the measurements (ZEIHR Nanosensors, Neuchatel, Switzerland). Cantilevers with a flexural resonance frequency of less than 120 kHz and a torsional resonance frequency below 1 MHz (typically 910 kHz) were selected. A spring constant of typically $19 (\pm 4)$ N/m was found for these cantilevers by standard calibration procedures²⁰. Amplitude modulation experiments were carried out with the system as delivered by the manufacturer (Fig. 1 (a)). A frequency modulation feedback was realized with an external phase-locked-loop unit (Easy PLL plus detector and controller, Nanosurf AG, Liestal, Switzerland). The FM unit was connected to the microscope controller via a signal access module, as sketched in Figure 1 (b). The microscope controller was set to standard operation, while the signals for feedback were

provided by the external electronics. Tracking of the resonant frequency was achieved by the PLL unit, while an automatic gain control (AGC) kept the oscillation amplitude constant (CA-Mode). The frequency shift was used as control signal for the z-feedback loop keeping the frequency shift constant. Note that the tip has to be engaged very carefully since the cantilever is very stiff and thus the tip can easily destroy the delicate surface structure of the specimen. Image processing was done using the software package SPIP (Image Metrology, Lyngby, Denmark).

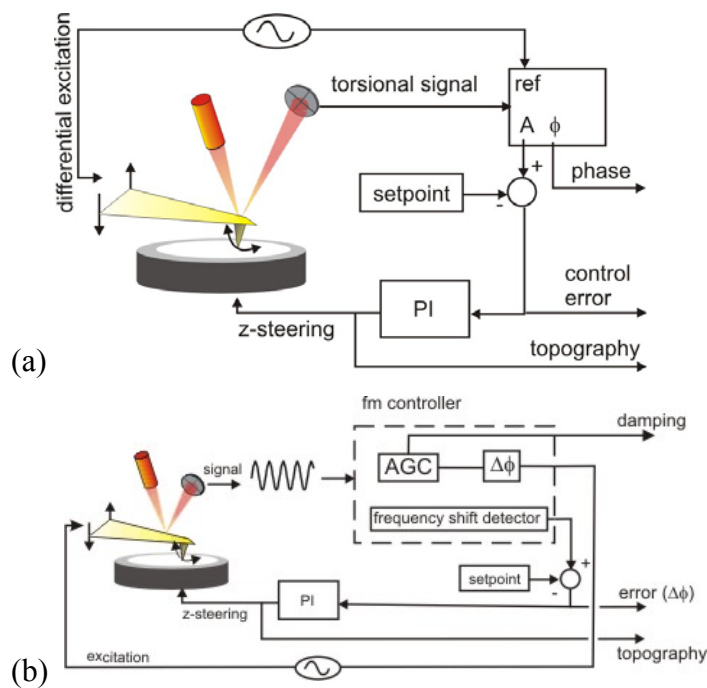


Figure 1. Scheme of the feedback circuitry used for (a) amplitude and (b) frequency modulation of torsional resonance imaging. The torsion signal is measured by a quadrant photodiode. (a) For AM the lock-in was used as delivered by the manufacturer. (b) For FM detection the torsion signal (signal left - right) was pre-amplified and then fed into the FM-controller. The frequency shift signal was used for feedback the damping was detected as amplitude variation by the automatic gain control (AGC).

A pennine specimen (also known as penninate) was cleaved (origin: Rimpfischwäng, Zermatt, Switzerland, Sample #17984 of the Bavarian Mineralogical State Collection, Munich). The mineral pennine is a variety of clinocllore ($Mg,Fe^{2+})_5Al[(OH)_8|AlSi_3O_{10}]$ and belongs to the chlorite group. The chlorite clinocllore is a 2:1:1 phyllosilicate consisting of alternating brucite-like and T-O-T (tetrahedral-octahedral-tetrahedral) layers which correspond to talc²¹. The brucite-like surface exhibits OH groups and is positively charged in the bulk whereas the talc-like layer presents oxygen and is negatively charged. Compared to muscovite micas,

where the layers are connected by an interlayer of K^+ cations, this interlayer is substituted by a full octahedral-sheet (brucite) in clinochlore. Thus, the T-O-T and brucite sheets are connected by hydrogen bonds between the layers²². Clinochlore is monoclinic with the cell parameters $a = 5.325 \text{ \AA}$, $b = 9.267 \text{ \AA}$, $c = 14.27 \text{ \AA}$, $\beta = 96.35^\circ$. The step height of a single layer is about 0.5 nm for brucite and 0.9 nm for T-O-T.

Results and Discussion

We imaged freshly cleaved chlorite to demonstrate the capabilities of the torsional resonance mode to image delicate specimen. Clinochlore exhibits heterogeneous surface properties due to alternating mineral layers. On such a freshly cleaved sample, both surface areas can be observed within a few square micrometers. Due to its heterogeneous surface properties after cleavage, chlorite minerals recently gained attention as substrates for the preparation of DNA samples²³. In the following we focus on friction measurements by torsional resonance mode AFM.

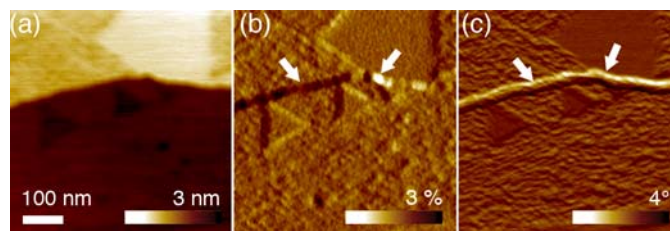


Figure 2. Torsional resonance mode images of the clinochlore surface obtained in amplitude modulation. (a) Topography, (b) amplitude (c) and phase. The amplitude in (b) is given relative to the amplitude set-point of 0.5 V.

For a comparison between amplitude and frequency modulation imaging we first imaged the mineral surface in amplitude modulation. This means that the amplitude was used for topography imaging while the phase between driving and response is used to create the phase image. In AM operation the excitation frequency was fixed to the maximum of the resonance peak as measured far away from the surface. Figure 2 shows images obtained in amplitude modulation. The scan direction was horizontally from right to left while the torsional oscillation was in vertical direction. The large step between the bright and the dark area of the height image in Fig. 2 (a) was $1.5 (\pm 0.1) \text{ nm}$, which is compatible with the height of the unit cell. The images at the step show interesting feature. In the amplitude image in Fig. 2 (b) the typical feedback errors of a scan in right to left direction prevailed while the phase image Fig. 2 (c) showed a variation between dark and bright at the vertical edge. Note that the dark bright

contrast remains the same while the feedback control error changes sign (arrows in Fig 2 (b) and (c)). The phase contrast at the edge is explained by the oscillating tip interacting with the edge laterally. An attractive lateral interaction can lead to a softening of the lateral interaction potential. Additionally, a repulsive interaction limits the oscillation when the tip is on the lower side of the step. The dark rim is less than 10 nm wide (full width at half maximum depth) which provides an upper boundary for the tip oscillation amplitude in this experiment (neglecting tip geometry and long range interactions). On the plateau close to the edge, the effective contact area is reduced decreasing elastic coupling and friction.

The topography image in Fig 2 (a) also showed a bright triangle on the upper right which was elevated by approximately $0.4 (\pm 0.1)$ nm with respect to the upper plateau. This feature may be explained as a brucite layer lying on top. The triangular holes are about $0.2 (\pm 0.1)$ nm deep. One plausible explanation for this feature is a missing tetrahedral layer in the T-O-T sheet. However, when discussing feature heights obtained in AM torsional resonance mode one should keep in mind that the oscillation amplitude can also encode friction. On features with increased friction, the feedback will retract the tip in order to compensate for the friction and vice versa. In the case of this mineral surface, the effect will be rather small since the phase image in Fig 2 (c) only shows a weak contrast, which implies only small frictional variations. However, in order to assess the influence of friction on the topography imaging in AM torsional resonance mode more precisely, an additional frequency modulation experiment is needed.

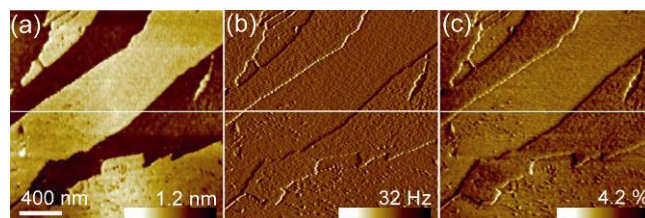


Figure 3. Images obtained in FM torsional resonance mode on a clinocllore (001) surface. On the surface brucite-like stripes are visible on a talc-like T-O-T layer. (a) Topographic image with the frequency error (Δf) z-control. Image (b) shows the frequency shift tracking error. Image (c) shows AGC output which corresponds to the dissipation. The color scale encodes the deviation from the mean dissipation in the image.

In the FM experiment, the oscillation amplitude of the cantilever was maintained by an automatic gain control (AGC). The shift in resonance frequency was used for topographic feedback regulation, while the output of the AGC provided a measure for the energy dissipation. Figure 3 shows maps of (a) topography, (b) frequency shift, and (c) energy dissipation measured simultaneously using the AGC in constant amplitude mode on the mineral surface. These data were obtained in a constant amplitude operation at a detuning set-point of 40 Hz. The frequency shift set-point was minimized in order to avoid sample damage. The topographic information (Fig. 3 (a)) shows distinct areas which are separated by 0.5 nm-steps. We conclude from the topographic information, that the topmost layer was brucite-like. In a perfectly structured clinocllore the second layer is a T-O-T sheet. In order to discern the different surfaces, additional information on the surface properties is necessary. The detuning of the oscillation frequency as shown in Figure 3 (b) cannot carry additional information on surface composition, because it is used as an input signal for FM-feedback. The dissipation image in Figure 3 (c), however, provides additional information on frictional properties. A small contrast between the different layers can be observed.

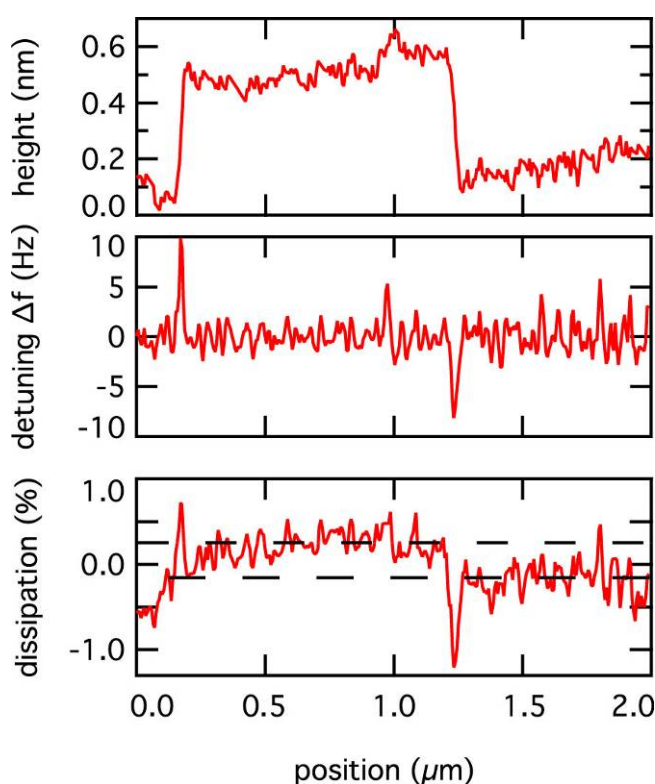


Figure 4. Cross sectional analysis of the image data shown in **Fig.3**

The cross sectional analysis of Figure 3 reveals a step height of 0.5 nm (Fig. 4). In the cross section of the detuning signal only a very small tracking error is found, which can be attributed to the response of the control loop. The contrast in dissipation between both surfaces is 0.5 % with respect to the dissipation averaged over the entire image. On the brucite-like surface, we observe less friction than on the talc layer. There are several potential origins for this friction contrast, since structure and surface chemistry of both layers are quite different. It is known from high-pressure experiments that the compression of the T-O-T layer of clinocllore involves the tetrahedra only. The octahedral sheets are not compressed even under high pressure conditions²². Thus, one can identify several parameters contributing to a frictional contrast. Firstly, the mechanical coupling between the tip and the brucite surface should be slightly stiffer than the contact with the talc-like surface region. Secondly, with respect to surface chemistry, the brucite-like layer is known to exhibit hydroxyl groups whereas the talc-like layer presents oxygen. Kelvin probe imaging with the same type of cantilever reveals a measured contact potential difference of typically 50 mV (data not shown). Thus, also Joule friction might play a role. Thirdly, both surfaces are structurally slightly different, which can cause differences in the elemental friction processes on the atomic scale. Although the atomistic origin of the friction contrast remains to be clarified several conclusions can be drawn regarding the AM experiment in Fig. 2. On the brucite-like layer energy dissipation is slightly decreased as compared to the TOT layer. In order to assess the possible degree of crosstalk between topography and friction in AM experiments the amplitude vs. distance relation has to be determined.

In order to decouple elastic and dissipative contributions we measured the relation between amplitude and distance in a constant excitation FM scheme. In this experiment the excitation frequency follows the detuning of the force sensor due to elastic coupling between tip and sample. A measured amplitude reduction is thus largely caused by damping¹⁸. A typical approach and retract cycle is shown in figure 5. During approach, the frequency shift, the amplitude reduction, and the vertical cantilever deflection remained at a constant level. At 0 nm, the tip snapped into contact with the surface (asterisk in figure 5). After snap-in, the cantilever deflection was negative, i.e. the cantilever was bent towards the sample by -4 nm (-80 nN). Coincidentally, an increasing detuning and a decrease of the oscillatory amplitude were observed. Approaching closer, the frequency detuning increases and the cantilever deflection towards the surface decreases until the cantilever deflection nearly reached zero at a detuning of 600 Hz. The cantilever deflection was nearly fully balanced at about 5 nm after the snap-in.

This snap-in can be explained by strong attractive forces due to van der Waals interaction and capillary condensation which induced a liquid neck between tip and sample during approach. The attractive surface forces pulled the cantilever towards the surface causing a frictional contact between tip and sample. The strong attractive force of about 80 nN at snap-in is typical for such high energy surfaces such as mica. The signals acquired during the approach-retract-cycle exhibited a strong hysteresis. Passing the point of snap into contact, the tip seemed to have gradually detached from the surface, which can be explained by pulling on the liquid neck. At a z-position of -5 nm, the tip finally detached from the surface.

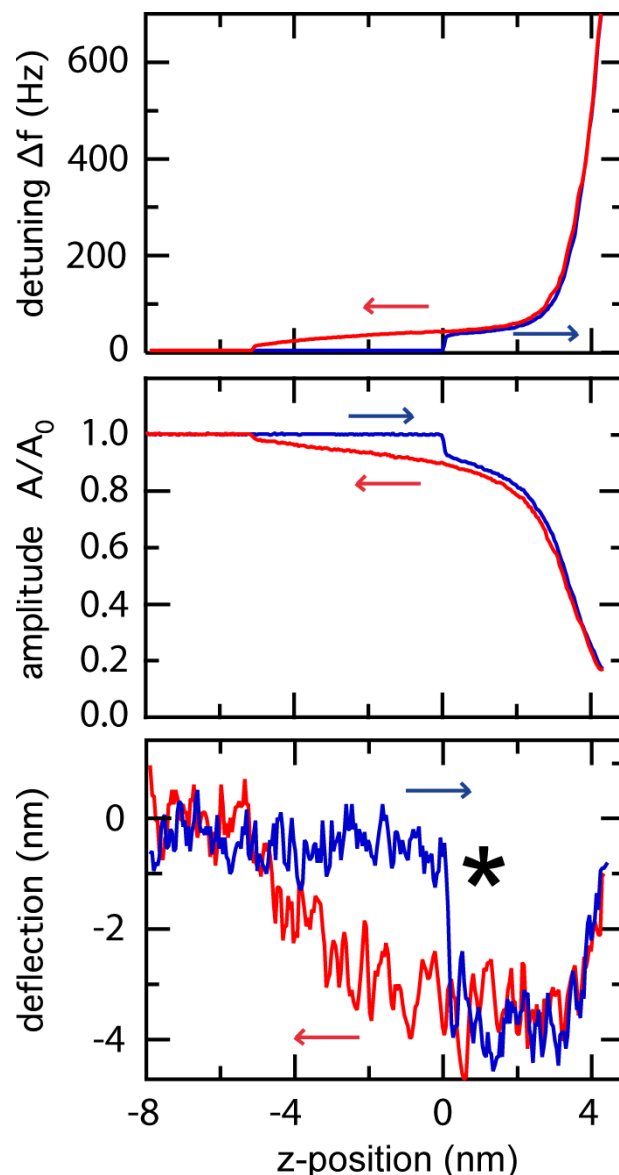


Figure 5. Dynamic approach and retract curves acquired in constant excitation mode. Torsional resonance detuning and oscillation amplitude were measured together with the static flexural cantilever deflection. The arrows indicate the direction of motion during data acquisition. The asterisk marks the snap-in which is associated with the onset of detuning and energy dissipation.

Several conclusions can be drawn from this experiment. At 50 % amplitude - which is a typical set-point for AM torsional resonance mode - the slope of the amplitude curve was approximately 0.5/nm. Due to the variation of surface properties, the energy dissipation on the brucite layer was increased by 0.5 %. In an AM feedback, this damping thus corresponds to a height difference of 0.1 Å, which is much smaller than the lattice parameters. Thus, on the clinocllore sample, the height error due to friction was negligible. However, large variations of the energy dissipation as they can occur e.g. on diblock co-polymers¹⁸ may affect the height measurements. In general, possible crosstalk between topography and friction in AM torsional resonance mode can be minimized by choosing an amplitude set-point at the steep part of the amplitude vs. distance curve.

The detuning vs. distance experiment also helps to answer the question if the tip-sample interaction was repulsive or attractive. The experimental results clearly show that for imaging at a frequency-shift set-point on the order of ten Hertz, the tip was in mechanical contact with the specimen. The contact was established by bending the tip towards the surface. Thus, the attractive interaction between tip and sample was balanced by the probe stiffness and an increasingly repulsive interaction as the set-point was increased. Although the image was taken close to the critical frequency shift for imaging, the experiment of Figure 3 can be understood as a shear force experiment where the degree of repulsive interaction could be varied by variation of the detuning set-point. In order to possibly stabilize the probe in the attractive regime and to avoid a snap to contact on a high-energy surface such as chlorite, stiffer cantilevers with higher resonant frequencies are needed.

In summary, torsional resonance mode images were obtained on a clinocllore surface with a amplitude and frequency modulation feedback. In both modes stable and non-destructive imaging could be obtained. In FM-mode an image contrast between exposed brucite-like and T-O-T layers was achieved in the topography and dissipation signals. From the frequency shift vs. distance curves we conclude that stable imaging can be obtained while the tip is in repulsive contact with the specimen in both AM and FM mode. This means that the image contrast observed in the dissipation channel in an FM experiment is a frictional contrast. With FM torsional resonance mode a wide field of applications in tribology can be addressed. In-

plane sample properties such as friction can be addressed dynamically with a very spatial high resolution.

Acknowledgments

We gratefully acknowledge financial support by the German Federal Ministry of Education and Research (BMBF) Nanofutur grant 03N8706 and the DFG cluster of excellence “Nanosystems Initiative Munich”. AY is supported by the scholarship of the Elite Network of Bavaria, International Doctorate Program Nano-Bio-Technology (IDK-NBT).

References

- ¹ L. Huang and C. M. Su, *Ultramicroscopy* **100** (3-4), 277 (2004).
- ² A. Yurtsever, A. M. Gigler, E. Macias, and R. W. Stark, *Appl. Phys. Lett.* **91** (25), 253120 (2007).
- ³ T. Drobek, R.W. Stark, M. Gräber, and W.M. Heckl, *New J. Phys.* **1**, 15 (1999); T. Drobek, R. W. Stark, and W. M. Heckl, *Phys. Rev. B* **64** (4), 045401 (2001).
- ⁴ H. U. Krottil, T. Stifter, and O. Marti, *Appl. Phys. Lett.* **77** (23), 3857 (2000); M. Reinstädler, U. Rabe, V. Scherer, U. Hartmann, A. Goldade, B. Bhushan, and W. Arnold, *Appl. Phys. Lett.* **82** (16), 2604 (2003).
- ⁵ K. Karrai and R. D. Grober, *Appl. Phys. Lett.* **66** (14), 1842 (1995); K. Karrai and I. Tiemann, *Phys. Rev. B* **62** (19), 13174 (2000).
- ⁶ H. Göttlich, R. W. Stark, J. D. Pedarnig, and W. M. Heckl, *Rev. Sci. Instrum.* **71** (8), 3104 (2000).
- ⁷ R. Brunner, O. Marti, and O. Hollricher, *Journal of Applied Physics* **86** (12), 7100 (1999).
- ⁸ M Antognozzi, MD Szczelkun, AN Round, and MJ Miles, *Single Molecules* **3** (2-3), 105 (2002).
- ⁹ M. Reinstädler, T. Kasai, U. Rabe, B. Bhushan, and W. Arnold, *J. Phys. D Appl. Phys.* **38** (18), R269 (2005).
- ¹⁰ O. Pfeiffer, R. Bennewitz, A. Baratoff, E. Meyer, and P. Grutter, *Phys. Rev. B* **65** (16) (2002).
- ¹¹ T. Kunstmann, A. Schlarb, M. Fendrich, D. Paulkowski, T. Wagner, and R. Moller, *Appl. Phys. Lett.* **88** (15) (2006).

- ¹² T. R. Albrecht, P. Grutter, D. Horne, and D. Rugar, *J. Appl. Phys.* **69** (2), 668 (1991).
- ¹³ Y. Sugawara, M. Ohta, H. Ueyama, and S. Morita, *Science* **270** (5242), 1646 (1995); F. J. Giessibl, *Science* **267** (5194), 68 (1995); K. Fukui, H. Onishi, and Y. Iwasawa, *Phys. Rev. Lett.* **79** (21), 4202 (1997).
- ¹⁴ M. Gauthier and M. Tsukada, *Phys. Rev. Lett.* **85** (25), 5348 (2000); B. Gotsmann, B. Anczykowski, C. Seidel, and H. Fuchs, *Appl. Surf. Sci.* **140** (3-4), 314 (1999); L. N. Kantorovich and T. Trevethan, *Phys. Rev. Lett.* **93** (23), 236102 (2004).
- ¹⁵ T. Fukuma, T. Ichii, K. Kobayashi, H. Yamada, and K. Matsushige, *J. Appl. Phys.* **95** (3), 1222 (2004); S. P. Jarvis, H. Yamada, K. Kobayashi, A. Toda, and H. Tokumoto, *Appl. Surf. Sci.* **157** (4), 314 (2000); C. Loppacher, R. Bennewitz, O. Pfeiffer, M. Guggisberg, M. Bammerlin, S. Schar, V. Barwich, A. Baratoff, and E. Meyer, *Phys. Rev. B* **62** (20), 13674 (2000).
- ¹⁶ H. Hölcher, B. Gotsmann, W. Allers, U. D. Schwarz, H. Fuchs, and R. Wiesendanger, *Phys. Rev. B* **64** (7), 075402 (2001); B. Gotsmann and H. Fuchs, *Phys. Rev. Lett.* **86** (12), 2597 (2001).
- ¹⁷ W. A. Atia and C. C. Davis, *Appl. Phys. Lett.* **70** (4), 405 (1997).
- ¹⁸ A. Yurtsever, A. M. Gigler, C. Dietz, and R. W. Stark, *Appl. Phys. Lett.* **92**, 143103 (2008).
- ¹⁹ I. I. Smolyaninov, W. A. Atia, S. Pilevar, and C. C. Davis, *Ultramicroscopy* **71** (1-4), 177 (1998).
- ²⁰ J. E. Sader, J. W. M. Chon, and P. Mulvaney, *Rev. Sci. Instrum.* **70** (10), 3967 (1999).
- ²¹ L. Pauling, *Proceedings of the National Academy of Sciences of the United States of America* **16**, 578 (1930); G. W. Brindley, B. M. Oughton, and K. Robinson, *Acta Cryst.* **3**, 408 (1950).
- ²² M. D. Welch and W. G. Marshall, *American Mineralogist* **86** (11-12), 1380 (2001).
- ²³ G. Valdre, M. Antognozzi, A. Wotherspoon, and M. J. Miles, *Philosophical Magazine Letters* **84** (9), 539 (2004); M. Antognozzi, A. Wotherspoon, J. M. Hayes, M. J. Miles, M. D. Szczelkun, and G. Valdre, *Nanotechnology* **17** (15), 3897 (2006).

2. Acknowledgements

This work would not have been possible without the help and support of many people. It is my pleasure to express my gratitude to all the people supporting me during my PhD.

First of all, I would like to thank my supervisor PD Dr. Robert Walter Stark, for giving me the opportunity to work in his research group at the Ludwig-Maximilians-Universität (LMU). He has provided me not only a working position in his group but also accompanied all my work. Moreover, I thank for his inspiring and encouraging way to guide me to a deeper understanding of scientific work, and his invaluable comments during the formation of this dissertation. I wish to thank him for everything he has taught me, and for the friendly relationship we have had over the years.

I want to thank Prof. Wolfgang Heckl for giving me the opportunity to work in his NanoScience research Group

Many thanks to Dr. Alexander Gigler for his fruitful scientific discussions about my PhD work and his advises about writing scientific papers.

This whole thesis could not have looked like it is without my friends, Marc Hennemeyer, Ferdinand Walther, Michael Bauer and Dr. Javier Rubio Sierra. I more than appreciate for their help. The technical assistance of Stefan Burghardt is gratefully acknowledged.

I want to thank Christian Dietz from the Technical university of Chemnitz for providing us polymer samples.

I want to thank Prof. Gilberto Weissmüller from the Instituto de Biofísica Carlos Chagas Filho, Universidade Federal do Rio de Janeiro, for the collaboration.

I want to express my gratitude to all the group members for their help to improve my presentation capabilities and their patience during the preparation of the conference talks.

For the financial support I would like to thank the German Federal Ministry of Education and Research (BMBF) under grant 03N8706. I would like to acknowledge the financial and

academic support of LMU and Center for NanoScience (CeNS) for the scholarship through the international Doctorate Program in "NanoBioTechnology".

I also have thanks to my undergraduate advisor Prof. Meral Aydin and Prof. Salim Ciraci from the Bilkent University. I would not have been here today without the inspiration of Prof. Salim Ciraci.

I wish to thank my parents for their constant support and encouragement in my education.

3. Curriculum Vitae

Personal information

Name: Ayhan Yurtsever

Date of birth: March 8, 1976

Place of birth: Ispir, Erzurum, Turkey

Nationality: Republic of Turkey

Education and scientific work

09.1989-08.1992 Secondary school: Ispir Endustri Meslek Lisesi, Erzurum, Turkey

09.1992-06.1994 High school: Ispir Endustri Meslek Lisesi, Erzurum, Turkey

06.1994-06.1999 Undergraduate study: Hacettepe University, Ankara, Turkey
Thesis topics: Renormalization Group Theory in Statistical Mechanics

06.2000-10.2002 Graduate study at Bilkent University Physics, Ankara, Turkey
Master Thesis: Correlation Effects in Coupled Quantum-Well and Quantum-wire systems

11.2004-01.2008 PhD student at Tribology and Nanomanipulation Group (TNMG),
Ludwig-Maximilians-Universität (LMU), Germany

Publications

- 1) **“Frequency modulated torsional resonance mode atomic force microscopy on polymers”**
Ayhan Yurtsever, Alexander M. Gigler, Christian Dietz, and Robert W. Stark, **Applied Physics Letters (APL) 92, 143103 (2008)**

- 2) **“Response of a laterally vibrating nano-tip to surface forces”**
Ayhan Yurtsever, Alexander M. Gigler, R. W. Stark, **Applied Physics Letters (APL) 91, 253120 (2007), Selected in Virtual Journal of Nanoscale Science & Nanotechnology: Vol. 17, 01 (2008)**

- 3) **“Amplitude and Frequency Modulation Torsional Resonance Mode Atomic Force Microscopy”**
Ayhan Yurtsever, Alexander M. Gigler, R. W. Stark, Submitted (2008)

- 4) **“Torsion mode atomic force microscopy and image processing for the analysis of Protein-DNA complex binding site”**
Gilberto Weissmüller, Ayhan Yurtsever , Lilian T. Costa, Ana B. F. Pacheco, Paulo M. Bisch, Wolfgang M. Heckl, Robert W. Stark, **Submitted (2008)**

- 5) **“Acoustical force nanolithography of thin polymer films”**
F. J. Rubio-Sierra , A. Yurtsever , M. Hennemeyer , W. M. Heckl and R. W. Stark, **Physics Status Solidi A, 203 (6), 1481-1486 (2006)**

- 6) **“Frequency modulation torsional resonance mode AFM on chlorite (001)**
Ayhan Yurtsever, Alexander M. Gigler, R. W. Stark, **Journal of Physics, 100, 052033 (2008)**

- 7) **“Many-body effects in the Coulomb drag between low density electron layers”**
Ayhan Yurtsever, V. Moldaveanu, B. Tanatar, **Solid State Com. 125 (2003) 575-579**

- 8) **“Dynamic correlations effects on the Plasmon dispersion in a two-dimensional Electron gas”**

Ayhan Yurtsever, V. Moldaveanu, B. Tanatar, Physical Review B, 67 115308 (2003)

- 9) **“Ladder Approximation in coupled quantum well systems”**

Ayhan Yurtsever, B. Tanatar, Physical Review B, 125320 (2002)

- 10) **“Model boson fluid with disorder in the self-consistent field approximation”**

Ayhan Yurtsever, B. Tanatar, Physics Letters A, 286 (2002), 362-368

- 11) **“Short-range Correlations in Coupled Quantum-wire Systems”**

Ayhan Yurtsever, B. Tanatar, T. Journal of Physics 26 (2002), 237-242

- 12) **“Dynamics imaging of the single-DNA-protein interaction using the torsional resonance mode AFM”**

Ayhan Yurtsever, G. Weissmüller, Lilian T. Costa, R. W. Stark, Proceedings of the VII Annual Linz Winter Workshop

Scientific talks and Contributions

Ayhan Yurtsever, A. M. Gigler, and R. W. Stark: Frequency modulation torsional resonance mode AFM, International NC-AFM conference, 16-20 September, Antalya, Turkey (2007)

Ayhan Yurtsever, A. M. Gigler, and R. W. Stark: Energy dissipation measurement with frequency modulated torsional resonance mode AFM (FM-TR-AFM), International Conference on Nano Science and Technology (ICN+T 2007), Stockholm, Sweden

Ayhan Yurtsever, A. M. Gigler, R. W. Stark: Shear force imaging with frequency modulation feedback in torsional resonance mode, Scanning Probe Microscopies and Organic materials, 26-28 September 2007, Hamburg, Germany

Ayhan Yurtsever, A. M. Gigler, R. W. Stark: Measuring energy dissipation with torsional resonance mode atomic force microscopy in frequency modulation, Regensburg, DPG-Spring- Meeting, 2007-03-26.

Ayhan Yurtsever, A. M Gigler, C. Dietz, R. Magerle, R. W Stark: Frequency modulation torsional resonance atomic force microscopy (FM-TR-AFM) for in-plane surface properties measurement, Macromolecular Systems for NanoScience - Chemistry, Physics and Engineering Aspects", Irsee September 6th-9th 2007, Germany

Ayhan Yurtsever, R. W. Stark: DNA-protein interaction analyzed by shear force AFM, ENNaB-Workshop, BMBF Junior Research Groups in Nanotechnology, April 2006 in München, Germany

Ayhan Yurtsever, R. W. Stark: Local Anodic Oxidation by Atomic Force Microscopy ENNaB-Workshop: Excellence Network NaNoBio Technology, Munich, Germany 2005

F.J. Rubio-Sierra, Ayhan Yurtsever, R. Vazquez, W. M. Heckl, R.W. Stark: Toward controlled surface manipulation at the nanometer scale by atomic force microscopy TNT 2005 "Trends in Nanotechnology", Oviedo, Spain

Ayhan Yurtsever, V. Moldaveanue, B. Tanatar: Coulomb Drag effect on bilayer electron system, Paul Scherrer institute (PSI), Switzerland 2003